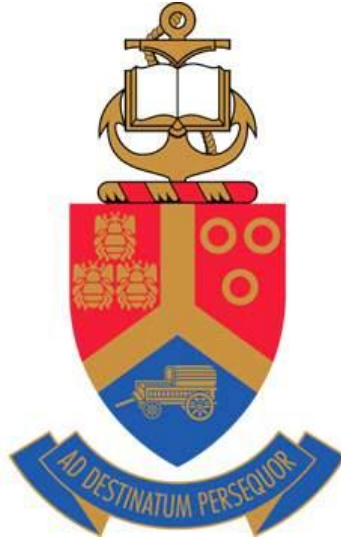# MODELING, FABRICATION, CALIBRATION AND TESTING OF A SIX-AXIS WHEEL FORCE TRANSDUCER

University of Pretoria

Department of Mechanical and Aeronautical Engineering

MSC 422: Final Report

Student Name	OMM Nouwens
Student Number	10389467
Study Leader	Prof. PS Els
Date	28 October 2013

MECHANICAL AND AERONAUTICAL ENGINEERING

MEGANIESE EN LUGVAARTKUNDIGE INGENIEURSWESE

INDIVIDUAL ASSIGNMENT COVER PAGE /INDIVIDUELE OPDRAG DEKBLAD

Name of Student / Naam van Student	O.M.M. NOUWENS
Student number / Studentenommer	10389467
Name of Module / Naam van Module	Research Project
Module Code / Modulekode	MSC 422
Name of Lecturer / Naam van Dosent	Prof. P.S. Els
Date of Submission / Datum van Inhandiging	28 October 2013
Declaration: 1. I understand what plagiarism is and am aware of the University's policy in this regard. 2. I declare that this <u>Thesis</u> (e.g. essay, report, project, assignment, dissertation, thesis, etc.) is my own, original work. 3. I did not refer to work of current or previous students, memoranda, solution manuals or any other material containing complete or partial solutions to this assignment. 4. Where other people's work has been used (either from a printed source, Internet, or any other source), this has been properly acknowledged and referenced. 5. I have not allowed anyone to copy my assignment.	**Verklaring:** 1. Ek begryp wat plagiaat is en is bewus van die Universiteitsbeleid in hierdie verband. 2. Ek verklaar dat hierdie _____ (bv. opstel, verslag, projek, werkstuk, verhandeling, proefskrif, ens.) my eie, oorspronklike werk is. 3. Ek het nie gebruik gemaak van huidige of vorige studente se werk, memoranda, antwoord-bundels of enige ander materiaal wat volledige of gedeeltelike oplossings van hierdie werkstuk bevat nie. 4. In gevalle waar iemand anders se werk gebruik is (hetsy uit ´n gedrukte bron, die Internet, of enige ander bron), is dit behoorlik erken en die korrekte verwysings is gebruik. 5. Ek het niemand toegelaat om my werkopdrag te kopieër nie.
Signature of Student / Handtekening van Student	
Mark awarded / Punt toegeken	

PROTOCOL

The relevant sections of the Protocol as compiled by the student prior to the initiation of the project are included. The objectives as mentioned in the Project Scope section of the protocol will form the basis of the Protocol Compliance Matrix.

PROBLEM STATEMENT

The objective of the research project is to implement a six axis wheel force transducer into a Baja, at the University of Pretoria, to determine the three force and three moment components transmitted through the tyre to the vehicle during operation. This will require the theoretical modeling and configuration of a designed wheel force transducer (from MOX 410 Design Project) using the correct methodology such that it can be fabricated, calibrated and tested in real-life conditions.

BACKGROUND

A wheel force transducer is typically found between the wheel hub and rim of a vehicle, thus creating an interface through which all forces and moments must be transmitted in order to travel from the tyre contact patch (vehicle-terrain interface) to the vehicle itself. Therefore, each wheel must be fitted with a force transducer if one wishes to capture all forces and moments generated at all the tyre contact patches.

A force transducer is a flexural system that undergoes monitored deformation or strain when a force or moment is transmitted through it. The deformation throughout the force transducer causes a specific strain field which can be analysed and resolved back into the transmitted forces and moments using careful mathematical or finite element modeling. The strain field can be characterized by using a series of strategically placed resistive strain gauges throughout the transducer.

The ability to accurately model the forces and moments transmitted to a vehicle provides great insight into vehicle dynamics. Wheel force transducers provide a means to experimentally determine the forces and moments transmitted to a vehicle through the tyre contact patch and can thus provide data to either create or verify vehicle simulations. The need for accurate vehicle

simulations and models is of great importance as it can provide information on vehicle characteristics, performance and limitations.

PROJECT SCOPE

The research project regarding the implementation of the six axis wheel force transducer will encompass the following aspects:

a) The student is required to compile a literature survey regarding the implementation and application of wheel force transducers. The student will be required to gain a full understanding of wheel force transducers and tyres such that all the required modeling, fabrication, calibration and testing can be completed.

A detailed design of the required wheel force transducer will be completed for the MOX 410 Design Project and made available to the project. The transducer will meet the specifications as required in the research project: The design will be based on the Baja's at the University of Pretoria.

b) The student is to complete the appropriate modeling of the wheel force transducer in context of functionality (not design). In other words the student is to model the force transducer such that applied loads can be predicted based on information from strain gauges, load cells etc.

c) The design of a calibration procedure and setup it to be completed for the force transducer. The transducer is to be calibrated by applying known forces and moments.

d) An experimental procedure to verify the theoretical predictions against experimental results is to be compiled: Calibration data is to be compared to the theoretical predictions.

e) An experimental procedure and setup must be compiled for the testing of the wheel force transducer on the Baja vehicle.

f) Fabrication of a full prototype wheel force transducer (according to the existing design) is to be completed. In addition, any fabrication required for calibration and vehicle implementation is to be completed.

g) The wheel force transducer is to be calibrated: The applicable procedures, as compiled by the student, for calibration should be used.

h) Implementation of an operational and calibrated wheel force transducer in the Baja is to be completed. Once implemented experimental data is to be collected during vehicle operation.

i) Verification of theoretical predictions against experimental results is to be completed.

An existing computational system to record all readings, for telemetry, from the wheel force transducer will be made available to the project. In this regard the student is only required to create an interface between the wheel force transducer and the computational system.

PROJECT PLANNING

Planning for the project is based on a predefined schedule, comprising of deadlines, as stated in the MSC 412/422 Study Guide. The resultant schedule with all activities is presented on a Gantt chart.

The critical deadlines are as follows:

- Handing in of protocol   18-02-2013
- First progress report   04-03-2013
- Half year report   27-05-2013
- Half year evaluation   14-06-2013
- Second progress report   12-08-2013
- Closure of workshops, and all computer facilities   14-10-2013
- Handing in of final report   28-10-2013
- Presentation and oral examination   15-11-2013
- Poster exhibition during final year function   28-11-2013

The required tasks are as follows:

- *Literature study of wheel force transducer implementation*: The outcomes of this task are explained in part a) of the *Project Scope* section.
- *Design of the transducer for fabrication (MOX 410):* This task represents the MOX 410 Design Project of the wheel force transducer. It has been included to outline an appropriate timescale till the design is available to the research project.

- *Functional modeling of the transducer:* The student is to model the force transducer such that applied loads can be predicted based on information from the strain gauges, load cells etc.

- *Selection of the transducer communication system:* As explained, the appropriate equipment is made available to the project for data recording; however the student will be required to select the system and the correct interface medium.

- *Design of the calibration procedure and setup*: A procedure and setup is to be designed to effectively calibrate the wheel force transducer while utilizing existing equipment.

- *Design of a procedure to verify theoretical predictions*: The student is to verify the models by compiling a procedure to compare the experimental data from calibration to the theoretical predictions.

- *Fabrication of the transducer and accessories for assembly*: This task represents all fabrication required for the wheel force transducer assembly and implementation into the Baja with the communications system.

- *Fabrication of the calibration setup*: If applicable, this task represents all fabrication required for calibration according to the calibration setup as previously designed.

- *Installation of the transducer into the Baja*: The wheel force transducer is to be installed into the Baja with all required communication systems. Only completed after calibration.

- *Calibration of the transducer*: The wheel force transducer is to be calibrated according to the calibration procedure as previously compiled.

- *Experimental verification of theoretical predictions*: The theoretical predictions are to be verified using the experimental verification procedure as previously compiled.

- *Testing of the transducer in the Baja*: The wheel force transducer is to be installed and tested in the Baja.

The student plans to complete all deliverables and reports more or less a week before the time to ensure the critical deadlines are met with a safety margin. This safety margin is presented on the Gantt chart included on the following page.

Important points to note on the Gantt diagram is that the design of the wheel force transducer for fabrication coincides with the MOX 410 Design Project initiation and deadline dates, thus it extends over the whole first semester.

Gantt chart — Project schedule (Week 6 – Week 48)

Category	Task	Scheduled period (approx.)
Literature survey	Literature study of wheel force transducer implementation	Week 7 – Week 13 (Feb – Mar)
Transducer design and modeling	Design of the transducer for fabrication (MOX 410)	Week 7 – Week 22 (Feb – May)
	Functional modeling of the transducer	Week 11 – Week 18 (Mar – Apr)
	Selection of the transducer communication system	Week 14 – Week 15 (Apr)
Procedures for the transducer	Design of the calibration procedure and setup	Week 14 – Week 17 (Apr)
	Design of a procedure to validate theoretical predictions	Week 15 – Week 17 (Apr)
	Design of a test procedure using the Baja	Week 14 – Week 16 (Apr)
Fabrication and installation	Fabrication of the transducer and accessories for assembly	Week 19 – Week 32 (May – Aug)
	Fabrication of the calibration setup	Week 19 – Week 22 (May)
	Installation of the transducer into the Baja	(Aug)
Analysis and testing	Calibration of the transducer	Week 33 – Week 36 (Aug – Sep)
	Experimental verification of theoretical predictions	Week 34 – Week 37 (Aug – Sep)
	Testing of the transducer in the Baja	Week 36 – Week 39 (Sep)
	Project protocol	Week 7 (Feb)
	First progress report	Week 9 (Mar)
	Half year report	Week 21 – Week 22 (May)
Deliverables and reports	Half year evaluation	Week 24 (Jun)
	Second progress report	Week 32 (Aug)
	Handing in of final report	Week 43 – Week 44 (Oct)
	Presentation and oral examination	Week 45 (Nov)
	Poster exhibition during final year function	Week 47 – Week 48 (Nov)

Column headings (months / weeks):
February: Week 6 (4–10), Week 7 (11–17), Week 8 (18–24), Week 9 (25–3) · March: Week 10 (4–10), Week 11 (11–17), Week 12 (18–24), Week 13 (25–31) · April: Week 14 (1–7), Week 15 (8–14), Week 16 (15–21), Week 17 (22–28) · May: Week 18 (29–5), Week 19 (6–12), Week 20 (13–19), Week 21 (20–26), Week 22 (27–2) · June: Week 23 (3–9), Week 24 (10–16), Week 25 (17–23), Week 26 (24–30) · July: Week 27 (1–7), Week 28 (8–14), Week 29 (15–21), Week 30 (22–28) · August: Week 31 (29–4), Week 32 (5–11), Week 33 (12–18), Week 34 (19–25), Week 35 (26–1) · September: Week 36 (2–8), Week 37 (9–15), Week 38 (16–22), Week 39 (23–29) · October: Week 40 (30–6), Week 41 (7–13), Week 42 (14–20), Week 43 (21–27), Week 44 (28–3) · November: Week 45 (4–10), Week 46 (11–17), Week 47 (18–24), Week 48 (25–1)

EXECUTIVE SUMMARY

The purpose of this research project was to model, fabricate, calibrate and test a six-axis wheel force transducer designed for the Baja vehicles at the University of Pretoria. The concept incorporated was that of the statically indeterminate four-cantilever-spoke and hub force transducers. Such six-axis transducers may be almost entirely decoupled in their operation by careful selection of the Wheatstone bridges and strain gauge layout.

The concept was advanced to the detailed design phase where a mathematical model was used to optimize the geometry of the transducer based on the design specifications of the Baja vehicles. After a convergent geometry had been obtained a final strain compliance (and calibration matrix) could be established by the mathematical model to fully characterize the transducer in its operation. The geometry was imported to a FE (Finite Element) model to confirm the results from the mathematical model. This formed the theoretical investigation of the report where it was found that a strong correlation existed between the two models.

An experimental investigation was formulated and completed to verify the results from the theoretical models and establish the wheel force transducer was operational. This was done in two stages: Firstly an experimental reconstruction of the calibration procedure was completed to obtain a strain compliance matrix of the actual fabricated transducer. It was found that the experimental and theoretical results compared very well regarding the calibration of the transducer. Finally tests were completed on the Baja vehicle itself to insure the wheel force transducer was operational in the environment it was designed for. Various maneuvers were completed to load specific axes of the device while on the Baja. The results from these tests correlated extremely well with the expected results based on vehicle dynamic behavior.

It could be concluded that a wheel force transducer had been successfully modeled, fabricated, calibrated and tested thus producing a working piece of equipment that will aid in the future development of the Baja vehicles at the University of Pretoria. However, slight improvements can be made to the existing design to provide a more sensitive and easier to fabricate wheel force transducer.

ABSTRACT

This report contains the details regarding the modeling and testing a six-axis wheel force transducer to be implemented on the Baja vehicles at the University of Pretoria. The purpose of the project was to eventually obtain a fully implementable wheel force transducer that will provide data for vehicle simulations. These simulations will aid in the development process of the Baja vehicles. A detailed mathematical and FE (Finite Element) modeling of an existing concept was completed such that the wheel force transducer could be fully characterized during its operation. To verify the models and operation of the wheel force transducer an experimental investigation was formulated and completed. The models allowed for a thorough theoretical investigation of the wheel force transducer where a strong correlation was found between the mathematical and FE models. Additionally, the experimental results also displayed a strong correlation. After implementing the wheel force transducer to the Baja vehicle is was found that the device was operational and capable of withstanding the required conditions. To improve the performance of the wheel force transducer it is recommended that the design loads be reexamined and characterized to possibly create less demanding design specifications. This will improve the sensitivity of the device if an iterative design process is followed.

PROTOCOL COMPLIANCE MATRIX

Requirement	Protocol (Scope)		Project Report	
	Part	**Page**	**Section**	**Page**
Complete a literature survey regarding the implementation, modeling and application of wheel force transducers.	a)	iv	3	4
Complete the appropriate modeling of the wheel force transducer in context of functionality.	b)	iv	5	34
Design of a calibration procedure and setup.	c)	iv	6	69
Design of an experimental procedure to verify the theoretical predictions against experimental results.	d)	iv	6.1.1	69
Design of a wheel force transducer test procedure on the Baja	e)	iv	6	69
Fabrication of a full prototype wheel force transducer.	f)	iv	6.2	72
Calibration of the wheel force transducer.	g)	iv	6.5	76
Implementation of a calibrated wheel force transducer in the Baja.	h)	v	6.6	83
Verification of theoretical predictions against experimental results.	i)	v	7	91

ACKNOWLEDGEMENTS

I would like to thank all parties which have contributed in making this project a success. Their kind and valued inputs are greatly appreciated:

- Prof. PS Els, whose continuous guidance and comprehensive past research in wheel force transducers allowed for great project progress throughout the year.
- Fellow student, Brett Kent, for very kindly undertaking the immense task of machining the transducer.
- My father, Pieter Nouwens, for all his valued support and continuous engineering input.
- My brother, Nicholas Nouwens, for all his past expertise and continued assistance in the fabrication process.
- Member of the Vehicle Dynamics Research Group at the University of Pretoria, Carl Becker, for his appreciated assistance throughout the year, especially in setting up the communications system for the wheel force transducer and arranging the eDAQs.
- Member of the Vehicle Dynamics Research Group at the University of Pretoria, Joachim Stallmann, for kindly demonstrating the necessary communications software.
- Members of the University of Pretoria Baja team who provided continuous assistance during the fabrication, assembly and testing of the wheel force transducer.

TABLE OF CONTENTS

LIST OF FIGURES

LIST OF TABLES

LIST OF SYMBOLS

English letters and symbols

A	Area	(m^2)
b	Breadth/width	(m)
$[B]$	Calibration matrix	(Nm/m ; Nm^2/m)
$[C]$	Strain compliance matrix	(m/Nm ; m/Nm^2)
$[CSC]$	Cross-sensitivity coefficient matrix	(-)
E	Modulus of elasticity	(Pa)
F	Force relative to the transducer	(N)
F'	Force relative to the vehicle	(N)
$\bar{F}$	Force and moment vector	(N ; Nm)
G	Shear modulus	(Pa)
h	Height	(m)
H^c	Centroidal bending stiffness	(Pa.m^4)
$[H]$	Transformation matrix	(-)
I	Second moment of area	(m^4)
K_f or K_{fs}	Fatigue stress concentration factor	(-)
K_s	Strain gauge factor	(-)
l	Length	(m)
l_o	Unstrained length of strain gauge	(m)
M	Moment relative to the transducer	(Nm)
M	Bending moment	(Nm)
M'	Moment relative to the vehicle	(Nm)
P	Tension	(N)
R	Resistance	(Ohm)
R_o	Unstrained resistance of strain gauge	(Ohm)
R	Reaction force or moment	(N ; Nm)
$\bar{R}$	Reaction force and moment vector	(N ; Nm)
S	Strain signal	(m/m)

$\bar{S}$	Strain signal vector	(m/m)
T	Temperature	(˚C)
T	Torsion	(Nm)
$\bar{u}$	Transverse displacement	(m)
V	Voltage	(V)
V	Shear force	(N)
w	Width (variant to b)	(m)
x	General dimension in X axis	(m)
y	General dimension in Y axis	(m)
z	General dimension in Z axis	(m)

Greek symbols

α	Coefficient of thermal expansion	(1/˚C)
α_r	Strain gauge resistance temperature coefficient	(1/˚C)
δ	Small change in	(-)
Δ	Change in	(-)
ε	Strain	(m/m)
ε_o	Observed strain	(m/m)
θ	Angular displacement	(radians)
ν	Poisson's ratio	(-)
σ	Normal stress	(Pa)
τ	Shear stress	(Pa)
ϕ	Angle of misalignment	(radians)
Ω	Resistance	(Ohms)

Superscripts

TC	At the tyre contact patch
M	Associated moment reaction
θ	Associated rotational stiffness

Subscripts

a	Amplitude
eff	Effective
$i; j; k; l$	Indicial notation
max	Maximum
in	Input
out	Output
rev	Reversed
SG	Of the strain gauge
sub	Substrate
X	In or about the X axis
Y	In or about the Y axis
Z	In or about the Z axis

1.   INTRODUCTION

A wheel force transducer is typically found between the wheel hub and rim of a vehicle, thus creating an interface through which all forces and moments must be transmitted in order to travel from the tyre contact patch (vehicle-terrain interface) to the vehicle itself.

A force transducer is a flexural system that undergoes monitored deformation or strain when a force or moment is transmitted through it. The deformation throughout the force transducer causes a specific strain field which can be analysed and resolved back into the transmitted forces and moments using careful mathematical or finite element modeling. The strain field can be captured by using a series of strategically placed strain sensors throughout the transducer.

The ability to accurately model the forces and moments transmitted to a vehicle provides great insight into vehicle dynamics. Wheel force transducers provide a means to experimentally determine the forces and moments transmitted to a vehicle through the tyre contact patch and can thus provide data to either create or verify vehicle simulations. The need for accurate vehicle simulations and models is of great importance as it can provide information on vehicle characteristics, performance and limitations.

Several methods exist in practice to capture the forces and moments transmitted through a wheel. Each method has its own associated advantages and disadvantages while attempting to accomplish one specific design parameter based on the application. Wheel force transducers can be designed to be extremely simple in their mechanical design, but inherently complex to characterize/model during operation. On the other extreme very complex designs exist that can be simply modeled for efficient operation. This project focuses on the modeling, testing and calibration of a six-axis wheel force transducer. There are currently techniques in place that utilize a series of one or two axis force sensors/transducers to create a single six axis force transducer. This is only to mention a few approaches for the design of wheel force transducers. Many different concepts could thus have been pursued during the design phase each of which would have led to different modeling, calibration and testing methods.

A major limitation in the implementation of a wheel force transducer was experienced during the undertaking of the project. Each wheel force transducer must be designed to be compatible with

a specific vehicle. In this project the vehicle at hand was the Baja vehicles as found at the University of Pretoria. The wheel setup of a Baja is extremely confined in space and in addition is subject to extremely high loads during operation. The wheel force transducer had to be specifically designed to withstand all the high loading while complying with the limited available space for implementation. This meant the selected concept for design had to be carefully selected in context of these limitations.

The undertaking of this project would provide great insight into the loading as experienced by the Baja vehicles at the University of Pretoria. The University of Pretoria hosts competitive Baja teams that are continually improving the design of their vehicles. Dynamic loading simulations with data produced by the wheel force transducer(s) will allow the teams to further develop and improve their vehicles.

During this report a literature review is completed that provides all the insights necessary to develop an effective wheel force transducer model based on the selected concept. The final design of the wheel force transducer is then included to provide all necessary context. Having established a well-founded background of the specific wheel force transducer, the modeling is then explained in detail as a theoretical investigation. With the wheel force transducer completely characterized theoretically an experimental investigation was formulated and completed to both verify the theoretical modeling and operation of the device in the Baja vehicle.

2.   SCOPE OF WORK

The student was required to complete the modeling, calibration, implementation and testing of a wheel force transducer for the Baja vehicle at the University of Pretoria. Comprehensive details regarding the project scope were provided in the Protocol on page iv.

This report is under the assumption that the wheel force transducer has been completely designed and optimized. This undertaking was completed in the MOX 410 Design Project where various types of wheel force transducers were analysed in the context of the Baja. The most viable concept was selected and thereafter underwent detailed design. This report can therefore immediately be focused in the final concept and associated modeling, testing and calibration requirements.

3.   LITERATURE REVIEW

The literature review in this report contains information regarding the modeling, calibration and testing of wheel force transducers. The methodology of the wheel force transducer is explained in detail such that a full understanding of the principles can be attained. It is in understanding the underlying principles that the correct modeling, calibrating and testing can be completed effectively. The literature review focuses more specifically on the wheel force transducer that will be implemented.

3.1.   FORCES IN WHEELS AND TRANSDUCERS

The function of a wheel force transducer is to capture all the forces and moments transmitted between the vehicle and the tyre contact patch. In Figure 1 the forces and moments generated at the tyre contact (TC) patch ($F_X^{TC}; F_Y^{TC}; F_Z^{TC}; M_X^{TC}; M_Y^{TC}; M_Z^{TC}$) are shown.

The wheel force transducer as researched in this project is centered on the axis of the wheel thus is offset by the radius of the wheel from the tyre contact patch (there may also be a slight axial offset). The forces generated at the tyre contact patch are thus translated by these offsets before being measured causing additional moment components at the transducer. The wheel force transducer is required to measure forces and moment in all six axes ($F_X'; F_Y'; F_Z'; M_X'; M_Y'; M_Z'$) as illustrated in Figure 1.
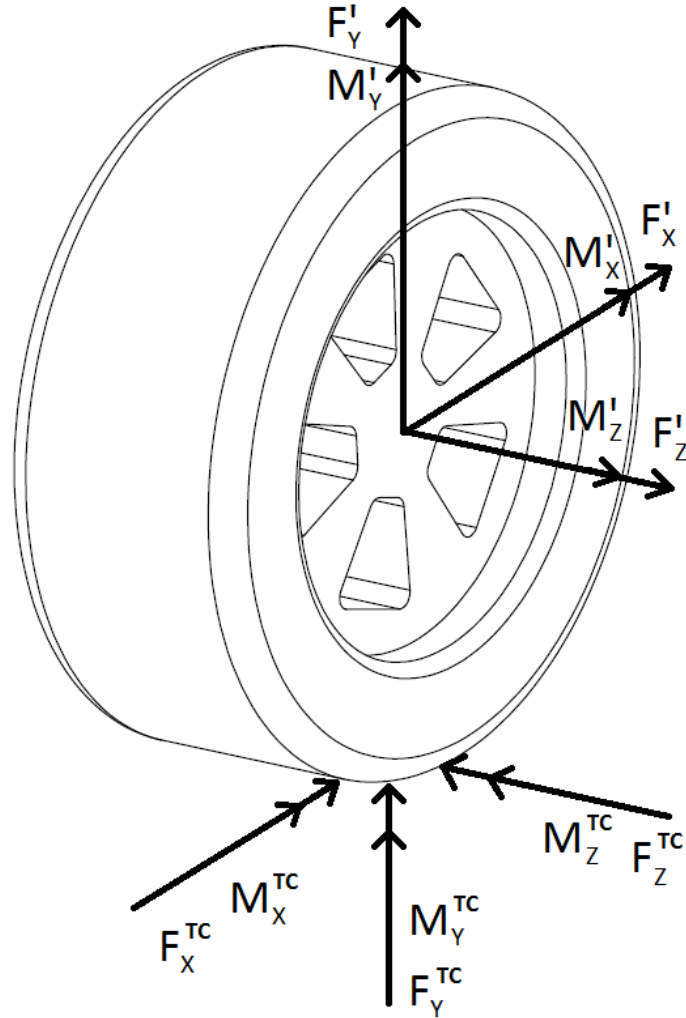
Figure 1: Wheel forces in a static reference frame

The forces and moments in Figure 1 will be very briefly explained: $F_X^{TC} = F_X'$ are the driving/braking forces (tractive force) responsible for the acceleration of the vehicle while M_Z' is the resultant driving/braking torque. The transverse steering loads $F_Z^{TC} = F_Z'$ (lateral force) cause the centripetal acceleration of the vehicle during a turning maneuver and M_X' is the resultant overturning moment induced by M_X^{TC} and F_Z^{TC} through the radius of the wheel. M_Y' is the moment (aligning torque) responsible for steering the wheel and resisting the self-aligning moment M_Y^{TC}. Finally $F_Y^{TC} = F_Y'$ are the normal forces (vertical force) mainly created by the mass of the vehicle and any load distribution under acceleration due to the vehicle's center of gravity above the wheel axis (MIDDLE, Tersius, 2007). The scope of this report does not entail a detailed analysis of wheel force generation but rather the capturing of these forces.

5

The force and moment components $(F_X'; F_Y'; F_Z'; M_X'; M_Y'; M_Z')$ represented by vector $\bar{F}'_{6\times1}$ exist in a static reference frame with respect to the vehicle. However, the wheel force transducer will be operating inside of a rotating reference frame with respect to the vehicle. The figure below illustrates the transducer's coordinate system with respect to the wheel's static system at a positive angular displacement θ.
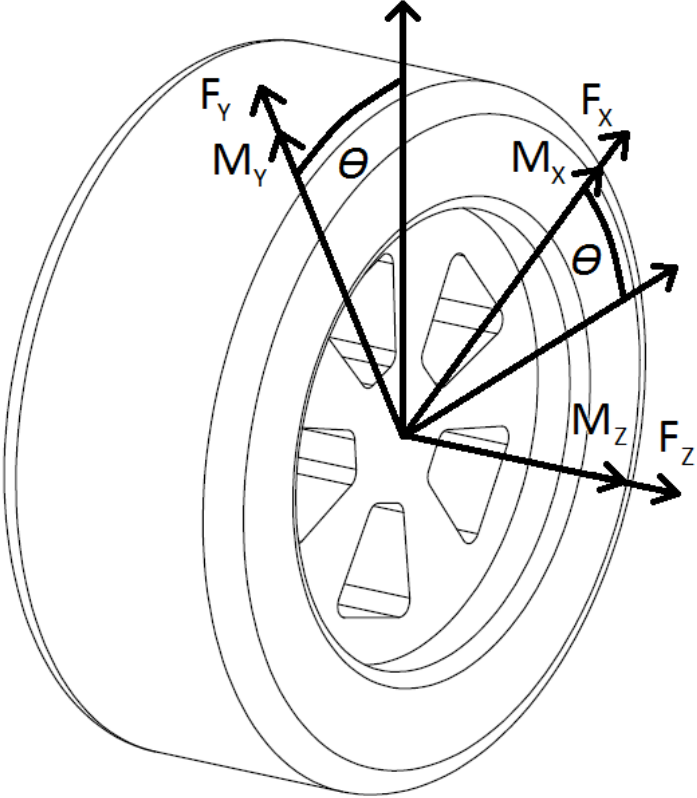
Figure 2: Rotated reference frame relative to the vehicle

It should be noted that the presented coordinate system, force and moment components in Figures 1 and 2 represents convention for the entirety of this report.

The force and moment components $(F_X; F_Y; F_Z; M_X; M_Y; M_Z)$ represented by vector $\bar{F}_{6\times1}$ are measured by the transducer in its coordinate system. Each force and moment component represents an active axis of the force transducer. $\bar{F}'$ and $\bar{F}$ are related through the following transformation (SLOCUM, A.H, 1992):

$$\begin{bmatrix} F'_X \\ F'_Y \\ F'_Z \\ M'_X \\ M'_Y \\ M'_Z \end{bmatrix} = \begin{bmatrix} \cos\theta & -\sin\theta & 0 & 0 & 0 & 0 \\ \sin\theta & \cos\theta & 0 & 0 & 0 & 0 \\ 0 & 0 & 1 & 0 & 0 & 0 \\ 0 & 0 & 0 & \cos\theta & -\sin\theta & 0 \\ 0 & 0 & 0 & \sin\theta & \cos\theta & 0 \\ 0 & 0 & 0 & 0 & 0 & 1 \end{bmatrix} \begin{bmatrix} F_X \\ F_Y \\ F_Z \\ M_X \\ M_Y \\ M_Z \end{bmatrix} \qquad (3.1)$$

Or simply $\bar{F}' = [H]\bar{F}$ where $[H]$ is called the transformation matrix.

3.2. IMPLEMENTATION OF WHEEL FORCE TRANSDUCERS

Unlike static force transducers, wheel force transducers exist inside a rotating reference frame as explained earlier. It is therefore necessary to track the angular position of the wheel force transducer relative to the vehicle such that the appropriate transformation can be executed as presented in Equation (3.1). To accomplish this angular displacement transducers are incorporated.

In addition telemetry systems are required to receive and process data from the force sensors. To prevent high noise in data transmission slip rings are avoided and rather the telemetry systems are placed in the same rotating reference frame as the force transducers. This raises the unsprung mass of the vehicle; however, efficient data transmission is accomplished. An alternate solution is to incorporate wireless systems for data transmission; however, these are usually associated with low data transfer rates. The latter approach will be adopted in the research project at hand.

3.3. TYPES OF WHEEL FORCE TRANSDUCERS

At this point in time it is important to realize that wheel force transducers comprise of several coupled or uncoupled (to be explained later) force sensors or force transducers. In doing this a wheel force transducer accomplishes the task of determining global forces and moments based on the information received from local forces/strains measured by several force sensors/transducers.

The most common method of creating force sensors is by the utilization of resistive strain gauges. There are many classical methods for the electronic measurement of a force. They are in no particular order: resistive, inductive, capacitive, piezoelectric, electromagnetic, electrodynamic, magnetoelastic, galvanomagnetic, vibrating wires, microresonators, acoustic and

gyroscopic. Each method presents a different principle involved and thus has associated advantages and disadvantages (STEFANESCU, Dan M and Anghel, Mirela A, 2012). In the application of wheel force transducers strain gauges, as incorporated in this project, are highly advantageous due to their relatively low cost, ability to withstand harsh conditions and versatility in Wheatstone Bridges. The principle of resistive strain gauges and measurement will be explained in detail in Section 3.4 as it will be required to understand some wheel force transducer concepts in the literature review.

Many types wheel force transducers that utilize resistive strain gauges exist in practice. Each method obviously has its own associated advantages and disadvantages while attempting to accomplish some specific design parameter. The most common design parameters to accomplish are:

- Create an uncoupled wheel force transducer for effective/efficient computational times (CHAO, Lu-Ping and Chen, Kuen-Tzong, 1997).
- Utilize the existing rim of the vehicle to minimize the unsprung mass and cost (CHELI, F et al., 2011).
- Utilize existing one or two axis force sensors to minimize the complexity of the system (CENTKOWSKI, Karol and Ulrich, Alfred, 2012).
- Create an essentially statically determinate system for simple modeling (GOBBI, M et al., 2011).

These design parameters each require the design of the wheel force transducer to be focused differently. This project focuses on the modeling, fabrication, calibration and testing of an uncoupled wheel force transducer. The exact implications of uncoupled wheel force transducers will only become clear in subsequent sections of the literature survey.

3.4.   STRAIN GAUGES

3.4.1.   PRINCIPLE OF STRAIN GAUGES

Resistive strain gauges, as will be incorporated in this project, detect a minute dimensional change as an electric signal. The resistance as seen across a strain gauge is mainly dependent on the elongation or contraction of the gauge. A strain gauge is applied to the surface of an object

by a specialized adhesive that is capable of transferring the strain from the object to the gauge. Thus when a strain gauge is placed on a specimen that undergoes elongation due to tensile loading, it will to be elongated if correctly orientated. The elongation will be detected as a change in resistance across the strain gauge (The same principle holds under contraction due to compression). The change in resistance δR can be related to the surface strain (where the gauge is placed only) by the following relation (PANAS, Robert.M, 2009)

$$\frac{\delta R}{R_o} = K_s \frac{\delta l}{l_o} = K_s \, \varepsilon \qquad (3.2)$$

Where R_o is the unstrained resistance, K_s the gauge factor coefficient, l_o the unstrained length, δl the change in length and ε the measured strain. The gauge factor is a property of the resistive element used in the strain gauge and describes its sensitivity. A common value for the gauge factor is approximately 2.

A strain gauge comprises of a resistive element in an electrical insulator of thin resin (Kyowa). The resistive element has a length of much higher order than its width or height and is laid out in a grid pattern such that the length is consumed in as much as possible the rated direction of the strain gauge. The result of this configuration is that a strain induced on the resistive element orthogonal to the direction of the strain gauge leads to a negligible δR i.e. it is only a strain along the length of the resistive element that causes a significant δR. The important consideration is therefore not the effect of transverse strain on the resistive element but rather the effect of transverse strain on the strain in the direction of the strain gauge. Consider the following general stress-strain relation for a linear isotropic material (PANAS, Robert.M, 2009):

$$\varepsilon_i = \frac{\delta l}{l_o} = \frac{1}{E}\left[\sigma_i - v(\sigma_j + \sigma_k)\right] \qquad (3.3)$$

In this expression E represents the modulus of elasticity of the material and $\sigma_{i,j,k}$ the stresses in the respective orthogonal $i; j; k$ axes. Here the Poisson effect is introduced by the Poisson's ratio v and demonstrates how an elongation (contraction) in one direction causes a proportional contraction (elongation) in the orthogonal axes. As explained earlier the resistive element can be approximated as being only exposed to strain along its longitudinal direction (direction of the

strain gauge): Let us consider this the X-axis direction. The strain gauge (SG) will therefore reflect the following orthogonal internal strains (PANAS, Robert.M, 2009):

$$\varepsilon_{XSG} = \frac{\sigma_{XSG}}{E_{SG}} \tag{3.4}$$

$$\varepsilon_{YSG} = -v_{SG}\varepsilon_{XSG} \tag{3.5}$$

$$\varepsilon_{ZSG} = -v_{SG}\varepsilon_{XSG} \tag{3.6}$$

In the above expression σ_{XSG} is the stress in the X-direction and E_{SG} and v_{SG} the modulus of elasticity and Poisson's ration of the strain gauge respectively. The X, Y and Z subscripts represent orthogonal axes. Equations (3.4) to (3.6) demonstrate the inability of a single strain gauge to reflect on the strains generated by transverse loads.

In addition to the Poisson effects an important consideration are thermal effects. A general expression for thermal strain in an isotropic material is given by the following relation:

$$\varepsilon_i = \alpha\Delta T \tag{3.7}$$

In this expression α is the coefficient of thermal expansion of the material and ΔT the change in temperature. In addition to mechanical strains, thermal strain will cause a change in resistance across the strain gauge according to the following relation (PANAS, Robert.M, 2009):

$$\frac{\delta R}{R_o} = \alpha_r \Delta T \tag{3.8}$$

The temperature coefficient α_r will be defined shortly. The major concern with temperature effects in strain gauges is the difference in thermal expansion coefficients of the strain gauge α_{SG} and the substrate α_{sub} (object being measured). A strain gauge on a substrate would undergo the following internal strains during a temperature change ΔT:

$$\varepsilon_{XSG} = \alpha_{sub}\Delta T = \frac{\sigma_{XSG}}{E_{SG}} + \alpha_{SG}\Delta T \tag{3.9}$$

$$\varepsilon_{YSG} = [(1 + v_{SG})\alpha_{SG} - v_{SG}\alpha_{sub}]\Delta T \tag{3.10}$$

$$\varepsilon_{ZSG} = [(1 + v_{SG})\alpha_{SG} - v_{SG}\alpha_{sub}]\Delta T \qquad (3.11)$$

It follows that thermal effects influence the strains of the substrate and strain gauge differently. It can be shown that a strain gauge resistance temperature coefficient α_r can be solved for to compensate for the variation in thermal expansion coefficients. The expression, derived from the previous equations (and others), is given by:

$$\alpha_r = (1 + 2v)\alpha_{sub} - (2 + 2v)\alpha_{SG} \qquad (3.12)$$

By appropriately selecting the correct α_{SG} for a specific substrate, so called 'coefficient matching', the effects of temperature can effectively be 'turned off'. The resulting resistance of the strain gauge R_{SG} can then be obtained by combining Equations (3.2) and (3.8):

$$R_{SG} = R_o(1 + K_s\varepsilon + \alpha_r\Delta T) \qquad (3.13)$$

3.4.2. PRINCIPLE OF STRAIN MEASUREMENT

The change in resistance across a strain gauge during deformation is extremely small, thus Wheatstone bridges are usually used to amplify the signal. The basic layout of a Wheatstone bridge consists of four approximately equal resistors (of resistance R1 to R4) connected as follows (PANAS, Robert.M, 2009):
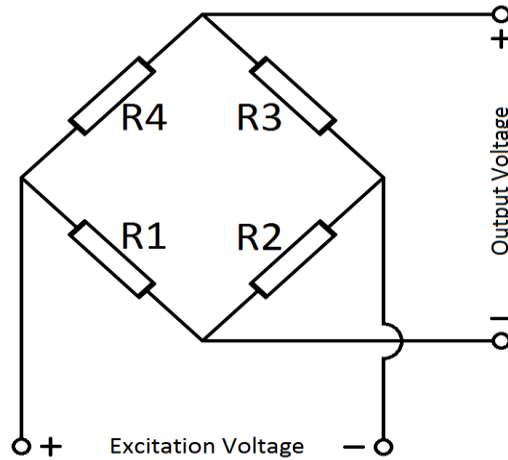
Figure 3: Wheatstone bridge

The Wheatstone bridge can be characterized by the following relation from simple direct current (DC) nodal analysis:

11

$$\frac{V_{out}}{V_{in}} = \frac{R3}{R4 + R3} - \frac{R2}{R1 + R2} \qquad (3.14)$$

Where V_{out} and V_{in} are the output and excitation voltages. From the expression we learn that four equal resistances (R1 to R4) will produce a zero volt output since the bridge removes the differential DC term. Any change in resistance will cause an offset in the output voltage, thus creating an associated signal. A Wheatstone bridge is defined by the number of active resistors (resistors with varying resistances) in it. This can range from a quarter bridge with one active resistor, to a half bridge with two active resistors to a full bridge with four active resistors.

The principle of Wheatstone bridges can be applied to strain gauges since a change in resistance of the strain gauge can cause it to act as an active resistor in the bridge. As an example consider the following: If R1 in Figure 3 represents a strain gauge of certain resistance R undergoing a change in resistance of ΔR such that $\Delta R \ll R$ and R2 to R4 represent resistors of the same resistance R, then the output voltage V_{out} can be closely approximated from (Kyowa):

$$V_{out} \cong \frac{1}{4} \cdot \frac{\Delta R}{R} V_{in} \qquad (3.15)$$

In this expression V_{in} is the excitation voltage. Substitution of Equation (3.2) into (3.15) yields:

$$V_{out} \cong \frac{1}{4} K_s \, \varepsilon V_{in} \qquad (3.16)$$

The approximation is as a result of the non-linearity associated with this specific type of Wheatstone bridge configuration. An exact solution to the output voltage for a quarter bridge under both strain and temperature changes can be represented by the Taylor series (PANAS, Robert.M, 2009):

$$\begin{aligned}
\frac{V_{out}}{V_{in}} = {} & \left[\frac{1}{4}(K_s \, \varepsilon) - \frac{1}{8}(K_s \, \varepsilon)^2 + \frac{1}{16}(K_s \, \varepsilon)^3 + \cdots \right] \\
& + \left[\frac{1}{4}(\alpha_r \Delta T) - \frac{1}{8}(\alpha_r \Delta T)^2 + \frac{1}{16}(\alpha_r \Delta T)^3 + \cdots \right]
\end{aligned} \qquad (3.17)$$

Equations (3.15) through (3.17) describe only one type of Wheatstone bridge configuration. There are many Wheatstone bridges involving different strain gauge layouts and bridge

configurations that allow one to specify desired properties of the strain measurement. The following properties are available through the correct configurations:

- Temperature compensation without 'coefficient matching' in Equation (3.12)
- Temperature annulment by the incorporation of 'dummy gauges' in full bridges
- Cancelation of strain gauge lead wire thermal effects
- Removal of non-linearities
- Elimination of bending strain
- Elimination of tensile/compressive strains
- Averaging of strains
- Addition or subtraction of strains (e.g. $\varepsilon = [\varepsilon_1 - \varepsilon_2 + \varepsilon_3 - \varepsilon_4]/4$ in a full bridge)
- Inclusion of Poisson's ratio
- Measuring of torsional strain
- Variation of sensitivity (e.g. full bridge more sensitive than quarter bridges)

In many cases a combination of these properties can be obtained and is entirely subject to the requirements of the measuring system.

Strain gauges should be placed in areas of high strain for the best sensitivities. It must be noted that a strain gauge has a finite length and is usually adhered to a substrate with a continuously varying surface strain. An ideal position for a strain gauge would be a surface with a high and constant strain over the span of the gauge. However, this is not always possible thus it should be noted that the strain gauge will record the average effective strain ε_{eff} over its length for varying surface strains. Consider a strain gauge of length x_{gauge} placed from x_0 in the X-axis direction over a surface with strain $\varepsilon_X(x)$ that varies along the X-axis direction. Then the ε_{eff} can be given by:

$$\varepsilon_{eff} = \frac{1}{x_{gauge}} \int_{x_0}^{x_0 + x_{gauge}} \varepsilon_X(x). dx \qquad (3.18)$$

Often strain gauges are misaligned accidentally during the adhesion process onto the substrate. Consider a strain gauge adhered to a surface in the XY plane that is misaligned at an angle ϕ from the X-axis. A relation exists to compensate for the misalignment as follows (Kyowa):

$$\varepsilon_o = \frac{1}{2}[(\varepsilon_X + \varepsilon_Y) + (\varepsilon_X - \varepsilon_Y)\cos 2\phi] \qquad (3.19)$$

Where ε_o is the observed strain, ε_X the strain in the X-direction and ε_Y the strain in the Y-direction. While misalignments can be corrected for they are of high inconvenience since an additional strain in the transverse direction will have to be solved for.

3.4.3. *ZERO-BALANCING OF WHEATSTONE BRIDGES*

In reality Wheatstone bridges produce an offset voltage due to mismatched strain gauges or fabrication tolerances. The offset may also be produced by varying resistances in the lead wires. The offset may be severe, often producing a reading that is out of range. Zero-Balancing of the Wheatstone bridge is therefore required. An effective method to manually zero the output voltage during fabrication is to incorporate a potentiometer R5 as follows (PANAS, Robert.M, 2009):
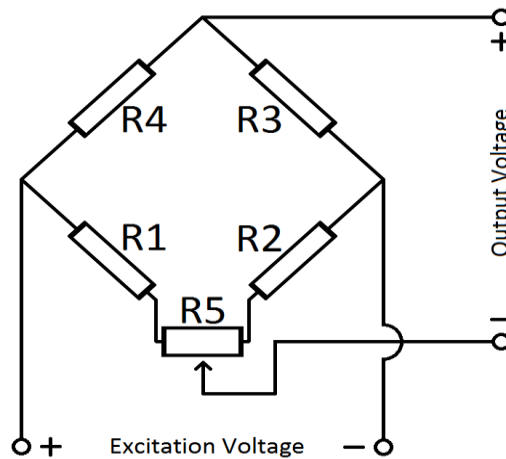
Figure 4: Wheatstone bridge with zeroing potentiometer

The temperature resistance coefficient of the potentiometer should ideally match that of the strain gauges to attenuate the thermal effects as much as possible.

3.5. CONSIDERATIONS IN TRANSDUCER MODELING

3.5.1. *FINITE ELEMENT MODELS VERSUS MATHEMATICAL MODELS IN STRAIN FIELDS*

When a force transducer is designed the appropriate modeling is required in order to obtain a theoretical prediction of the strain field in the structure of the transducer. By knowing the position of the strain gauges and Wheatstone bridge configurations the strain field can be used to predict outputs of the force transducer using strain compliance as will be explained in Section 3.5.2. The challenge lies in creating either a mathematical or finite element model that can accurately capture the strain field under various loads. Both methods present their own limitations and advantages thus a preference is dependent on the application of the model and geometry of the transducer.

A mathematical model can be used to describe transducers of simple geometry and thus provide a means of explicit optimization (PARK, Joong-Jo and Kim, Gab-Soon, 2005). Once optimized, the mathematical model can efficiently solve for the strains at the desired locations. However, when the geometry of the transducer is complex it often becomes challenging to describe any deformations mathematically. In such cases Finite Element (FE) methods are used usually associated with time consuming optimization, but accurate results under full consideration of the geometry.

Ultimately the best solution is to incorporate both a mathematical model and FE method. Once the geometry is known through optimization using the mathematical model, FE methods can be used to validate the final results.

3.5.2. *STRAIN COMPLIANCE AND COUPLING*

Before the selected wheel force transducer design is addressed a governing principle of force transducers is to be understood. This is the principle of strain compliance which relates the strain field in a transducer to the forces and moments applied to it. Measurement of the strain field is accomplished by the use of several strain gauges incorporated in various Wheatstone bridge configurations.

Consider a transducer's force and moment components to be measured $(F_X; F_Y; F_Z; M_X; M_Y; M_Z)$ represented by vector $\bar{F}_{6\times1}$ as before. In addition consider all strain signals from the n Wheatstone bridges $(S_1; S_2; S_3 \ldots S_{n-1}; S_n)$ as vector $\bar{S}_{n\times1}$. These strain signals depend on the selected Wheatstone bridge configurations and strains in the m strain gauges $(\varepsilon_1; \varepsilon_2; \varepsilon_3 \ldots \varepsilon_{m-1}, \varepsilon_m)$. Strain compliance is then defined as the following provided the force sensors operate in the linear elastic region (CHAO, Lu-Ping and Chen, Kuen-Tzong, 1997):

$$\bar{S} = \begin{bmatrix} S_1 \\ S_2 \\ S_3 \\ \vdots \\ S_{n-1} \\ S_n \end{bmatrix} = [C]\bar{F} \tag{3.20}$$

$$\bar{F} = [B]\bar{S} \tag{3.21}$$

Where $[C]$ is called the strain compliance matrix. The inverse of $[C]$ is called the calibration matrix represented by $[B]$. When vector $\bar{S}$ is not a $[6 \times 1]$ size matrix then special inverse techniques will be required to solve for $[B]$. The linear elastic behavior of the material is responsible for a constant strain compliance matrix $[C]$ (CHAO, Lu-Ping and Yin, Ching-Yan, 1999). The presented strain compliance relations hold for all strain based sensors/transducers and is not restricted to six-axis transducers: The same principle can be applied to one or two axis force transducers for instance.

The development of $[C]$ is of great importance: It is essentially arbitrary but some strain compliance configurations will be far more effective than others. By correctly defining $[C]$ the system can be decoupled resulting in a simpler and more effective system that can reduce further computational times.

At this time it is appropriate to define the meaning of a coupled and uncoupled system. A force transducer is said to be coupled when one component of force or moment is applied but is received as output on more than one axis. Force transducers can be split into two types according to their calibration matrix (CHAO, Lu-Ping and Chen, Kuen-Tzong, 1997):

- *Coupled*: Associated with simple mechanical designs but complex calibration matrices. Operation of the force transducer is inherently complex and computation times are usually too high for real time telemetry.
- *Uncoupled*: Associated with complex mechanical designs but simple calibration matrices. Operation of the force transducer is simple as a result making real time telemetry possible.

It is almost impossible to develop a completely uncoupled force transducer; however, multi-axis force transducers with extremely low coupling effects have been developed. To develop an essentially uncoupled force transducer strong consideration must be given to the mechanical design and strain compliance matrix $[C]$. Without getting into too much detail, the compliance matrix $[C]$ is compiled as follows (CHAO, Lu-Ping and Chen, Kuen-Tzong, 1997):

- Given: The mechanical design of a force transducer and positions of m strain gauges to report the respective strains $(\varepsilon_1; \varepsilon_2; \varepsilon_3 \ldots \varepsilon_{m-1}, \varepsilon_m)$.
- Identify the active sensor axes and strain gauges that offer the best sensitivity (given their positions) for each axis.
- Configure n Wheatstone bridges using all strain gauges but only once each: This configuration is arbitrary. Ideally, however to create a six-axis decoupled force transducer six Wheatstone bridges should be created, each allocated to an axis i.e. each Wheatstone bridge only produces a high/distinct strain signal under load of their allocated axis.
- Assign each row in $[C]$ to the corresponding Wheatstone bridge strain signal. For instance every element in the nth row will be associated with the same strain signal from the nth given Wheatstone bridge.
- Using FE analysis or mathematical models solve for the strains ε_1 to ε_m under the rated (designed) load for each axis and compile $[C]$. Every element in each column will be associated with different strain signals. The first column will be compiled by substituting the strain values in under the rated load of the first axis, the second column under rated load of the second axis and so on. Note, these axes should be loaded independently.

17

As an example, if ε_1 and ε_2 undergo high tensile strain and ε_3 and ε_4 high compressive strain during load F_X, then since F_X is the first axis we are considering the first row in $[C]$ namely C_{1i}. A full Wheatstone bridge can be configured to produce $\frac{V_{out}}{V_{in}} = \frac{K_s}{4}(\varepsilon_1 + \varepsilon_2 - \varepsilon_3 - \varepsilon_4)$ resulting in a very high strain signal for the specific axis, therefore $C_{1i} = \frac{1}{4}(\varepsilon_1 + \varepsilon_2 - \varepsilon_3 - \varepsilon_4)$. Care must be taken to ensure low values for C_{1i} are generated for loads in the other axes.

When the calibration matrix $[B]$ is solved for from $[C]$ the coupling or cross-sensitivity effects can be determined. Consider an n axis force transducer and Equation (3.21) with n Wheatstone bridge sensors: We see that a purely diagonal matrix $[B]$ will result in Wheatstone bridge sensor readings each allocated to a specific force or moment component:

$$F_i = B_{ii}S_i \ for \ i \in [1; n] \tag{3.22}$$

A system such as this is completely uncoupled and $\bar{F}$ can be solved for efficiently. If $[B]$ was not purely diagonal under the same conditions but Equation (3.22) was to be utilized for efficient computations, then coupling effects would be encountered since the exact solution is not calculated. The components of the cross-sensitivity coefficient matrix $[CSC]$ are then (LIU, Sheng A and Tzo, Hung L, 2002):

$$CSC_{ij} = \frac{C_{ji}}{Q_i} \tag{3.23}$$

$$Q_i = \sum_{j=1}^{n} |C_{ji}| \tag{3.24}$$

When Equation (3.22) is not utilized and more Wheatstone bridge sensors are present than axes, then Gauss elimination and/or least squares must be utilized to solve for $\bar{F}$. This is very challenging, if not impossible, to complete in real time telemetry. However, if this approach is used then theoretically there will be no coupling effects in the output readings.

If Equation (3.22) is not utilized as a result of the calibration matrix $[B]$ not being well estimated by a purely diagonal matrix then we say the system is coupled. Again, the system may be coupled but coupling effects will not be present if the exact solution is calculated from Equation (3.21).

The above theory on strain compliance is applicable to the wheel force transducer as will be incorporated in this project. This will become clear when the concept of the selected wheel force transducer is discussed.

3.5.3. LINEARITY

During the FE or mathematical modeling it is assumed the wheel force transducer operates in the linear elastic region (linear material). When this is done it must be insured that yielding does not occur, thus Hooke's law of linear elasticity can be assumed (RADOVITZKY, Raul, 2012):

$$\sigma_{ij} = E_{ijkl}\varepsilon_{kl} \tag{3.25}$$

This expression linearly relates the second order stress σ_{ij} and strain ε_{kl} tensors through the forth order tensor of Elastic moduli E_{ijkl}. In addition small deformations can be assumed resulting in an inherently linear system. These assumptions greatly simply modeling as any non-linear analysis is generally very involved.

A linear system such as this combined with the linearity assumed in strain gauge operation will result in linear correlations between the loads, strains and output readings.

3.5.4. STRENGTH VERSUS SENSITIVITY

A force transducer is required to withstand all loads experienced during vehicle operation while creating a sufficient strain field for appreciable strain gauge readings. These two design criteria are each more individually satisfied while forcing the design in opposite manners. Consider again Hooke's law of linear elasticity in Equation (3.25) that will be assumed. In order to reach higher safety factors in the design the stresses must be lowered, however this lowers the strains linearly. In order to obtain high strain gauge readings the strains should be increased, however this raises the stresses linearly. An optimum balance between stress and strain (safety and transducer sensitivity) is required.

3.5.5. STIFFNESS AND NATURAL FREQUENCIES

Another tradeoff in force transducers is encountered: High stiffness versus high sensitivity. High sensitivity in force transducers is highly desirable but requires high strains/deformation in the

transducer structure. High deformations are associated with low stiffness and as a result low natural frequencies in the first modes. The natural frequencies of the force transducer must be determined to ensure operating frequencies do not cause resonance (CHAO, Lu-Ping and Chen, Kuen-Tzong, 1997).

3.6. STATICALLY INDETERMINATE FOUR-CANTILEVER-SPOKE AND HUB FORCE TRANSDUCERS

At this point the underlying concept behind statically indeterminate four-cantilever-spoke and hub force transducers must be addressed. This is the concept that was used in the detailed design of the wheel force transducer as it proved to be the most viable during the concept selection phase in the MOX 410 Design Project. The theory addressed in Section 3.5.2 is highly applicable to this section.

The transducer consists of a central hub and four protruding cantilever spokes on the same plane. Consider the following figure:
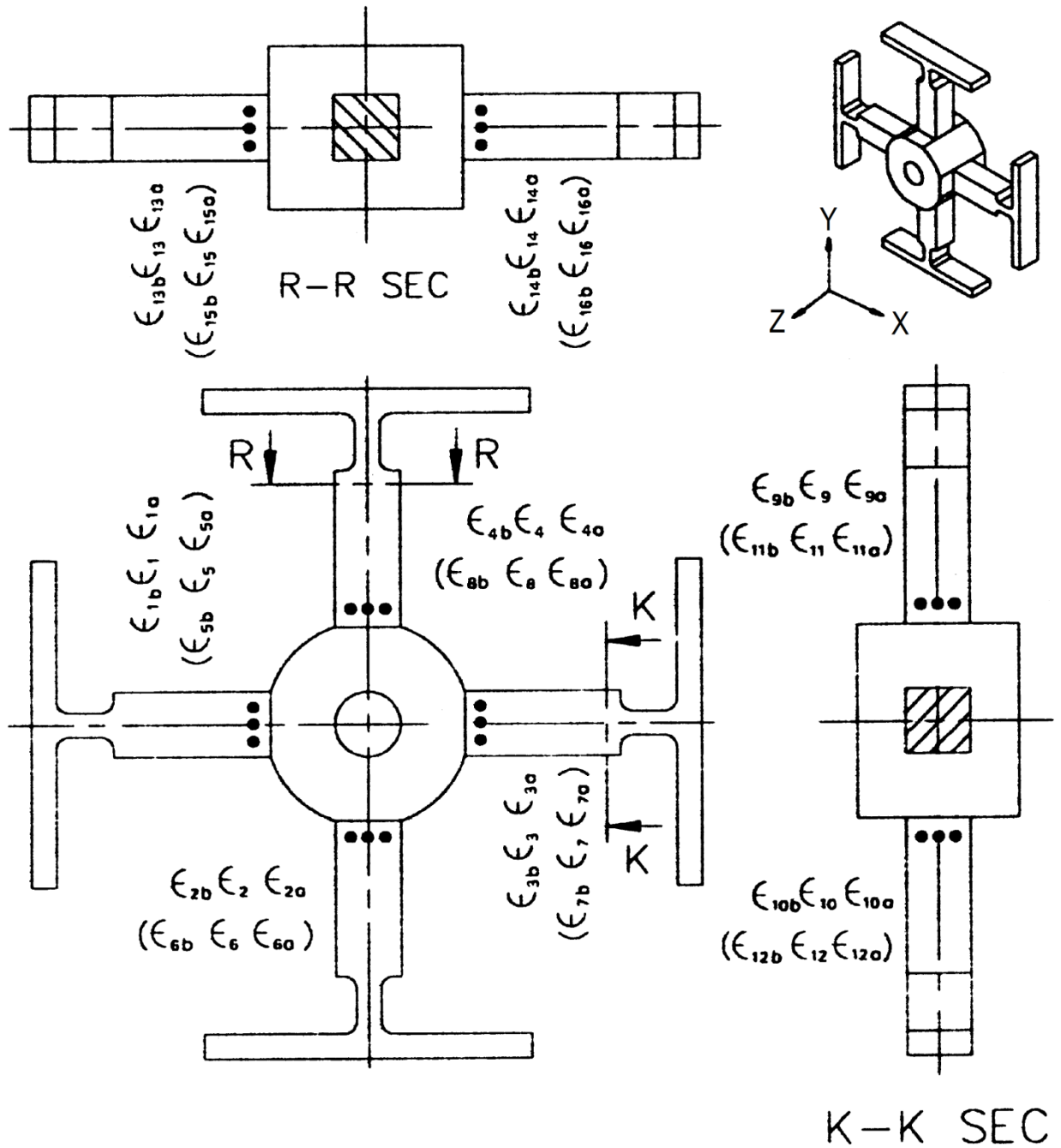
Figure 5: Junyich's six-axes force transducer with strain gauge locations (CHAO, Lu-Ping and Chen, Kuen-Tzong, 1997)

Figure 5 displays specifically the design of a Junyich's six-axis force transducer, however, the principle involved can be applied to all Maltese shaped force transducers as used in this project. These four-spoke transducers are applied to many applications in force sensing due to the simplicity of the structure: it consists of only one piece. These transducers are found in large part

in robotics sensors in places such as the wrist or angle. In the application of wheel force transducers the central hub is adapted to fit onto the vehicles wheel hub while the four spokes protrude to the rim. The force from the tyre contact patch must therefore pass through the four spokes and hub in order to be transmitted to the rest of the vehicle.

In Figure 5 we see the positions of 16, 32 or 48 strain gauges placed in areas of high strain (the dots indicate strain gauges and parenthesis the reverse side). Each strain gauge is orientated axially along each spoke. Now consider the following strain compliance for the use of 16 strain gauges obtained by using gauges on opposite sides of each beam as a Wheatstone bridge half (CHAO, Lu-Ping and Chen, Kuen-Tzong, 1997):

$$C_{1i} = \frac{(\varepsilon_1 - \varepsilon_5)}{2}; \; C_{2i} = \frac{(\varepsilon_2 - \varepsilon_6)}{2}; \; C_{3i} = \frac{(\varepsilon_3 - \varepsilon_7)}{2};$$

$$C_{4i} = \frac{(\varepsilon_4 - \varepsilon_8)}{2}; C_{5i} = \frac{(\varepsilon_9 - \varepsilon_{11})}{2}; C_{6i} = \frac{(\varepsilon_{10} - \varepsilon_{12})}{2}; \quad\quad (3.26)$$

$$C_{7i} = \frac{(\varepsilon_{13} - \varepsilon_{15})}{2}; \; C_{8i} = \frac{(\varepsilon_{14} - \varepsilon_{16})}{2}$$

In this strain compliance eight Wheatstone bridges are utilized. We notice immediately that this system is coupled: Firstly the strain compliance matrix is not square (it is a $[8 \times 6]$ sized matrix) and secondly independent loading of axes results in substantial strain signals in various Wheatstone bridges. Take for example is positive 3rd axis load F_Z: Under this load ε_1 to ε_4 all increase positively under tension and ε_5 to ε_8 all increase negatively under compression. This creates high signals in C_{1i}, C_{2i}, C_{3i} and C_{4i} from Equation (3.26). There are many coupling pairs in this strain compliance configuration. The following strain compliance was obtained in FE modeling by Lu-Ping Chao and Kuen-Tzong Chen (1997) using Equation (3.26) in the Junyich's six-axes force transducer:

$$C_{ij}(10^6)$$

$$= \begin{bmatrix}
33.7 & -2 \times 10^{-6} & 869 & 4 \times 10^{-6} & 1110 & -7 \times 10^{-6} \\
2 \times 10^{-6} & 33.1 & 866 & 1110 & -4 \times 10^{-6} & 7 \times 10^{-6} \\
-33.7 & 2 \times 10^{-6} & 869 & 4 \times 10^{-6} & 1110 & 7 \times 10^{-6} \\
2 \times 10^{-6} & -33.1 & 866 & 1110 & -4 \times 10^{-6} & -7 \times 10^{-6} \\
270 & -26.1 & 47 & 72 & -7.7 & -779 \\
270 & 26.1 & 47 & -72 & -7.7 & 779 \\
-27 & 277 & 47 & 7.9 & 72 & -782 \\
27 & 277 & 47 & 7.9 & -72 & 782
\end{bmatrix} \quad (3.27)$$

The compliance matrix was obtained under the rated loads $F_X = F_Y = 392N, F_Z = 784N, M_X = M_Y = 20Nm, M_Z = 29Nm$. The compliance matrix displays the high degree of coupling in the strain signals. Finding the calibration matrix from the inverse of $[C]$ and then the solution from a given strain field will require substantial computational time.

Now consider again the Junyich's six-axis force transducer and 16 strain gauges from Figure 5. This time however, we consider the following alternate strain compliance:

$$C_{1i} = \frac{(\varepsilon_9 + \varepsilon_{10})}{2}; \quad C_{2i} = \frac{(\varepsilon_{13} + \varepsilon_{14})}{2};$$

$$C_{3i} = \frac{(\varepsilon_2 + \varepsilon_3 - \varepsilon_5 - \varepsilon_8)}{4}; \quad C_{4i} = \frac{(\varepsilon_4 + \varepsilon_6)}{2}; \quad (3.28)$$

$$C_{5i} = \frac{(\varepsilon_1 + \varepsilon_7)}{2}; \quad C_{6i} = \frac{(\varepsilon_{11} - \varepsilon_{12} + \varepsilon_{15} - \varepsilon_{16})}{4}$$

Using the same rated loads the following compliance matrix was obtained by Lu-Ping Chao and Kuen-Tzong Chen (1997):

$$C_{ij}(10^6) = \begin{bmatrix}
270 & 0 & 47 & 0 & -7.7 & 0 \\
0 & 277 & 47 & 7.9 & 0 & 0 \\
-16.8 & 16.8 & 867 & 2 \times 10^{-6} & -2 \times 10^{-6} & 6 \times 10^{-6} \\
2 \times 10^{-6} & 0 & 0 & 1110 & 0 & 0 \\
0 & 0 & 0 & 0 & 1110 & 0 \\
-13.5 & -13.1 & 0 & -36 & 36 & 781
\end{bmatrix} \quad (3.29)$$

By only changing the Wheatstone bridge configurations while using the same strain gauges as before, the compliance matrix has been greatly decoupled. In addition the compliance matrix is square thus the computation times will be greatly improved when solving for the solution from a given strain field. It is possible to reduce the degree of coupling further by implementing more

strain gauges (such as 32 or 48) and selecting an appropriate strain compliance matrix. The principles involved are identical thus, will not be illustrated.

Equations (3.26) to (3.29) illustrate the significance of strain compliance and how it must be planned carefully. Consider again the design of the Junyich's six-axis force transducer: Notice at the ends of each spoke (near the rim) how they are thinned out, in addition how thin the rim is in comparison to the rest of the structure. This reduction in cross sectional area gives rise to a low torsional and axial stiffness in each spoke, thus a more compliant/free boundary condition at the rim. Such boundary conditions are hugely advantageous if implemented correctly with the appropriate stain compliance. As an example consider the strain compliance presented in Equation (3.28): If a load F_X was applied to the structure then the vertical spokes in Figure 5 would virtually carry the entire load under bending creating high tensile loads in ε_9 and ε_{10}, thus a high strain signal in C_{1i} for load F_X as planned. The horizontal spokes would not carry load axially due to their compliance at the rim boundary. Lower strain signals would therefore be recorded in the other bridges. In short, compliant boundary conditions concentrate the loading in certain axes to specific members in the structure thus improving sensitivity and reducing coupling. Several methods exist to create these highly advantageous compliant boundaries. The implementation of flexural boundaries has already been introduced. It is for instance also possible to utilize bearings (rubber or ball bearings) at the boundaries to obtain more ideal boundary conditions. In this project flexural boundaries as illustrated in Figure 5 will be utilized as was decided during the concept selection phase in the MOX 410 Design Project.

3.7. CALIBRATION AND EXPERIMENTAL VERIFICATION

During the modeling phase of a transducer a strain compliance matrix would have been determined. This compliance would theoretically describe the characterization of the transducer under the rated loads. To insure a transducer with its implemented strain gauges operate as expected, experimental data is required for validation against these theoretical results.

3.7.1. CALIBRATION OF TRANSDUCERS

A force transducer must be calibrated by applying known static loads. Every axis of the force transducer should receive independent loading under or at the rated (designed) load (CHAO, Lu-

Ping and Yin, Ching-Yan, 1999). During the modeling of the force transducer the strain signal from each Wheatstone bridge ($S_1; S_2; S_3 \ldots S_{n-1}; S_n$) would have been predicted under the rated loads. These strain signals can similarly be obtained experimentally. In other words the assemblage of the compliance matrix is completed experimentally as done theoretically in Section 3.5.2. If the rated loads are too high for practical calibration loads then smaller loads can be used since a linear system is assumed. The load-reduction factor should just be noted and applied accordingly.

The experimental strain compliance matrix can then be constructed as it was during the theoretical modeling phase. The experimental strain compliance matrix is obviously more applicable to the calibrated force transducer than the theoretical strain compliance, thus should rather be implemented during operation. However, the theoretical and experimental strain compliance matrixes should correspond strongly. If great deviations exist then it is known that the transducer as used during experimentation may be defective as a result of faulty strain gauges, Wheatstone bridges or telemetry. The transducer can then undergo the appropriate post-experimental investigation and alterations.

3.7.2. *ZEROING STRAIN GAUGE READINGS*

Theoretically zero strain signals will be produced when no loads exist on a force transducer. During experimentation however, non-zero strain signal may be produced at zero loading as a result of pre-stressed strain gauges or non-ideal unstrained gauge resistances R_o. The appropriate zeroing of strain gauge readings could be completed as suggested in Section 3.4.3. A simpler alternate solution exists as a result of the processing capabilities of some telemetry systems (as will be implemented in this project). The strain signals generated at zero loading can be noted prior to any experimental procedures. The strain signals can then be appropriately offset during operation to produce the correct results.

3.7.3. *VALIDATION OF COUPLING EFFECTS*

Validation of the coupling effects will depend on the approach used as explained in Section 3.5.2: If Equation (3.22) is utilized then the coupling/cross sensitivity effects would have been theoretically calculated by Equation (3.23) at the rated loads. Experimental coupling effects are

required for comparison. They can similarly be obtained as in Section 3.5.2 by applying the known rated loads to the individual axes and noting the Wheatstone bridge strain signals $(S_1; S_2; S_3 \ldots S_{n-1}; S_n)$: The elements of the strain compliance matrix can then be determined and the cross-sensitivity coefficient matrix $[CSC]$ compiled experimentally.

3.8.   TESTING OF TRANSDUCERS

3.8.1.   GENERAL FORCE MEASUREMENT

No fixed standards exist to which wheel force transducers must be tested. Generally, after the calibration procedure has been completed, tyre testers are used to apply and monitor dynamic loads on a wheel force transducer. The input forces and moments as compiled by the wheel force transducer are then compared to that measured by the tyre tester. These results may verify that the wheel force transducer is operational. The accuracy of the wheel force transducer can also be determined depending on the accuracy of the tyre tester.

Additionally the wheel force transducer may be installed onto a vehicle and specific maneuvers completed to excite certain load axes. The loads as measured by the wheel force transducer should correspond to the expected loading for the maneuver. For instance acceleration and braking tests should produce high loads in F_X' (tractive force) and M_Z' (driving/braking torque).

It is important to note that in both cases the wheel force transducer is tested dynamically unlike during calibration. This will entail the rotation of the transducer and the requirement of the angular transformation from Equation (3.1).

3.8.2.   DETERMINATION HYSTERESIS EFFECTS

Hysteresis effect may come into effect after the transducer has undergone server loading during operation or experimentation. It may therefore be necessary to zero and recalibrate the transducer after such loading conditions to reevaluate the strain compliance. To determine the degree to which the transducer underwent hysteresis the strain signals at zero loading can be examined after the transducer has been heavily loaded. Prior to the loading the strain signals would have been zeroed, therefore any nonzero strain signal produced after loading would be as a result of hysteresis effects in the transducer.

4. WHEEL FORCE TRANSDUCER DESIGN

The final design of the wheel force transducer is known from the MOX 410 Design Project. To provide the necessary context the final design will briefly be illustrated and explained throughout this section. For full details regarding the wheel force transducer the MOX 410 report entitled *DETAIL DESIGN OF A SIX-AXIS WHEEL FORCE TRANSDUCER* (NOUWENS, Oscar, 2013) should be referred to.

It was previously explained that the final design would incorporate a statically indeterminate four-cantilever-spoke and hub force transducer. The transducer alone defines the performance and characteristics of the entire wheel force transducer. All other components involved in the assembly merely allow the transducer to be fitted to the rim in the appropriate manner while complying with all design specifications. For this reason, it was only the transducer that was required to undergo comprehensive modeling and optimization while in consideration of the strain gauge positions and strain compliance/bridge configurations.

The modeling required for the transducer will be explained in the *Theoretical Investigation* section of this report. This section only deals with the transducer as optimized and all other designed components in the final assembly.

4.1. WHEEL FORCE TRANSDUCER DESIGN APPROACH

Several important design approaches were adopted by the student that greatly affected the resultant wheel force transducer design. These will be briefly underlined such that the motivation behind the design can be understood:

- It was decided to utilize the existing wheel rims of the Baja instead of designing new custom rims specifically for the transducer. Custom rims may have resulted in a more space efficient solution since the design would be completed in mind of the transducer, however, custom rims can be both complex and expensive to implement. It was therefore decided to utilize the existing rims since they provided a much simpler and cost effective solution.

- By simple analysis it was determined that the existing space inside the Baja rims would not be sufficient for an effective four-cantilever-spoke and hub force transducer. It was

therefore necessary to locate the transducer outside the rim where space was more abundant. A spacing ring would be necessary to translate the transducer outward axially.

- New wheel hubs would be designed to meet the geometric specifications of the existing Baja hubs while creating the correct offset in the wheel in consideration of the entire wheel force transducer assembly. The alternate solution would be to implement hub adapters; however, this would complicate the final assembly.

- An existing telemetry system would be mounted to the outer side of the wheel force transducer were sufficient space would be available. Details regarding the telemetry system are provided in Section 4.2.

- A CBL (Center Bore Location) ring would be utilized to position/center the transducer relative to the wheel hubs during assembly.

- Dust covers would be designed to ensure all electronics are protected.

- All fastening and securing would be accomplished with non-permanent bolted joints.

The implications of these design approaches will become clearer upon presentation of the final assembly design in Section 4.3.

4.2.   TELEMETRY SYSTEM

A telemetry system has been prescribed for the research project. The telemetry system is responsible for recording data from the strain sensors while monitoring the angular position of the wheel. The telemetry system in question is the Kraus Messtechnik GmbH (KMT) CT 4/8-Wheel.

This specific telemetry system, as will be incorporated, is capable of recording all required data but does not allow for real time telemetry, rather a post-processing approach had been adopted in the telemetry system. The telemetry system is capable of recoding 8 different channels simultaneously. However, 2 of the 8 channels are required to monitor the angular position of the wheel to produce θ in Equation (3.1). Thus 6 channels remain for the Wheatstone bridges, but this is ideal for the final selected strain compliance as will be made clear in Section 5.2.4. The telemetry system receives an analogue voltage signal, amplifies it and then converts it to a digital signal to be transmitted via wireless interface to the receiver. The wireless transmission both reduces dimensional occupancy and noise by avoiding the use of slip rings.

The telemetry system is shown in the follow figure:

Figure 6: KMT CT4/8-Wheel Telemetry System (KMT Telemetry)

This telemetry system will be mounted to the wheel force transducer at the *TELEMETRY BASE MOUNT* in Figure 6 by utilizing the four holes on the PCD of $175mm$. The angular position transducer is not shown in the Figure 6 however it simply fastens over the top of the telemetry system. This will become clear in Section 6 where the entire wheel force transducer assembly is displayed as used during the experimental investigation. Finally it should be noted that the telemetry system utilizes an independent onboard power supply, thus power connectors are not required during operation.

4.3. WHEEL FORCE TRANSDUCER ASSEMBLY

In this section the ***basic*** assembly drawings of the wheel force transducer are provided. Once again further details regarding the wheel force transducer can be found in the MOX 410 Design Project report entitled *DETAIL DESIGN OF A SIX-AXIS WHEEL FORCE TRANSDUCER.*

The following exploded assembly drawings are displayed such that all the components can be seen. In the first exploded assembly drawing the telemetry system is excluded for clarity;

however the telemetry mounting interface is illustrated on the subsequent exploded assembly drawing. A *simplified* parts list is included at the end:
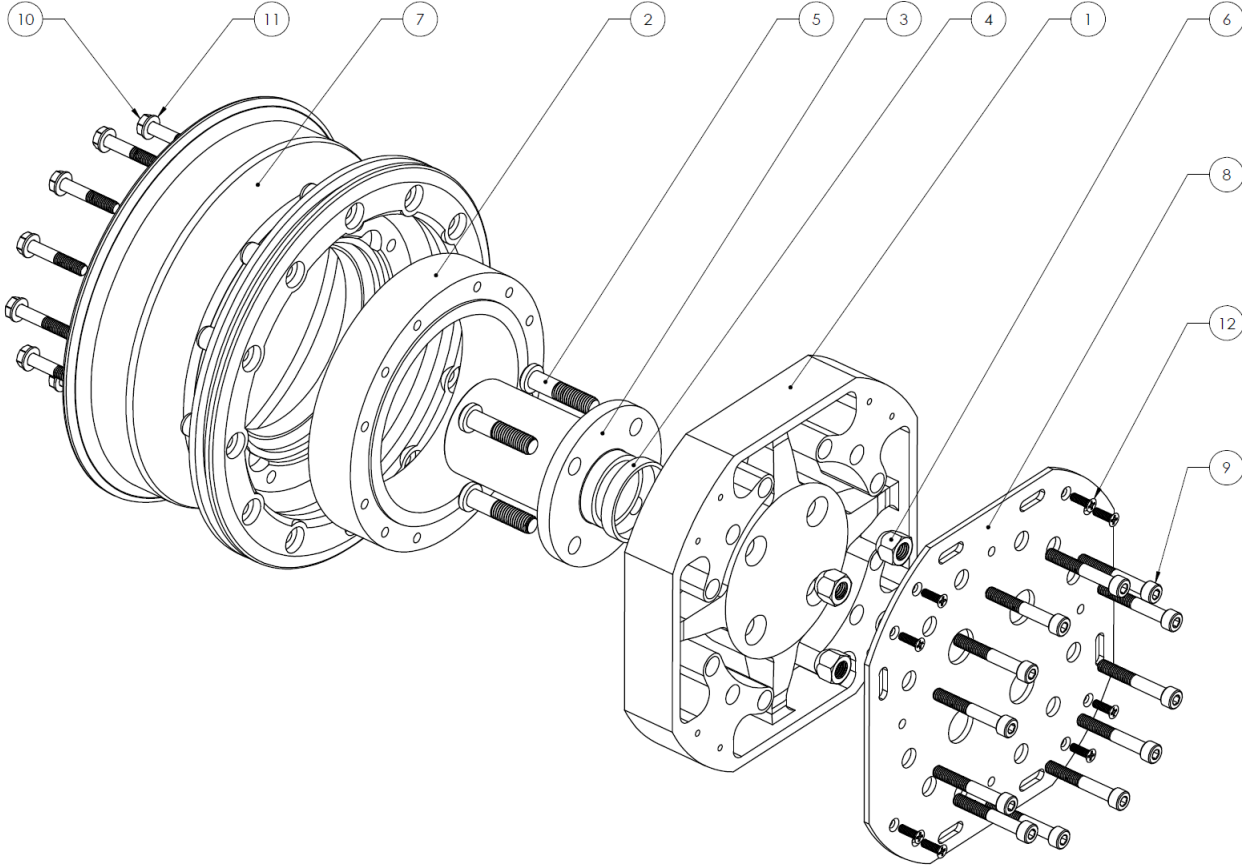
Figure 7: Exploded assembly drawing of the final design
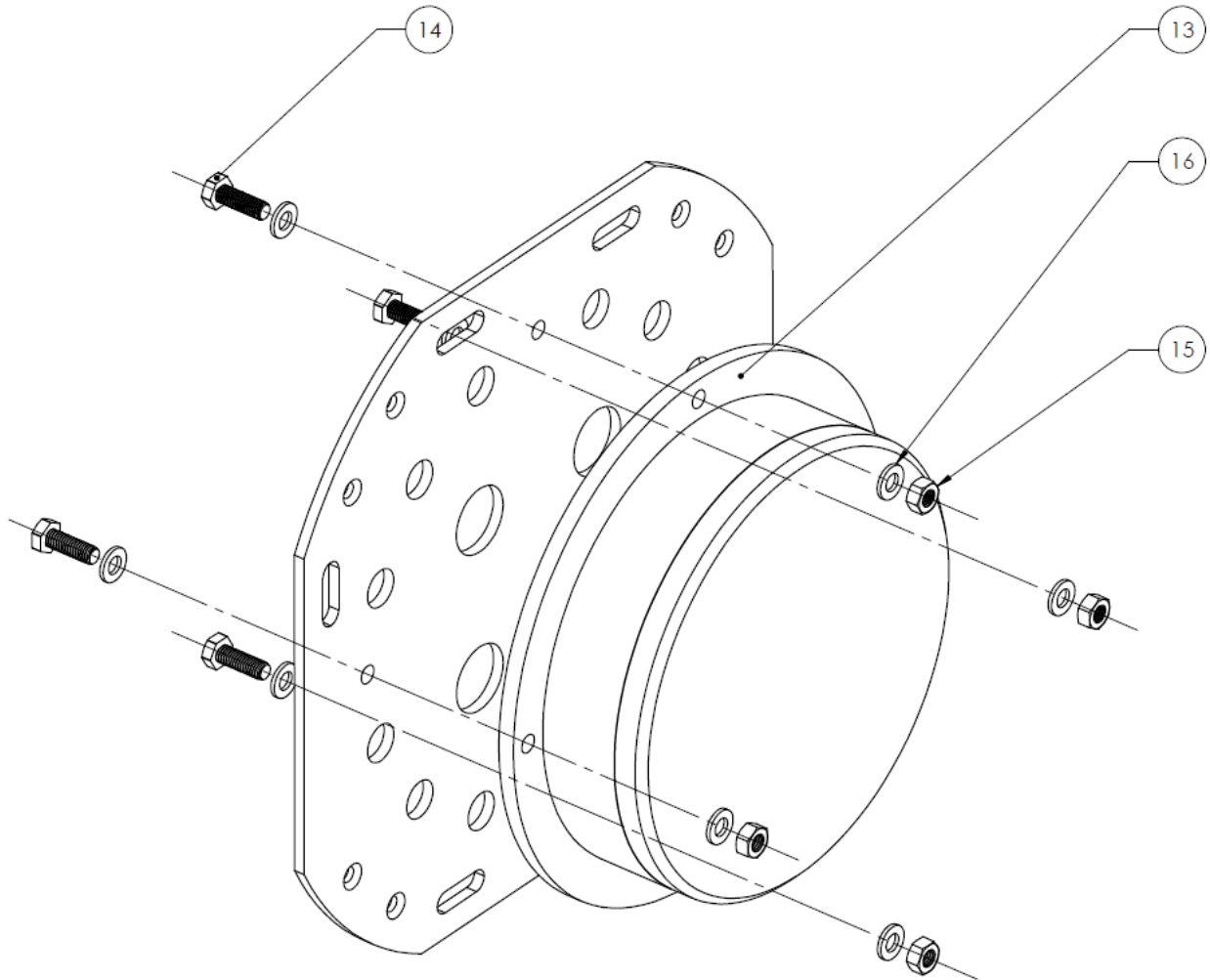
Figure 8: Exploded assembly drawing of the telemetry mounting interface

Table 1: Simplified assembly parts list

Part	Description	Quantity
1	Transducer	1
2	Securing/spacing ring	1
3	Wheel hub (front or back)	1
4	CBL ring	1
5	M12 Stud	4
6	M12 Lug nut	4
7	Baja rim	1
8	Outer dust cover	1

9	M8 Allen cap screw	12
10	M8 Bolt	12
11	M8 Washer	12
12	M5 countersunk flat head screw	8
13	Telemetry base	1
14	M6 Bolt	4
15	M6 Nut	4
16	M6 Washer	8

The following assembly drawing provides further clarity (The telemetry system is not included in this drawing):
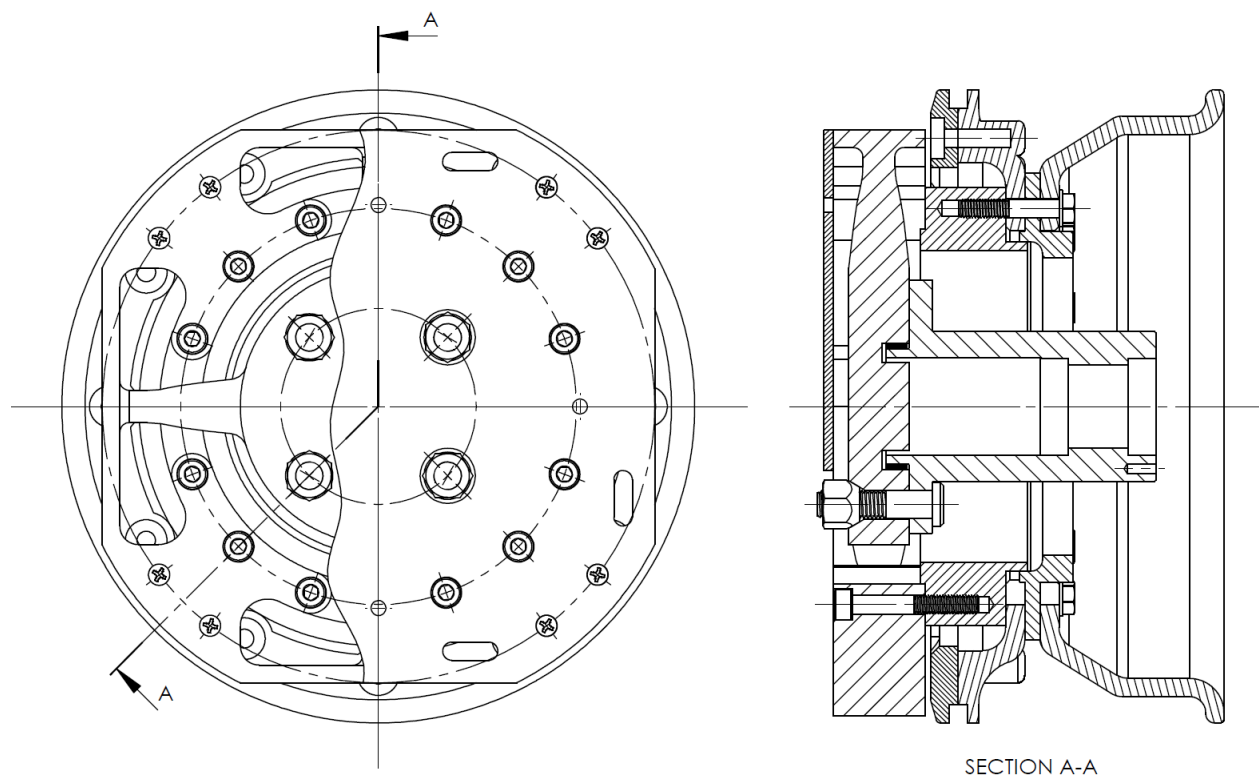
SECTION A-A

Figure 9: Sectioned assembly drawing of the final design

As mentioned previously the component of major interest is the transducer (Part ① in Figure 7). The transducer was fully optimized during the detailed design phase in MOX 410. In order to optimize and characterize the transducer complete modeling was required. This will be the scope of the theoretical investigation addressed in Section 5. Finally the following rendered isometric image of the wheel force transducer creates a much better perspective of the entire assembly (The telemetry is again excluded in this view):
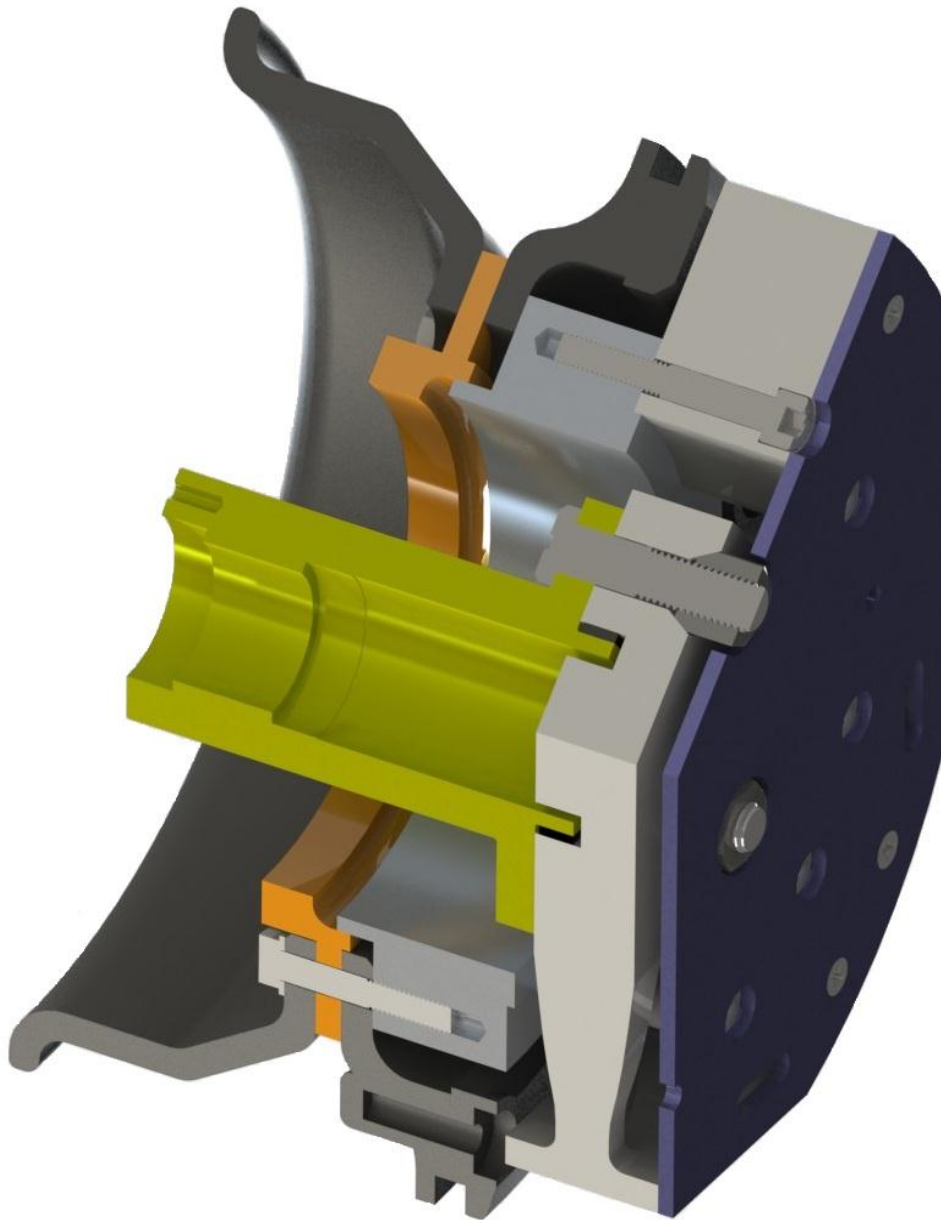
Figure 10: Rendered isometric image of the wheel force transducer (Sectioned view)

5.   THEORETICAL INVESTIGATION

The theoretical investigation of this project encompasses the modeling of the transducer as it alone determines the performance and characteristics of the entire wheel force transducer. The final design of the transducer is shown in the following figure:
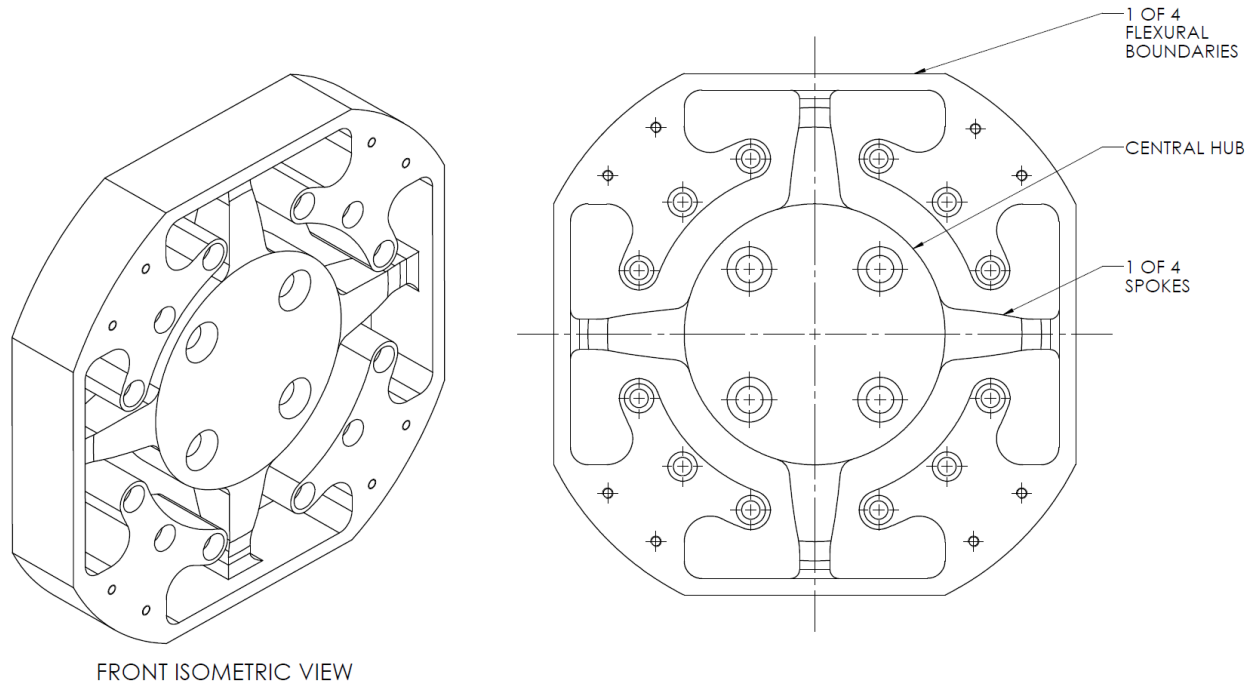
Figure 11: Final design of the transducer

In Figure 11 we see the transducer as an extension of the indeterminate four-cantilever-spoke and hub force transducer with flexural boundaries as introduced in Section 3.6. Using the convention as presented in Section 3.1 that transducer was designed to operate at the following maximum loads (PENNY, W.C.W, 2012):

$$F'_{Xmax} = F'_{Ymax} = F'_{Zmax} = 5200N$$

$$M'_{Xmax} = M'_{Ymax} = M'_{Zmax} = 1400N$$

At this point many other details regarding the design of the transducer will not be clear to the reader. The final geometry of the transducer can only be motivated through the detailed design procedure which included mathematical modeling and optimization with finite element verification.

The theoretical investigation of this research report will encompass the modeling and optimization of the transducer as was completed during the detailed design phase.

5.1. OBJECTIVES AND MODELING PROCEDURE

The final design of the transducer is an extension of the concept reviewed in Section 3.6 which utilizes the strain compliance theory as addressed in Section 3.5.2. Thus, the objectives of the theoretical investigation are as follows:

- Development of a mathematical model to establish a strain compliance matrix for any generic statically indeterminate four-cantilever-spoke and hub force transducer.
- Optimization of the transducer geometry to obtain maximum sensitivity while complying with all design specifications.
- Verification of the mathematical model with a suitable FE model.
- Assemblage of the final strain compliance matrix according to the mathematical and FE model.
- Determination of the first modal frequencies according to the FE model.

Details/aspects of the transducer regarding assembly in the wheel force transducer shall be avoided to maintain coherency. From a theoretical standpoint the above objectives signify all obtainable theoretical results in terms of the transducer's functionality. In other words, once the strain compliance matrix and natural frequencies are known then transducer is fully described and the experimental investigation can be pursued.

5.2. TRANSDUCER DETAILED MODELING AND OPTIMIZATION

During this section the modeling of a generic statically indeterminate four-cantilever-spoke and hub force transducer will be explained in detail. Thereafter the utilization of this model during the optimization process, as completed during MOX 410, will be discussed. The design parameters that constrain the model during optimization will also be discussed. Finally the FE verification of the model will be addressed as was completed after the optimization process. The theoretical objectives developed in Section 5.1 can therefore be achieved.

5.2.1. TRANSDUCER MODELING

The need for geometric optimization was motivated in Section 3.5.4 where it was explained that a balance between a transducer's strength/safety and sensitivity is required. Optimization can more effectively be accomplished in a mathematical model specifically designed for the transducer.

In order to optimize the design of the transducer the student compiled a mathematical model relating the geometry of the transducer and flexural boundaries to the displacements, stresses and strains under specific loads. The development of the mathematical model will be fully explained during the remaining of Section 5.2.1. The model is developed from a generic standpoint (where the transducer's final geometry is still unknown and has not undergone optimization).

5.2.1.1. BOUNDARY REACTION FORMULATION

The first step in the transducer modeling is to formulate the forces and moments that exist in the transducer given the transducer's geometry. Consider first a simplified schematic of the transducer:
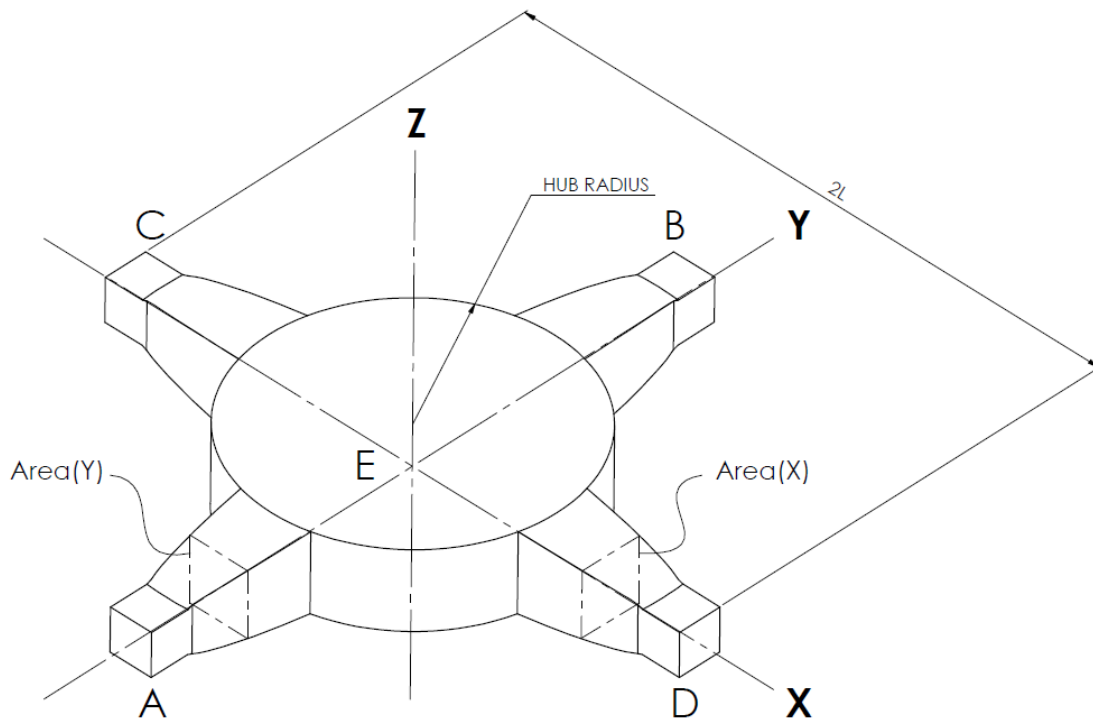
Figure 12: Simplified diagram of the transducer without flexural boundaries

Figure 12 illustrates a representation of the transducer without the flexural boundaries. At every boundary, marked from A to D, we have a reaction in every axis (three force and three moment reactions). We mark the reaction at a boundary with the following notation:

$$\bar{R} = [R_X, R_Y, R_Z, R_X^M, R_Y^M, R_Z^M] \qquad (5.1)$$

The M superscripts mark <u>M</u>oment reactions. For instance we have the reaction $\bar{R}_A$ at boundary A:

$$\bar{R}_A = \left[R_{X_A}, R_{Y_A}, R_{Z_A}, R_{X_A}^M, R_{Y_A}^M, R_{Z_A}^M\right]$$

In addition, at every boundary we have a stiffness in every axis (three translational and three rotational). We mark the stiffness at a boundary with the following notation:

$$[k] = \left[k_X, k_Y, k_Z, k_X^\theta, k_Y^\theta, k_Z^\theta\right] \qquad (5.2)$$

The θ superscripts mark <u>R</u>otational stiffness. The boundaries A to D are identical thus each will have the same boundary stiffness $[k]$ in a local coordinate system. At center point E we see the external loading. The loading at point E is given by the following notation:

$$\bar{F} = [F_X, F_Y, F_Z, M_X, M_Y, M_Z] \qquad (5.3)$$

This notation is in accordance with that presented in Section 3.1. Modeling the external loading as a point force is an approximation made to simplify the model. We notice immediately the system is statically indeterminate (as expected), thus a displacement formulation will have to be incorporated to determine reactions through rigidity.

A modeling strategy must be established at this point. To reduce the complexity of the analysis we will model $Beam\ AB$ and $Beam\ CD$ as separate beams that are coupled through translational and angular displacements at the center point E. In addition the beams will be coupled through balancing of the external loading. The coupling of the beams will become clearer as the model is explained further. We have the following free body diagrams of $Beam\ AB$ and $Beam\ CD$ as separate beams:
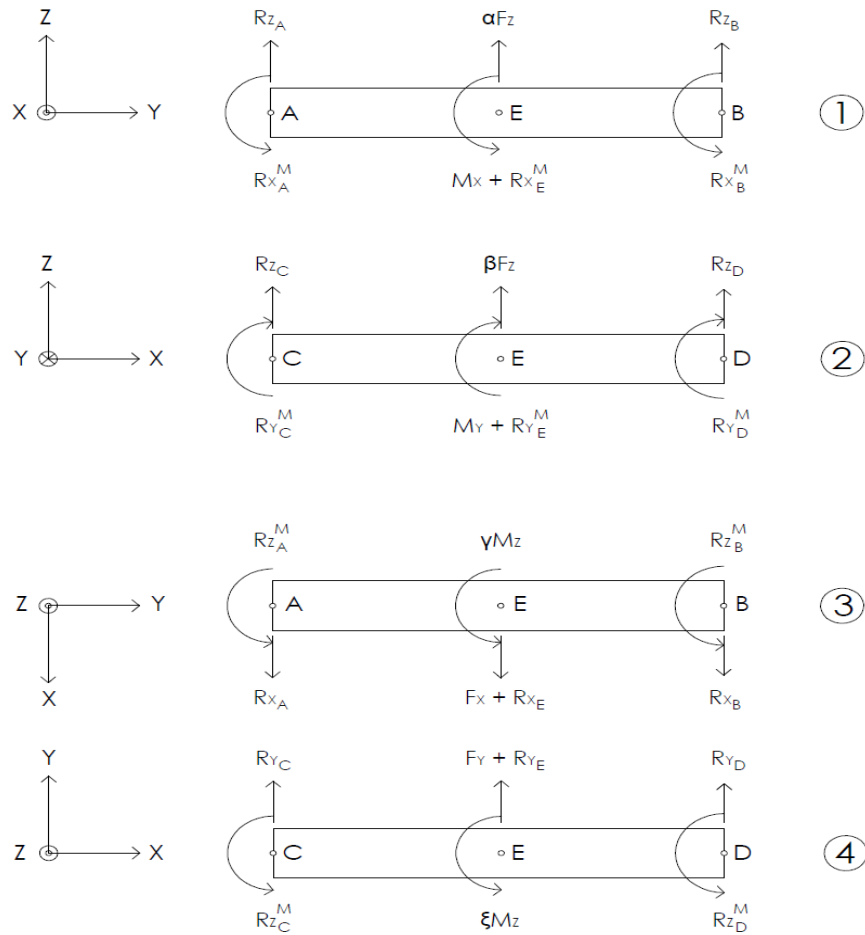
Figure 13: Free body diagrams of Beam AB and Beam CD

From Figure 13 the coupling between the beams can be made clearer: The forces R_{X_E} and R_{Y_E} and moments $R_{X_E}^M$ and $R_{Y_E}^M$ represent the coupling reactions between the beams under a displacement field. Forces R_{X_E} and R_{Y_E} will exist when point E is displaced/translated in the X and Y axes respectively. For instance, when point E has a positive X displacement in $Beam\ AB$ (see case ③ in Figure 13) then $Beam\ CD$ will act against this displacement with an opposing force directly proportional to the product of the displacement and an associated stiffness k_{X_E}. Similarly moments $R_{X_E}^M$ and $R_{Y_E}^M$ will exist when point E is displaced angularly about the X and Y axes respectively. Further coupling between $Beam\ AB$ and $Beam\ CD$ must exist in the common Z axis: For this coupling the applied external loads F_Z and M_Z are distributed between the two beams such that:

$$\alpha + \beta = 1$$
$$\gamma + \xi = 1 \tag{5.4}$$

Since $Beam\ AB$ and $Beam\ CD$ are identical we expect $\alpha = \beta = \gamma = \xi = 0.5$. This will have to be verified in the model to insure the results are valid.

Axial reaction forces have been excluded from Figure 13 for clarity. We have the following relations relating the axial reaction forces at the boundaries to the coupling forces R_{X_E} and R_{Y_E} and moments $R_{X\ E}^M$ and $R_{Y\ E}^M$:

$$R_{X_C} + R_{X_D} = -R_{X_E}$$
$$R_{Y_A} + R_{Y_B} = -R_{Y_E}$$
$$R_{X\ C}^M + R_{X\ D}^M = -R_{X\ E}^M \tag{5.5}$$
$$R_{Y\ A}^M + R_{Y\ B}^M = -R_{Y\ E}^M$$

The relations above simply explain that the axial forces and moments generated at the boundaries are transferred to the center point E.

We now attempt to use Euler beam bending theory to characterize the deformation of $Beam\ AB$ and $Beam\ CD$. Under the Euler-Bernoulli assumptions we assume the cross sections of the beams do not deform under the application of axial or transverse loading and that they remain planar and normal to the deformed axis. The governing equation is given as follows (RADOVITZKY, Raul, 2012):

$$M_X(y) = H_{XX}^c(y)\bar{u}_Z''(y)$$
$$H_{XX}^c(y) = \int_{A(y)} Ez^2 . dA \tag{5.6}$$

This expression relates the transverse displacement in Z ($\bar{u}_Z(y)$) to the bending moment about X ($M_X(y)$) through the centroidal bending stiffness about X ($H_{XX}^c(y)$). Similar relations exist for other orthogonal axes and Equation (5.6) provides only the governing relation for case ① in Figure 13.

Considering Figure 12 the transducer is designed to be symmetric about the XY, XZ and YZ planes thus eliminating the need to obtain the modulus weighted centroid: The origin for the centroidal bending stiffness expression in Equation (5.6) can be placed in the middle of each

cross section. In addition the modulus of elasticity is constant and each cross section will be rectangular through the X and Y axis. This greatly reduces the expression for the centroidal bending stiffness to a more familiar expression:

$$H_{XX}^c(y) = \frac{Eb(y)(h(y))^3}{12} \tag{5.7}$$

Here $b(y)$ is the width in X and $h(y)$ the height in Z. Once again the Equation (5.7) marks only the case for one set of orthogonal axes (case ① in Figure 13) and the relation can be extended to the other axes. Due to the varying cross sectional areas $A(x)$ and $A(y)$ an analytical solution to Equation (5.6) promises to be extremely challenging even with the simplification in Equation (5.7). For this reason it was decided to discretize $Beam\ AB$ and $Beam\ CD$ into a series of Euler beams. Each Euler beam will have a finite length and constant centroidal bending stiffness. We consider again case ① in Figure 13:
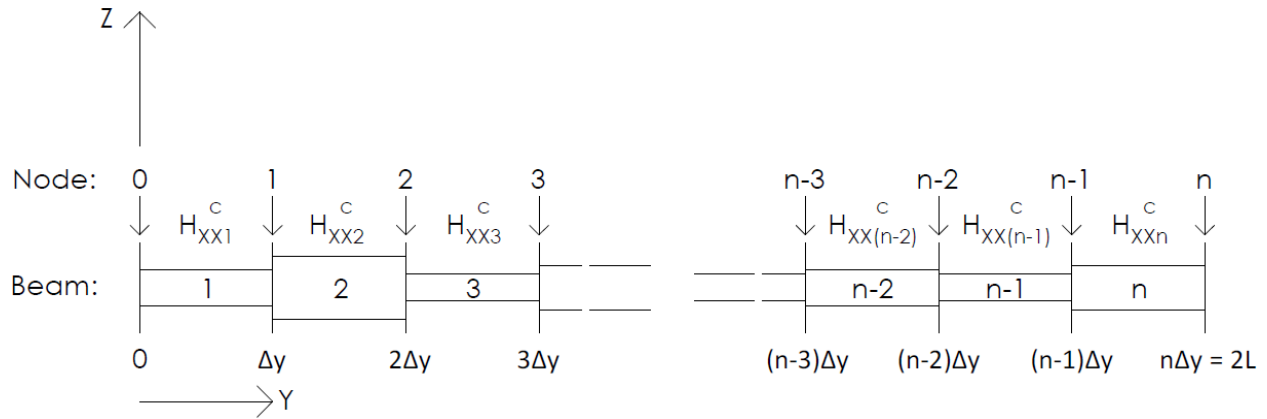
Figure 14: Free body diagram of case ①

In Figure 14 we see $Beam\ AB$ discretized into n finite Euler beams. Figure 14 only illustrates the discretization of case ①; however, the principle can be extended to the other three cases. The length of $Beam\ AB$ and $Beam\ CD$ is $2L$, thus the length of each finite Euler beam is given by:

$$\Delta y = \frac{2L}{n} \ for\ Beam\ AB$$
$$\Delta x = \frac{2L}{n} \ for\ Beam\ CD \tag{5.8}$$

40

We are now required to find the translational and angular displacements at each node in terms of the bending moment that exists in each finite Euler beam. Again, the derivation will only be provided for case ① in Figure 13 but can just as easily be applied to the other cases by simply changing the coordinate system. Due to the nature of the assumed loads and boundary reactions the bending moment, in each beam, for all cases in Figure 13 will be linear. We now consider finite beam i in Figure 14 with a local axial coordinate $\tilde{y}$:
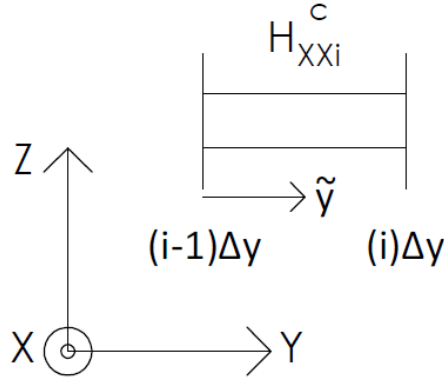
Figure 15: Finite beam with a local coordinate system

We know beam i will be subject to a bending moment of the form:

$$M_X(y) = Ay + B \tag{5.9}$$

Thus we have:

$$M_X(\tilde{y}) = A\tilde{y} + A\Delta y(i - 1) + B \tag{5.10}$$

Now from Equation (5.6) and $H^c_{XXi} = constant$ we have for beam i:

$$\bar{u}'_Z = \frac{1}{H^c_{XXi}} \int M_X(\tilde{y}).d\tilde{y} \tag{5.11}$$

$$\bar{u}_Z = \frac{1}{H^c_{XXi}} \iint M_X(\tilde{y}).d\tilde{y}^2 \tag{5.12}$$

We express the boundary conditions for beam i as follows:

$$\bar{u}'_Z(\tilde{y} = 0) = \bar{u}'_{ZOi}$$
$$\bar{u}_Z(\tilde{y} = 0) = \bar{u}_{ZOi} \tag{5.13}$$

41

These boundary conditions describe the angular and translational displacements at the beginning of beam i. The deflection in beam i is then given by the following expressions:

$$\bar{u}_Z' = \frac{1}{H_{XXi}^c}\left\{\frac{A\tilde{y}^2}{2} + [A\Delta y(i-1) + B]\tilde{y}\right\} + \bar{u}_{ZOi}' \tag{5.14}$$

$$\bar{u}_Z = \frac{1}{H_{XXi}^c}\left\{\frac{A\tilde{y}^3}{6} + \frac{[A\Delta y(i-1) + B]\tilde{y}^2}{2}\right\} + \bar{u}_{ZOi}'\tilde{y} + \bar{u}_{ZOi} \tag{5.15}$$

The general angular and translational displacements at the nodes are unknown thus is will be important to relate successive nodal displacements. Since the displacements must be continuous in the entire beam we notice that the displacements at the beginning of beam $(i+1)$ must be the same as the displacements at the end of beam i. We express this relation by evaluating Equations (5.14) and (5.15) at $\tilde{y} = \Delta y$:

$$\bar{u}_{ZO(i+1)}' = \frac{1}{H_{XXi}^c}\left\{\frac{A(\Delta y)^2}{2} + [A\Delta y(i-1) + B]\Delta y\right\} + \bar{u}_{ZOi}' \tag{5.16}$$

$$\bar{u}_{ZO(i+1)} = \frac{1}{H_{XXi}^c}\left\{\frac{A(\Delta y)^3}{6} + \frac{[A\Delta y(i-1) + B](\Delta y)^2}{2}\right\} + \bar{u}_{ZOi}'\Delta y \tag{5.17}$$
$$+ \bar{u}_{ZOi}$$

Equations (5.16) and (5.17) illustrate that if the bending moment through a finite Euler beam is known then the nodal displacements can be related through the geometric properties of that same beam. We can now simply determine the transverse shear force and bending moment for case ① in Figure 13:

$$\left.\begin{array}{l} V_Z(y) = R_{Z_A} \\ M_X(y) = R_{Z_A}y - R_{X~A}^M \end{array}\right\} 0 \le y < L \tag{5.18}$$

$$\left.\begin{array}{l} V_Z(y) = -R_{Z_B} \\ M_X(y) = R_{Z_B}(2L - y) + R_{X~B}^M \end{array}\right\} L < y \le 2L \tag{5.19}$$

Equations (5.16) to (5.19) describe the general nodal displacements, however global boundary conditions are still required for $Beam~AB$. We know the following for the first and last finite beams:

$$\bar{u}'_{ZO1} = -\frac{R^M_{X\,A}}{k^\theta_{X\,A}}$$

$$\bar{u}_{ZO1} = -\frac{R_{Z\,A}}{k_{Z\,A}}$$

$$\bar{u}'_{ZO(n+1)} = -\frac{R^M_{X\,B}}{k^\theta_{X\,B}}$$

$$\bar{u}_{ZO(n+1)} = -\frac{R_{Z\,B}}{k_{Z\,B}}$$

(5.20)

In addition we have the following coupling moment due to torsion in $Beam\ CD$:

$$R^M_{X\,E} = -k^\theta_{X\,E} \times (\bar{u}'_{ZO})_E = -k^\theta_{X\,E} \times \bar{u}'_{ZO(\frac{n}{2}+1)} \qquad (5.21)$$

It is important to note that $\{n \geq 2, \in Even\}$: This creates nodes at point E and allows each finite beam to either fully described by Equations (5.18) or (5.19). Finally we have the following force and moment equilibrium equations for $Beam\ AB$:

$$\sum F_Z = 0 \therefore R_{Z\,A} + R_{Z\,B} + \alpha F_Z = 0$$

$$\sum M_X = 0 \therefore R^M_{X\,A} + R^M_{X\,B} + M_X + R^M_{X\,E} + L\alpha F_Z + 2LR_{Z\,B} = 0$$

(5.22)

At this point it may be important to note all the unknowns in the problem. We are still considering only case ① in Figure 13:

- $R_{Z\,A};\ R_{Z\,B};\ R^M_{X\,A}; R^M_{X\,B}; R^M_{X\,E}; \alpha \ \therefore (6\ unknowns)$
- $\bar{u}'_{ZO}\ at\ nodes\ 0 \to n \ \therefore (n+1\ unknowns)$
- $\bar{u}_{ZO}\ at\ nodes\ 0 \to n \ \therefore (n+1\ unknowns)$

We have to total of $6 + 2(n + 1)$ unknowns. Thus far we have the following equations:

- 7 equations from (5.20) to (5.22)
- $2n$ equations form (5.16) to (5.19) (two equations per finite beam)

We have a total of only $7 + 2n$ equations. There are not enough equations to relate all the unknowns. However we note that case ① and ② in Figure 13 are coupled through Equation (5.4) and the common translational displacement at point E:

$$\bar{u}_{ZO(\frac{n}{2}+1)}\Big|_{Beam\ AB} = \bar{u}_{ZO(\frac{n}{2}+1)}\Big|_{Beam\ CD} \qquad (5.23)$$

We therefore have an additional 2 equations. Now we follow exactly the same approach for case ② from Equations (5.9) to (5.22) noting only that the coordinate system has changed. We now have an additional $6 + 2(n + 1)$ unknowns and $7 + 2n$ equations. In total:

- $Unknowns = 2\big(6 + 2(n + 1)\big) = 16 + 2n$
- $Equations = 2(7 + 2n) + 2 = 16 + 2n$

The coupled cases ① and ② can now be fully solved under knowledge of the transducer geometry, boundary stiffness $k^{\theta}_{X_E}$ and $k^{\theta}_{Y_E}$.

The coupled cases ③ and ④ are similarly solved and the derivation will not be included to avoid reiterating the same concepts. The only major differences are that the coupling reactions at point E are a result of **translational** displacements and that case ③ and ④ are coupled through the common **angular** displacement at point E. The equivalent of Equations (5.21) and (5.23) are then given by:

$$R_{X_E} = -k_{X_E} \times (\bar{u}_{XO})_E = -k_{X_E} \times \bar{u}_{XO(\frac{n}{2}+1)} \quad for\ case\ ③ \qquad (5.24)$$

$$\bar{u}'_{XO(\frac{n}{2}+1)}\Big|_{Beam\ AB} = \bar{u}'_{YO(\frac{n}{2}+1)}\Big|_{Beam\ CD} \qquad (5.25)$$

At this point the reactions at point E ($R_{X_E}, R_{Y_E}, R^{M}_{X_E}$ and $R^{M}_{Y_E}$) are known given the coupling stiffness at point E ($k_{X_E}, k_{Y_E}, k^{\theta}_{X_E}$ and $k^{\theta}_{Y_E}$). As illustrated in Equation (5.5) the coupled reactions at point E are transferred from the boundaries. Since these boundaries are identical we can safely assume that these coupling reactions are equally distributed. Therefore, we can extend Equation (5.5):

$$R_{X_C} = R_{X_D} = -\frac{R_{X_E}}{2}$$

$$R_{Y_A} = R_{Y_B} = -\frac{R_{Y_E}}{2}$$

$$R_{X_C}^M = R_{X_D}^M = -\frac{R_{X_E}^M}{2}$$

$$R_{Y_A}^M = R_{Y_B}^M = -\frac{R_{Y_E}^M}{2}$$

(5.26)

It can be concluded that if the geometry of the transducer, boundary stiffness and coupling stiffness at point E are known then the reactions at the boundaries and point E can be determined in the statically indeterminate system under specific loads. Given these reactions the transverse shear forces, bending moments, torsion and tension in the beams can be determined (The tension and torsion derivation will be elaborated in the following section). It is therefore important to determine the boundary stiffness and coupling stiffness at point E as will be done in Section 5.2.1.3.

5.2.1.2. TRANSDUCER STRESS FORMULATION

In the previous section we were able to determine the transverse shear forces, bending moments, torsion and tension at any point in the transducer given the geometry, boundary stiffness, coupling stiffness at point E and loading.

We have already determined the transverse shear forces and bending moments in each beam (for case ① we had Equations (5.18) and (5.19)). It is still necessary to determine the tension and torsion in each beam from the given parameters. This is extremely simple since we already know the axial reaction force and moment at each boundary from Equation (5.26): The tension and torsion in each beam is simply given by the axial force and axial moment reaction at each boundary, up to point E. As an example the tension P and torsion T of $Beam\ CD$ from point E to D is given by:

$$\left. \begin{array}{l} P_{X\,BeamCD} = R_{X_D} \\ T_{X\,BeamCD} = R_{X_D}^M \end{array} \right\} L < x \le 2L$$

The stress in a rectangular beam due to transverse shear stresses, bending moments and tension can be easily characterized. Unfortunately the stress due to torsion in a rectangular beam creates

45

some difficulties. To illustrate how this difficulty was overcome the stress formulation for *Beam AB* is given (BUDYNAS, Richard G. and Nisbett, J. Keith, 2011):

$$Normal\ Stress\ \sigma_{YY} = \frac{-M_X(y)z}{I_{XX}} + \frac{M_Z(y)x}{I_{ZZ}} + \frac{P_Y(y)}{0.85A}$$

$$Shear\ Stress\ \tau_{YZ} = \frac{3V_Z(y)}{2A}\left(1 - \frac{z^2}{z_{max}^2}\right) + \tau_{max} \qquad (5.27)$$

$$Shear\ Stress\ \tau_{YX} = \frac{3V_X(y)}{2A}\left(1 - \frac{x^2}{x_{max}^2}\right) + \tau_{max}$$

Very similar relations exist for *Beam CD*. In the above expressions $z_{max}(y)$ and $x_{max}(y)$ mark the height and width of the rectangular cross section and $A = z_{max}(y)x_{max}(y)$. We also note $I_{XX}(y)$ and $I_{ZZ}(y)$ as the second moments of area about the X and Z axes respectively. We also have τ_{max} as the maximum shear stress due to torsion in a rectangular cross section. Since the stress due to torsion is difficult to characterize we simply add τ_{max} to both shear stress components to be conservative in our uncertainty. Specifically for Equation (5.27) τ_{max} is given by the following relation (BUDYNAS, Richard G. and Nisbett, J. Keith, 2011):

$$\tau_{max} = \frac{T_Y(y)}{bc^2}\left(3 + \frac{1.8c}{b}\right)\ with\ b \geq c \qquad (5.28)$$

Here τ_{max} marks the maximum shear stress due to torsion in a rectangular $b \times c$ cross section. We must now establish a von Mises stress equivalent for Equation (5.27) in context of a fatigue analysis. In Section 5.2.3 we will use the assumption that the transducer undergoes fully reversed stress cycles, thus we only required a von Mises stress equivalent for the stress amplitude (BUDYNAS, Richard G. and Nisbett, J. Keith, 2011):

$$\sigma_a' = \left\{\left[\left(K_f\right)_{bending}(\sigma_a)_{bending} + \left(K_f\right)_{axial}\frac{(\sigma_a)_{axial}}{0.85}\right]^2 \right.$$
$$\left. + 3\left[\left(K_{fs}\right)_{torsion}(\tau_a)_{torsion} + (\tau_a)_{shear}\right]^2\right\}^{1/2} \qquad (5.29)$$

The load factor for axial loading is included as the 0.85 divisor. The load factor for torsion of 0.59 is accounted for in the derivation of the von Mises equation. After undergoing optimization with safety factors the transducer was analysed in a FE program to insure stress concentrations are sufficiently low. This reduces the complexity of the transducer model and since all stress

concentration factors can be set to unity. We substitute the expressions in Equation (5.27) into (5.29) to obtain:

$$\sigma'_a = \{\sigma_{YY}{}^2 + 3[\tau_{YZ}{}^2 + \tau_{YX}{}^2]\}^{1/2} \tag{5.30}$$

As will be explained in Section 5.2.3 σ'_a had to be kept below a maximum allowable reversed stress $\sigma_{rev_{max}}$ during optimization at all points.

5.2.1.3.   BOUNDARY AND COUPLING STIFFNESS WITH STRESS FORMULATION

The notation as previously used in Section 5.2.1.1 is applicable and will be required in this section. The importance of the boundary stiffness and coupling stiffness at point E was signified previously. We begin by modeling the boundary stiffness. Consider first a simplified schematic of a boundary:
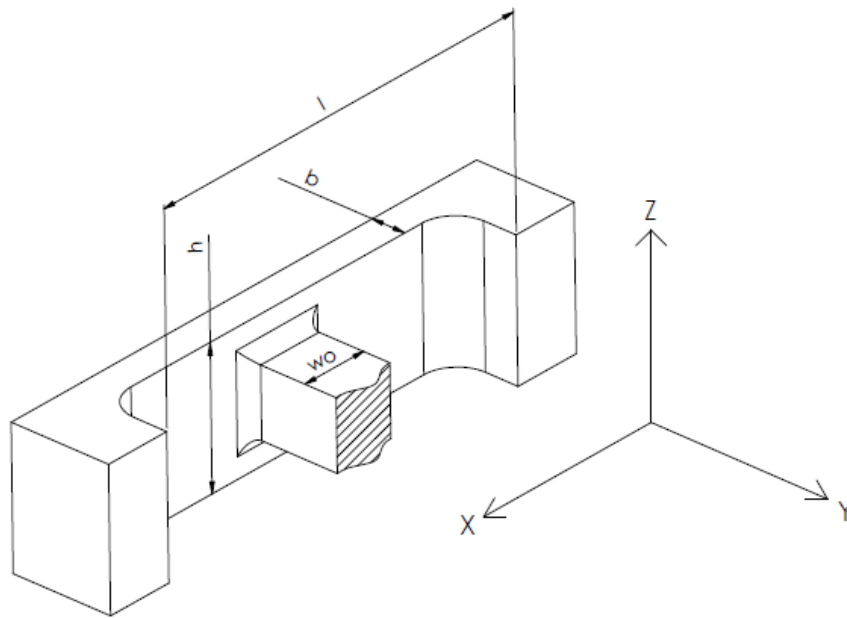
Figure 16: Simplified diagram of a flexural boundary

In Figure 16 we see an approximate representation of one-of-four identical boundaries orientated such that the axial direction of the spoke lies in the Y axis. This local coordinate system will be used throughout this sub-section. Here l is the length of the boundary, h the height, b the width and w_o is the width of the spoke at the root. We need to establish a stiffness and resultant stress caused by loading in each respective axis at the boundary. The stiffness must be determined at

the root of the spoke. The reaction at the boundary is given as before by the following expression:

$$\bar{R} = [R_X, R_Y, R_Z, R_X^M, R_Y^M, R_Z^M]$$

We begin with the simplest axis:

Application of R_X:

When reaction R_X is applied we can simply model the boundary as two identical tensile/compressive springs in parallel, thus we have:
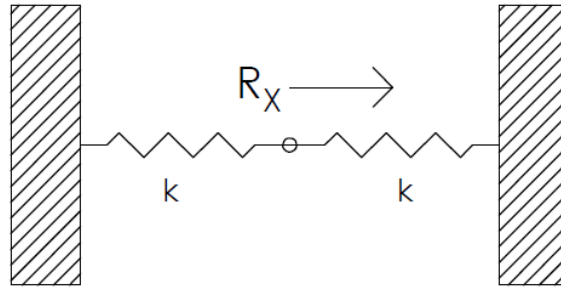
Figure 17: Model of boundary under reaction loading (1)

$$k_X = 2k = 2\left(\frac{Area \times E}{Spring\ Length}\right) = \frac{4bhE}{l - w_O} \tag{5.31}$$

In the above expression we assume the stiffness is infinitely large where the spoke merges with the boundary, hence the w_O correction. The stress experienced in the boundary under this reaction is tensile/compressive, thus we have the following normal stress.

$$Normal\ Stress\ \sigma_{XX} = \frac{1}{2} \times \left(\frac{R_X}{Area}\right) = \frac{R_X}{2bh} \tag{5.32}$$

Application of R_Y and R_Z^M:

Modeling the boundary under these loads requires us to split the boundary into three Euler beam on account of the spoke. As before we assume the stiffness is infinitely large where the spoke merges with the boundary. Consider the following diagrams:
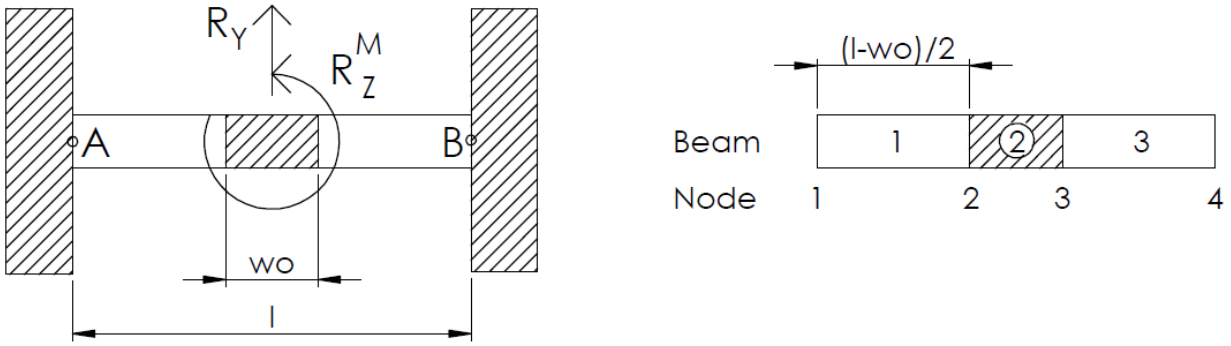
Figure 18: Model of boundary under reaction loading (2)

We notice that this discretization of the boundary into separate Euler beams is like that done in Section 5.2.1.1 with $Beam\ AB$ and $Beam\ CD$. The points A and B in the Figure 18 have no relation to points A and B in $Beam\ AB$ (they just represent points at the boundary's boundaries). The task is however greatly simplified since the end conditions are modeled as being ideal (rigid). Thus the angular and translational displacements at $nodes$ 1 and 4 in Figure 18 are zero. Consider the free body diagram of the boundary:
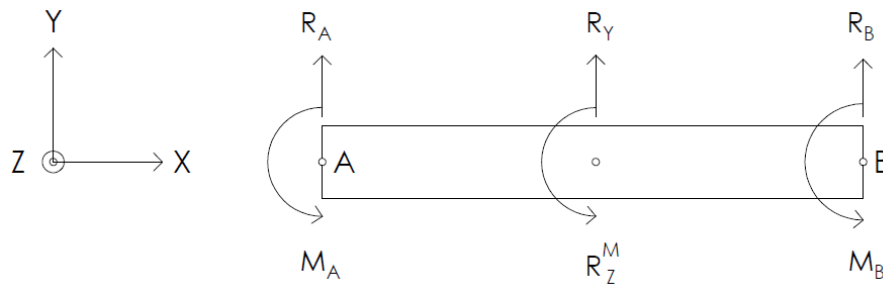
Figure 19: Free body diagram of the boundary in the XY plane

The following shear force and bending moment equations can be obtained for the boundary:

$$\left.\begin{aligned} V_Y(x) &= R_A \\ M_Z(x) &= R_A x - M_A \end{aligned}\right\} 0 \le y < l/2 \qquad (5.33)$$

$$\left.\begin{aligned} V_Y(x) &= -R_B \\ M_Z(x) &= R_B(l - x) + M_B \end{aligned}\right\} l/2 < y \le l \qquad (5.34)$$

The bending moments are linear thus the relations in Equation (5.16) and (5.17) are applicable and do not have to be redefined for this case. If we use the zero displacement end conditions,

49

infinite rigidity for *beam* 2, given lengths of each beam and Equations (5.33) and (5.34), we can derive the following equations:

$$\bar{u}'_{YO2} = \frac{1}{EI_{ZZ}} \left\{ \frac{A(l-w_O)^2}{8} + \frac{B(l-w_O)}{2} \right\}$$

$$\bar{u}_{YO2} = \frac{1}{EI_{ZZ}} \left\{ \frac{A(l-w_O)^3}{48} + \frac{B(l-w_O)^2}{8} \right\} \tag{5.35}$$

$$\text{with } A = R_A; B = -M_A$$

$$\bar{u}'_{YO3} = \bar{u}'_{YO2}$$

$$\bar{u}_{YO3} = \bar{u}'_{YO2}w_O + \bar{u}_{YO2} \tag{5.36}$$

$$\bar{u}'_{YO3} = -\frac{1}{EI_{ZZ}} \left\{ \frac{C(l-w_O)^2}{8} + \left[\frac{C(l-w_O)}{2} + D \right] \frac{(l-w_O)}{2} \right\}$$

$$\bar{u}_{YO3} = -\frac{\bar{u}'_{YO3}(l-w_O)}{2}$$

$$- \frac{1}{EI_{ZZ}} \left\{ \frac{C(l-w_O)^3}{48} \right. \tag{5.37}$$

$$+ \left. \left[\frac{C(l-w_O)}{2} + D \right] \frac{(l-w_O)^2}{8} \right\}$$

$$\text{with } C = -R_B; D = M_B + R_B l$$

In the above equations we have $I_{ZZ} = \frac{bh^3}{12}$. If we include global force and moment equilibrium equations the displacements at all the nodes can be solved for and the stiffness obtained for the two axes under load:

$$k_Y = \frac{R_Y}{\bar{u}'_{YO2}\frac{w_O}{2} + \bar{u}_{YO2}} \tag{5.38}$$

50

$$k_Z^\theta = \frac{R_Z^M}{\bar{u}_{YO2}'}$$ (5.39)

We have the following associated normal and shear stresses:

$$\sigma_{XX} = -\frac{M_Z(x)y}{I_{ZZ}} \quad and \quad \tau_{XY} = \frac{3V_Y(x)}{2bh}\left(1 - \frac{4y^2}{b^2}\right)$$ (5.40)

Application of R_Z and R_Y^M:

The modeling of the boundary under these loads can be approached in exactly the same manner as done for the application of R_Y and R_Z^M and the method will not be reiterated.

Application of R_X^M:

The application of R_X^M creates torsion in the boundary about the local X axis: Consider the following diagram:
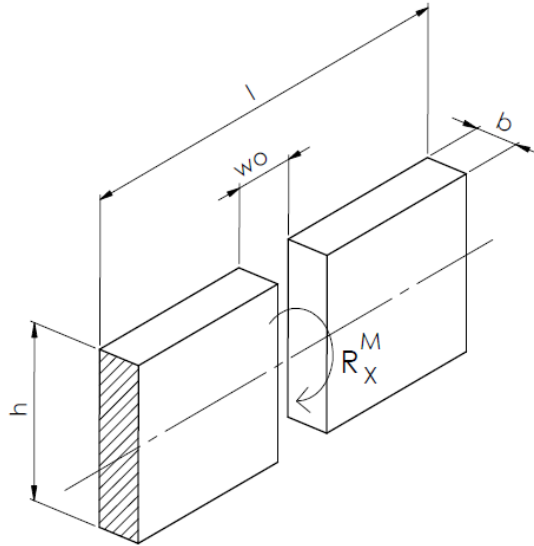
Figure 20: Model of boundary under reaction loading
(3)

The boundary can be modeled as two torsional springs acting in parallel. Since we expect that $h \geq b$ we obtain the following (BUDYNAS, Richard G. and Nisbett, J. Keith, 2011):

51

$$k_X^\theta = 2 \left[\frac{\beta h b^3 G}{\left(\frac{l - w_O}{2} \right)} \right] = \frac{4\beta h b^3 G}{l - w_O} \tag{5.41}$$

Here $\beta = \beta(h/b)$ for a rectangular $h \times b$ cross section and is often presented in tabulated form such as in the literature of R.G. Budynas and J.K. Nisbett in *Shigley's Mechanical Engineering Design*. The shear modulus of the material is given by G.

Due to the uncertainty of the shear stress under torsional load in a rectangular cross section we add the maximum shear stress due to torsion to both shear components as done previously:

$$\tau_{XY} = \tau_{XZ} = \tau_{max} = \frac{R_X^M}{hb^2} \left(3 + \frac{1.8b}{h} \right) \tag{5.42}$$

At this point we have a boundary stiffness in every axis at the root of the spoke and associated stresses under load. The von Mises stress equivalent approach for fatigue presented in Section 5.2.1.2 is applicable to the boundary and will not be reiterated.

The coupling stiffness at point E is still required but can be simply formulated. The axial stiffness of each spoke acts as a spring in series to k_Y (axial stiffness of the boundary) connecting each boundary to point E. Since the stiffness of the boundary is expected to be far smaller we can closely approximate the axial stiffness connecting point E to each boundary as k_Y. In each axis point E has two such connections working in parallel thus we know:

$$k_{X_E} = k_{Y_E} \approx 2 \times k_Y \tag{5.43}$$

To determine $k_{X_E}^\theta$ and $k_{Y_E}^\theta$ it should be noticed that each entire spoke acts as a torsional spring in parallel to k_Y^θ (torsional stiffness of boundary about the axial direction). Unlike the translational stiffness we expect the torsional stiffness of each spoke to be reasonably small, thus must be calculated. Consider the following diagram:
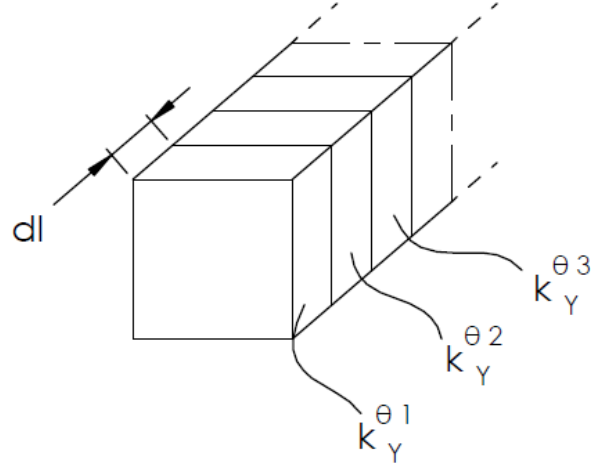
Figure 21: Model of spoke under axial torque loading

In Section 5.2.1.1 the spokes are discretized into many rectangular sections. Each one of these sections has an associated torsional stiffness about the axial direction represented by $k_Y^{\theta 1}, k_Y^{\theta 2}, k_Y^{\theta 3}$ ... which all act in series. Each rectangular $b \times c$ section has a torsional stiffness that can be calculated from the following expression:

$$k_Y^{\theta i} = \frac{\beta b c^3 G}{dl} \; with \; b \geq c \qquad (5.44)$$

Again $\beta = \beta(b/c)$ and G is the shear modulus of the material. In Section 5.2.1.1 *Beam AB* and *Beam CD* are each discretized into n sections. Therefore the series connection of $k_Y^{\theta i} \; i \in \left[1, \frac{n}{2}\right]$ acts in parallel with the series connection of $k_Y^{\theta i} \; i \in \left[\frac{n}{2} + 1, n\right]$, connecting point E to the boundaries. We can now determine $k_{X_E}^{\theta}$ and $k_{Y_E}^{\theta}$ from the following equation:

$$k_{X_E}^{\theta} = k_{Y_E}^{\theta} = \left[\frac{1}{k_Y} + \sum_{i=1}^{\frac{n}{2}} \frac{1}{k_Y^{\theta i}}\right]^{-1} + \left[\frac{1}{k_Y} + \sum_{i=\frac{n}{2}+1}^{n} \frac{1}{k_Y^{\theta i}}\right]^{-1} \qquad (5.45)$$

Due to symmetry in the transducer we can actually rewrite Equation (5.45) as the following:

$$k_{X_E}^{\theta} = k_{Y_E}^{\theta} = 2\left[\frac{1}{k_Y} + \sum_{i=1}^{\frac{n}{2}} \frac{1}{k_Y^{\theta i}}\right]^{-1}$$

53

At this point all that is required to determine the stresses throughout the transducer and its boundaries is the geometry and input forces.

5.2.1.4. STRAIN GAUGE READINGS

Thus far the stresses throughout the transducer can be determined. While this is required to insure the transducer meets all design specifications it does not allow us to determine its performance. The performance of the transducer is dependent on the strain field generated at each strain gauge. This section will deal with the strain gauge reading formulation. As involved as this may seem we should consider the literature addressed on the functionality of strain gauges presented in Section 3.4. We learn in this section that a strain induced on the resistive element of a strain gauge orthogonal to the direction of the strain gauge leads to a negligible δR i.e. it is only a strain along the length of the resistive element that causes a significant δR. The important consideration is therefore not the effect of transverse strain on the resistive element but rather the effect of transverse strain on the strain in the direction of the strain gauge. Consider the following stress-strain relation for linear elastic isotropic materials (RADOVITZKY, Raul, 2012):

$$\varepsilon_{ij} = \frac{1}{E}\left[(1+v)\sigma_{ij} + v\delta_{ij}\sigma_{kk}\right]$$

$$\delta_{ij} = \begin{matrix} 1 \; if \; i = j \\ 0 \; if \; i \neq j \end{matrix}$$

(5.46)

Let us say we are interested in measuring the principle strain ε_{11} with a strain gauge. We see that if no other principle stresses are present (except σ_{11}) then we simply have $\varepsilon_{11} = \frac{\sigma_{11}}{E}$. We note that the shear stresses have no effect on the principle strain ε_{11} of interest. In the case of the transducer we have such a situation: The strain gauges are placed on the spokes such that they measure the stain on the surface of a spoke in the axial direction of the same spoke (the axial direction of the spoke is equivalently the radial direction of the transducer). From the stress formulation we see no other principal stresses are present except the normal stress (previously represented as σ_{YY} in Equation (5.27)) which lies in the axial direction of each spoke. We can simply substitute Equation (5.27) into (5.46) while dropping the correction for the axial load factor. We therefore obtain the following strain as will be read by the strain gauges:

$$Normal\ Strain\ \varepsilon_{YY} = \frac{1}{E}\left[\frac{-M_X(y)z}{I_{XX}} + \frac{M_Z(y)x}{I_{ZZ}} + \frac{P_Y(y)}{A}\right] \qquad (5.47)$$

The notation is as presented in Section 5.2.1.2. Again the above expression represents the strains only on $Beam\ AB$. A very similar expression exists for $Beam\ CD$. If the positions of the strain gauges are known then a strain compliance matrix can be compiled as described in Section 3.5.2.

From Section 3.4.2 we had Equation (3.18) explaining the importance of accounting for a varying strain field along the strain gauge. This must be accounted for, however, due to the undertaken optimization process the stresses are maximized at every cross sectional point on $Beam\ AB$ and $Beam\ CD$. While it cannot be illustrated at this point we will learn from Section 5.2.6 that the strain along the surfaces (onto which the strain gauges are secured) have very linear, if not constant, strains in the axial direction of each spoke (direction of the strain gauges) due to maximizing the stresses. This greatly simplifies the strain measurement. Consider Equation (3.18) again, but $\varepsilon_X(x) = ax + b$ as a linear function:

$$\varepsilon_{eff} = \frac{1}{x_{gauge}} \int_{x_0}^{x_0 + x_{gauge}} (ax + b).dx$$

$$\varepsilon_{eff} = a\left(x_0 + \frac{x_{gauge}}{2}\right) + b \qquad (5.48)$$

We see the measured strain can be approximated as the strain at the center of the strain gauge for both a linearly varying and a constant strain field. It will just be required to verify that the strains are constant or linear in the region of the strain gauge.

Throughout Section 3.4 the importance of accounting for thermal strains and misalignments was signified. The transducer in its application will not be subject to appreciable thermal stresses and to simplify the model we assume no misalignments in the strain gauges. Additionally during implementation of the Wheatstone bridges 'dummy gauges' will be incorporated to create full bridges which completely annul all thermal effects provided the strain gauges are identical and attached to the same material at the same temperature (explained further in Section 5.2.4). These two assumptions are reasonable and greatly simplify the model.

The optimization of the geometry with the utilization of the model explained in Sections 5.2.1.1 through 5.2.1.4 will be explained further in Section 5.2.5 and 5.2.6.

5.2.2. TRANSDUCER MATERIAL SELECTION

The most suitable material for the force transducer was determined during the detailed design phase. The selected material was the aluminium alloy Al-7075-T651 with the following properties (ASM Aerospace):

- Ultimate tensile strength $\sigma_{ut} = 572MPa$
- Yield strength $\sigma_y = 503MPa$
- Modulus of elasticity $E = 71.7GPa$
- Effective endurance limit $Se' = 159MPa$ (RR Moore specimen for 5×10^8 cycles)
- Poisson's ration $v = 0.33$

This material was selected since the transducer should be as light as possible to conserve the unsprung-mass of the vehicle. The transducer requires a material with a high yield strength and effective endurance limit to deal with the extreme loading conditions in a confined space, but low modulus of elasticity to produce high strains (for better sensitivity) at the strain gauges. For these criteria Al-7075-T651 is very suitable.

5.2.3. TRANSDUCER FATIGUE ANALYSIS

During the detailed design phase a fatigue analysis was completed for the transducer. The objective of the fatigue analysis was to determine a maximum allowable reversed stress $\sigma_{rev_{max}}$ that the transducer could be subject to such that it would still comply with all design life specifications and safety factors.

A reasonable assumption of fully reversed loading was argued as follows: None of the forces or moments to measure, $(F_X'; F_Y'; F_Z'; M_X'; M_Y'; M_Z')$ as illustrated in Figure 1, are biased (explicitly have a non-zero mean) except F_Y'. The weight of the vehicle creates a non-zero mean for F_Y', however, since F_Y' exists radially to the wheel the rotating transducer will still experience a zero mean. All the forces therefore produce zero mean loading (in general) thus fully reversed loading can be assumed.

Assuming fully reversed loading simplified the analysis and allowed $\sigma_{rev_{max}}$ to be specified explicitly for the transducer. It was calculated at $\sigma_{rev_{max}} = 240 MPa$ as the upper-bound stress. The upper-bound stress would be incorporated in the model as one of the constraining parameters and explained in seen in Section 5.2.1.2.

For full details regarding the fatigue analysis the MOX 410 Design Report entitled *DETAIL DESIGN OF A SIX-AXIS WHEEL FORCE TRANSDUCER* should be referred to. Details have been excluded from this research report to maintain coherency in the modeling and optimization rather than the design.

5.2.4. TRANSDUCER STRAIN COMPLIANCE AND BRIDGING

Before optimization could commence it was necessary to define a strain compliance as would be incorporated in the final design. The literature presented in Section 3.5.2 is strongly applicable here.

In Section 4.2 the telemetry system was specified and it was stated that real time telemetry would not be necessary in the wheel force transducer. Instead the data is recorded from the strain sensors and post processing is done. The major advantage of the pursued concept it that the transducer can be made to be almost entirely decoupled in its operation. A decoupled transducer such as this allows for very efficient data processing as was noted in the literature survey. However, since post processing will be done the need for efficient computational times is not entirely necessary. Despite this a decoupled force transducer is still majorly advantageous as it can be incorporated in nearly every telemetry system (such as real time) without modification to the transducer. The designed transducer in this project shall utilize, but is not limited to, the specified telemetry system.

In addition to the telemetry system versatility, a decoupled force transducer is advantageous as its results are more stable and can more easily be modeled and understood. The number of Wheatstone Bridges or force sensors is also at a minimum for a decoupled force transducer (one sensor per axis), thus the minimum number of channels is utilized.

However, an attempt to *fully* decouple the force transducer by utilizing inordinate amounts of strain gauges was not made. In Section 3.6 the Junyich's six-axis force transducer was presented.

This concept was extended to the current design thus the number and positioning of strain gauges is applicable to our case. The Junyich's six-axis force transducer makes way for 16, 24, 32 and 48 strain gauges. An increased number of strain gauges allows us to decouple the transducer to a greater degree (CHAO, Lu-Ping and Chen, Kuen-Tzong, 1997). From a cost perspective however, the 16 strain gauges was the best solution given that a fully decoupled transducer is not entirely necessary in context of the specified transducer. If the telemetry system is altered more strain gauges can be added and a new strain compliance defined.

The following figure illustrates the positioning and numbering of the 16 strain gauges in a simplified diagram of the transducer:
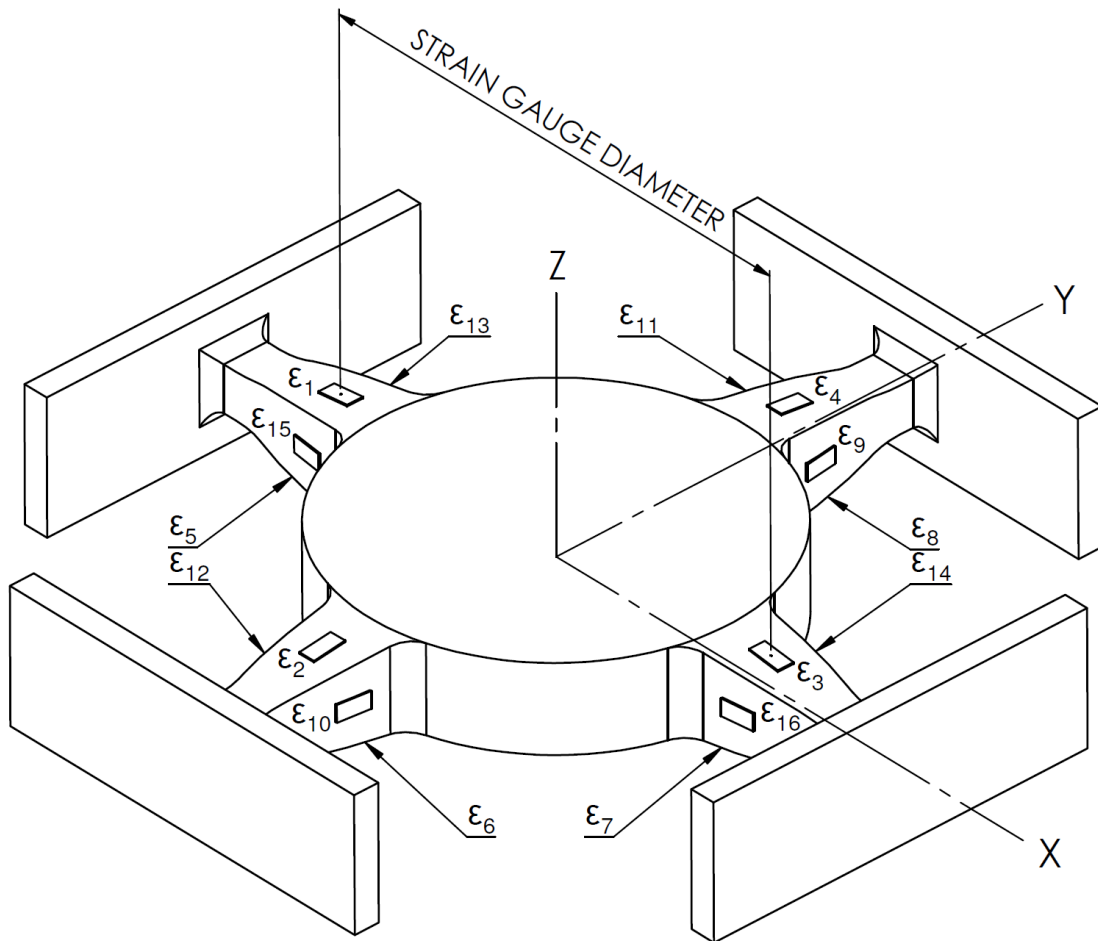
Figure 22: Simplified diagram of the transducer with strain gauge positions

In Figure 22 the placement of the strain gauges are shown and labeled from ε_1 to ε_{16}. Essentially each spoke has one strain gauge per side. The arrows in Figure 22 represent strain gauges on the

faces not visible. Each strain gauge will be placed the same distance from the center of the hub illustrated by the STRAIN GAUGE DIAMETER dimension.

The associated strain compliance matrix is given by Equation (3.28) which is provided again for convenience:

$$C_{1i} = \frac{(\varepsilon_9 + \varepsilon_{10})}{2}; \ C_{2i} = \frac{(\varepsilon_{13} + \varepsilon_{14})}{2};$$

$$C_{3i} = \frac{(\varepsilon_2 + \varepsilon_3 - \varepsilon_5 - \varepsilon_8)}{4}; \ C_{4i} = \frac{(\varepsilon_4 + \varepsilon_6)}{2}; \tag{5.49}$$

$$C_{5i} = \frac{(\varepsilon_1 + \varepsilon_7)}{2}; \ C_{6i} = \frac{(\varepsilon_{11} - \varepsilon_{12} + \varepsilon_{15} - \varepsilon_{16})}{4}$$

Wheatstone Bridges can simply be configured to produce this strain compliance while utilizing 6 channels of the telemetry system (C_{ji} requires one channel per row for $j \in [1,6]$). Provided identical strain gauges in a full Wheatstone bridge are attached to the same material under the same temperature, all thermal effects will be negated. This highly demandable effect can be understood by considering the output/signal voltage in a full Wheatstone bridge when all the strain gauges have an equal change in resistance due to thermal strain (there will be no net effect on the output voltage). Wheatstone bridges C_{3i} and C_{6i} in Equation (5.49) already exhibit this property; however the other half bridges do not. For this reason 'dummy gauges' will be incorporated in the half bridges to account for thermal effects. Dummy gauges are placed in areas such that they encounter only thermal strain. For this reason eight extra strain gauges will be required as dummy gauges.

5.2.5. TRANSDUCER OPTIMIZATION

At this point all the required information to compile optimization code for the transducer was in place. A model could be compiled that uses input forces and geometry to determine the stresses at any point as presented in Section 5.2.1. In addition the strain compliance and design parameters were known to constrain the model appropriately during optimization.

An optimized geometry of the transducer is one where the maximum stresses at any cross sectional point through $Beam\ AB$ and $Beam\ CD$ (from Section 5.2.1.1) is the maximum

allowable reversed stress $\sigma_{rev_{max}}$ presented in Section 5.2.3. This ensures the stresses and therefore strains are as high as possible while complying with the required design specifications. The boundaries of the transducer also required optimization. The boundaries were optimized such that they mimic ideal boundary conditions as much as possible to reduce coupling effects. Ideal boundary conditions have been addressed previously but in context of the model an ideal boundary would have the following stiffness in every axis from Section 5.2.1.3:

$$[k] = \left[k_X = \infty, k_Y = 0, k_Z = \infty, k_X^\theta = 0, k_Y^\theta = 0, k_Z^\theta = 0\right]$$

While being optimized to obtain these ideal conditions, the boundary could experience at most the maximum allowable revered stress $\sigma_{rev_{max}}$. The following flow chart illustrates the optimization algorithm:
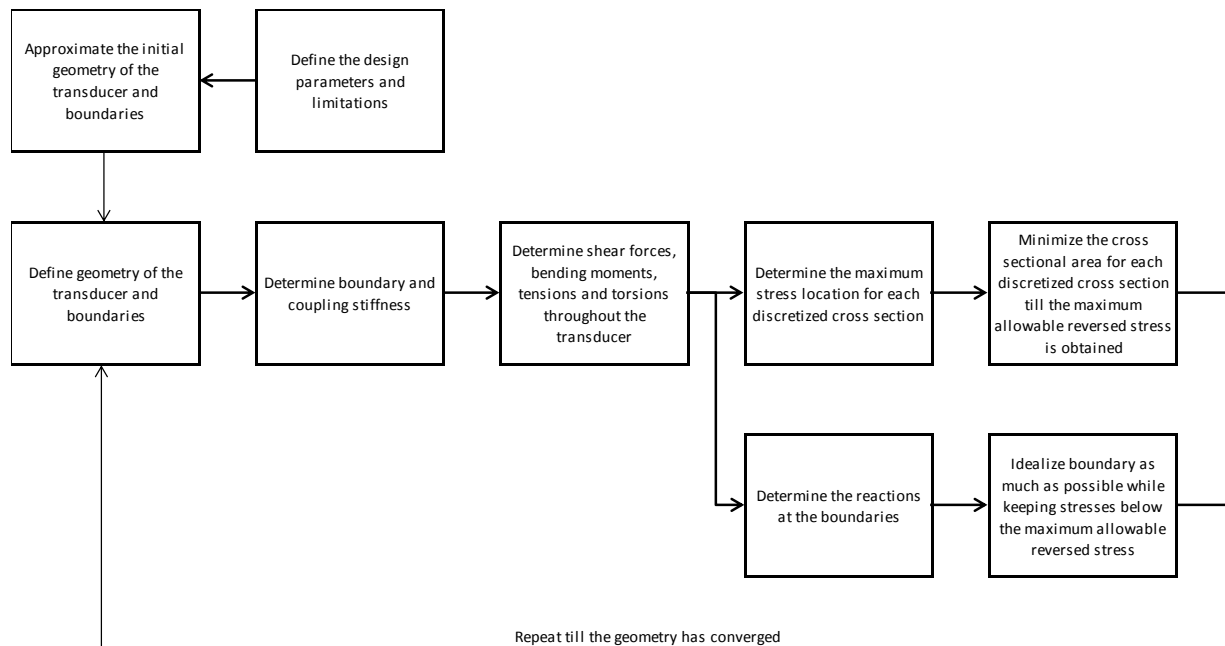
In the flow chart we see the optimization was initiated from a stage where we "Define the design parameters and limitations". These parameters include the following:

- Maximum allowable reversed stress $\sigma_{rev_{max}}$ (given as $240 MPa$)
- Maximum input forces with a safety factor (From MOX 410)
- Beam length (Represented as $2L$ in Figure 12)
- Hub radius (Represented as $HUB\ RADIUS$ in Figure 12)

60

- Maximum height of the boundary (Represented as h in Figure 16)

- Maximum length of the boundary (Represented as l in Figure 16)

- Material properties (Given for Al-7075-T651)

- The number of Euler beams n to use in the discretization of $Beam\,AB$ and $Beam\,CD$ (from Section 5.2.1.1)

Once these parameters were confirmed the optimization could continue till the geometry had converged. The optimization code has been included in Appendix E but will not provide further insight as it has been compiled and executed exactly as explained. The only point worth noting is that since the transducer exists in a rotating reference frame, with respect to the tyre contact patch, the maximum of the shear forces, bending moments, torsions and tensions throughout the transducer (all as a function of the axial position down each beam) were all assumed to act on the same beam during the stress formulation. This provided a very conservative approach since the characterization of forces in a rotating reference frame are challenging to model.

The optimization code was run several times for different design parameters and the following observations were made:

- Increased beam length $2L$ increases the overall performance of the transducer by increasing the strains where the strain gauges will be placed.

- Increased $HUB\,RADIUS$ increases the strains where the strain gauges will be placed but reduces the uniformity of the strain field along the surface.

- Increased $HUB\,RADIUS$ decreases the uniformity of the sensitivity for the various axes.

- Increased l and h decreases coupling effects (l more than h).

After many optimization configurations the following variable design parameters were found to be most effective:

- Beam length $2L = 225mm$

- Hub radius $HUB\,RADIUS = 60mm$

- Maximum height of the boundary $h = 40mm$

- Maximum length of the boundary $l = 120mm$

These design parameters maximized the outer diameter of the transducer and ensured all other components in the wheel force transducer assembly could meet the required design specifications.

Given these final design parameters the transducer could be optimized and a final geometry obtained. The optimization code was executed using $n = 1200$ Euler beams throughout the transducer. The results cannot be given as an explicit function, thus are presented as coordinates. The following graph illustrates the width and height of one spoke (half of beam $Beam\ AB$ or $Beam\ CD$):
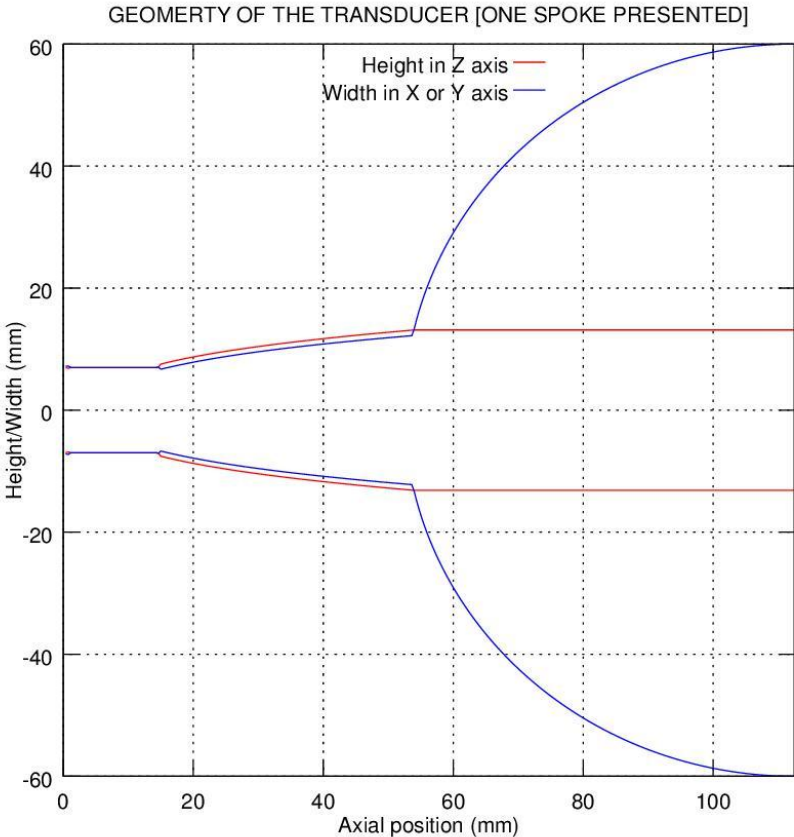
Figure 23: Optimized geometry of the transducer according to the mathematical model

We notice some interesting aspects about the optimized geometry: The width and height is constant from a zero axial position to approximately $15mm$. In this region the maximum stresses are induced by shear forces at the center of the cross section thus are linearly related to the area of the cross section. Since the shear forces are constant in this region so is the height and width.

62

We see after the constant cross sectional area region that the height and width increase along a curve. In this region maximum stresses are induced by bending moments at the edges thus are non-linearly related to the second moment of area about the respective axes. This trend is followed till to imposed hub radius is encountered. The results produced by the optimization model are thus in agreement with our expectations.

The boundaries were optimized to the following dimensions:

- Height $h = 40mm$
- Length $l = 120mm$
- Width $b = 7.6876 \approx 7.7mm$

While the width could not be predicted, the height and length is in accordance with our expectations: The height and length converged to the maximum values. Increasing the length as much as possible greatly reduces stiffness of the boundary, which in turn reduces the reaction loading at the boundary. A more idealized boundary is obtained which concentrates the loading on the beams in the transducer rather than the boundaries. Increasing the height allows the boundary to remain strong enough to withstand the reaction loads while increasing compliance in the desired axes (allows the width to be reduced).

5.2.6. TRANSDUCER AND MODEL VERIFICATION

The geometry of the transducer was solved for in the previous section using the model presented throughout Section 5.2. However, the limitations of the optimization must now be noted: We see in Section 5.2.1.2 that stress concentrations were negated on account of the complexities they would induce. It was stated that the geometry as presented by the optimization model would be imported into a FE program to insure stress concentrations were sufficiently low. Since the mathematical model had been addressed in detail and the FE program just provided verification of the results, there was no need for an in depth FE analysis. SolidWorks® 2012 was used as the FE program due to its simplicity.

Appropriate fillets were added to nullify the stress concentration effects to the greatest degree while not greatly altering the geometry as presented by the model. By completing this task the geometry of the transducer could be verified and finalized. The following figure displays the

von-Mises equivalent stress under simultaneous application of all the maximum loads after addition of the fillets:
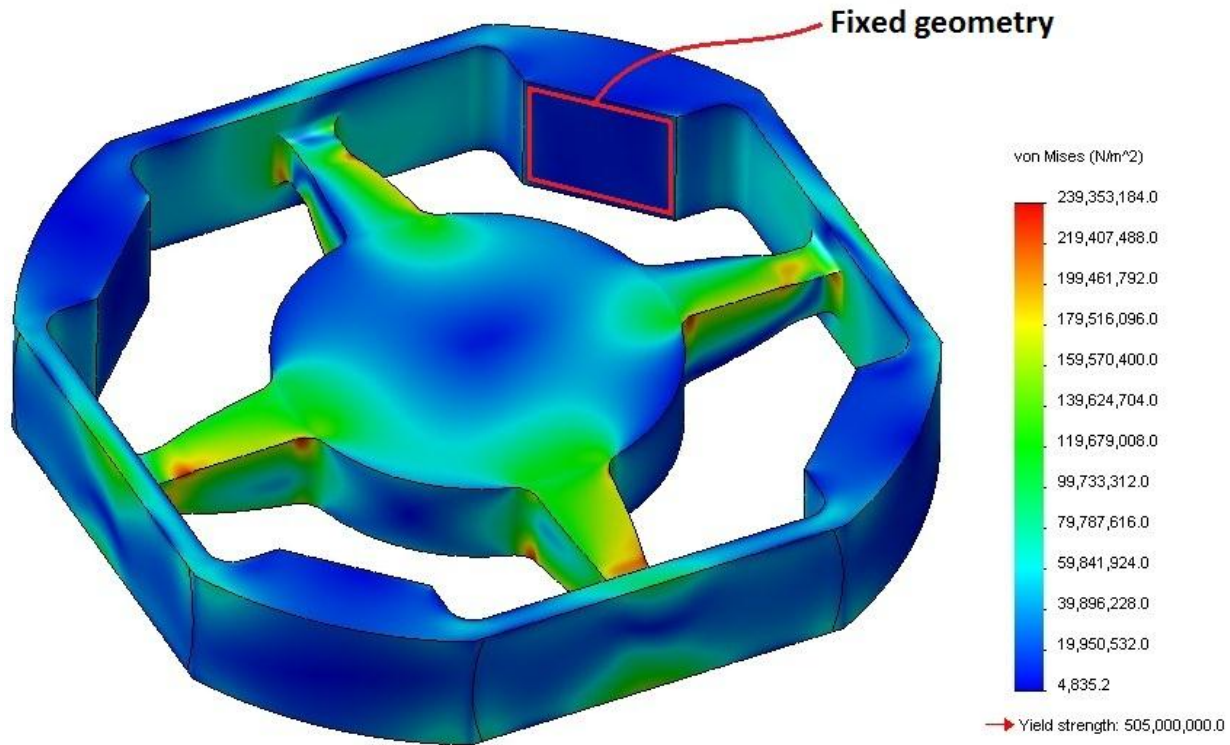
Figure 24: FE von Mises stress equivalent model of the transducer under application of all the maximum loads

For the FE model in Figure 24 a very fine mesh was utilized that was able to capture the stresses at extreme curvatures such as at the fillets. The FE model was loaded at the central cylindrical hub using distributed loads over both the top and bottom surfaces (No loads were applied on the spokes). The model incorporated fixed geometries at the four faces (one of these four faces are represented in Figure 24. These loading and boundary conditions resulted in all loading passing through the transducer's spokes and flexural boundaries as desired.

We see that the maximum experienced von Mises stress equivalent was approximately $240MPa$. This is the maximum allowable reversed stress as determined previously, thus the transducer was deemed acceptable in terms of stress concentrations (with the fillets).

The FE model allowed for the appropriate placement of the strain gauges. To avoid regions of stress concentration the strain gauges were placed $15mm$ out from the edge of the central hub. This created a STRAIN GAUGE DIAMETER (from Figure 22) of $150mm$. With the strain

gauge placement known the strain compliance under maximum loads according to the mathematical model and the FE model could be determined. This would allow for verification of the mathematical model. The FE model was constructed such that an extremely fine mesh was created on the spokes for accurate strain gauge readings.

Since the transducer was optimized to maximize the stress at the surface of the strain gauges, the strains were almost constant along these curved surfaces. This is extremely desirable in transducers and the concept of strain measurement in this context was explained in Section 5.2.1.4. To illustrate the constant strains consider a transverse load F_X on the transducer in a FE analysis:
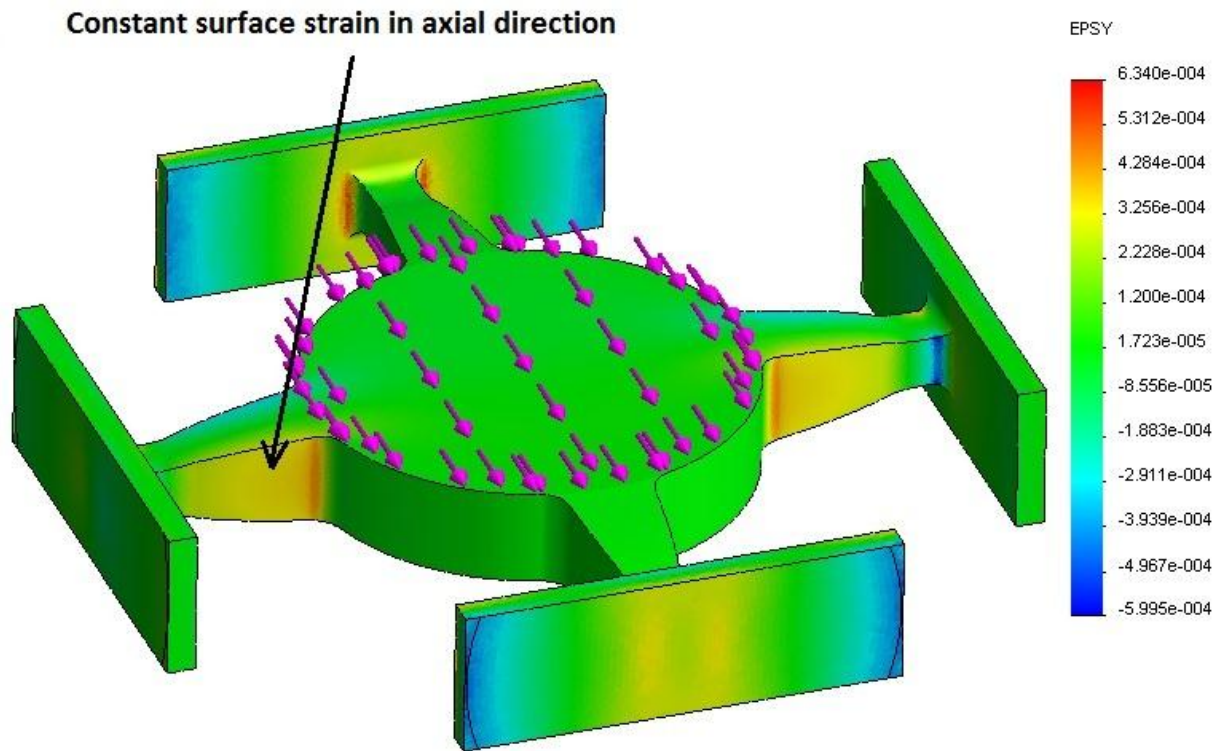
Figure 25: FE strain model of the transducer to demonstrate constant surface strain

From the FE model in Figure 25 we see extremely constant strains on the surfaces to contain the strain gauges. Loading conditions are as before, however, this simplified FE model incorporated fixed geometries at the ends of the flexural boundaries (All loading still passes through the spokes and flexural boundaries). The represented/pointed out surface is used to measure the applied load F_X. This is confirmed by results from the mathematical model:

65
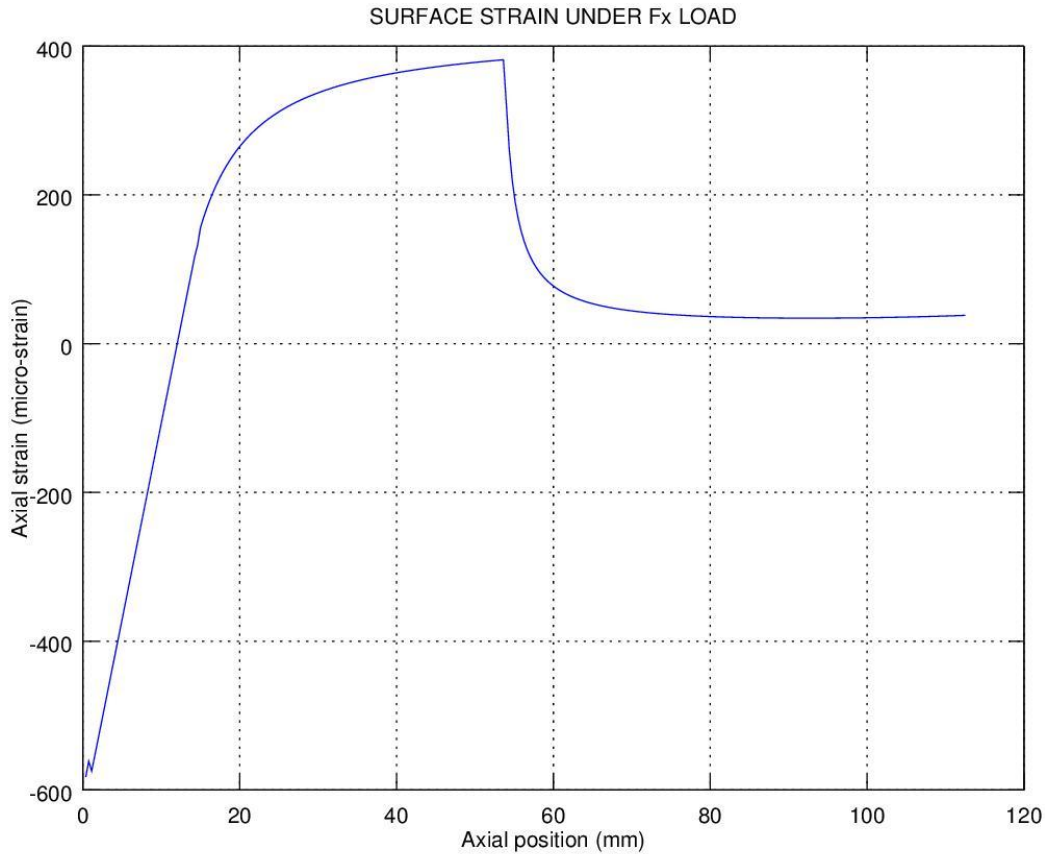
Figure 26: Mathematical axial strain model demonstrating constant surface strain

In the Figure 26 the axial strain is shown on the surface were a strain gauge would be placed to measure strain under load F_X according to the mathematical model. The surface corresponds to that represented in Figure 25. The strain gauges will be placed at an axial position of $37.5mm$ and we can see that the strains here are at almost their highest, but more importantly are nearly linear if not constant. The same observation can be made for all other loads but have not been included to maintain coherency.

From these observations it could be concluded that Equation (5.48) is valid and can be utilized to express the strain in both the mathematical and FE model. This greatly reduces the complexity of the situation and thus the strain compliance matrixes can be drawn up from Equation (5.49) for both the mathematical and finite element model.

According to the mathematical model we have the following strain compliance matrix:

$$
C_{ij}(10^6) =
\begin{bmatrix}
359.1 & 0 & 0 & 0 & 0 & 0 \\
0 & 359.1 & 0 & 0 & 0 & 0 \\
-12.9 & 12.9 & 301.3 & 0 & 0 & 0 \\
0 & 0 & 0 & 1562 & 0 & 0 \\
0 & 0 & 0 & 0 & 1562 & 0 \\
12.9 & -12.9 & 0 & 0 & 0 & 769.7
\end{bmatrix}
$$

And according to the FE model we have the following strain compliance matrix:

$$
C_{ij}(10^6) =
\begin{bmatrix}
341.6 & 0 & 3.1 & 34.0 & 0.9 & -1.6 \\
0 & 340.9 & 2.5 & -0.7 & 24.5 & 6.7 \\
-13.7 & 13.9 & 306.1 & -0.9 & 1.0 & -12.4 \\
4.7 & 0 & 0 & 1581 & 0 & 0 \\
0 & -0.1 & 0 & -0.1 & 1583 & 11.1 \\
14.4 & -15.3 & -0.2 & -1.9 & 9.7 & 803.7
\end{bmatrix}
$$

The results are presented in micro-strain per maximum/design load. The design loads were presented at the beginning of Section 5. When considering the diagonal elements i.e. C_{ii} we see the mathematical and FE model deviate at most by 5.34% using the FE model as the reference. The two models are therefore in strong agreement considering the diagonal correlation. This strong correlation between the two models verifies that the mathematical optimization was effective and did not converge to a geometry in error.

However, the FE model did encounter coupling effects that the mathematical model was not able to predict. This is especially apparent for the moment loads. This may at first seem like a large deviation between the two models; however, if we compile the cross-sensitivity coefficient matrix $[CSC]$ from Section 3.5.2 we see the effects are not severe.

According to the mathematical model we have the following cross-sensitivity coefficient matrix:

$$
CSC_{ij}(\%) =
\begin{bmatrix}
93.3 & 0 & -4.3 & 0 & 0 & 1.7 \\
0 & 93.3 & 4.3 & 0 & 0 & -1.7 \\
0 & 0 & 100 & 0 & 0 & 0 \\
0 & 0 & 0 & 100 & 0 & 0 \\
0 & 0 & 0 & 0 & 100 & 0 \\
0 & 0 & 0 & 0 & 0 & 100
\end{bmatrix}
$$

And according to the FE model we have the following cross-sensitivity coefficient matrix:

$$CSC_{ij}(\%) = \begin{bmatrix} 91.2 & 0 & -4.4 & 0.3 & 0 & 1.7 \\ 0 & 92.1 & 4.5 & 0 & 0 & -1.8 \\ 0 & 0.7 & 98.2 & 0 & 0 & 0 \\ 9.1 & -0.2 & -0.3 & 97.6 & -0.1 & -0.2 \\ 0.2 & 6.6 & 0.3 & 0 & 97.8 & 1.2 \\ -0.4 & 1.8 & -4.0 & 0 & 0.7 & 96.2 \end{bmatrix}$$

The results are presented in percentage. The largest deviation on the diagonal entries of the $[CSC]$ matrixes is only 3.8%. The largest variation is a 9.1% or 6.6% coupling effect the mathematical model was not able to detect.

Finally we use the same FE model to determine the first modal frequencies of the transducer. To complete this task we use the modal analysis feature in SolidWorks® since an analytical approach may present major difficulties on account of the complex geometry of the optimized transducer. Boundary conditions were incorporated in the FE modal analysis as presented in Figure 24.

The results were as follows:

Table 2: Modal analysis results

Mode	Modal Frequency (Hz)	Excitation
1st	1153	*Translation in Z*
2nd	1294	*Translation in X*
3rd	1294	*Translation in Y*
4th	2717	*Rotation about X*
5th	2717	*Rotation about Y*
6th	3294	*Rotation about Z*

In Table 2 the excitation refers to the displacement of the central hub. We see the lowest modal frequency is 1153Hz which is far higher than the minimum frequency that was specified in the design specifications.

At this point we have completed all the experimental objectives and attained all required results. The experimental investigation may now be addressed.

6. EXPERIMENTAL INVESTIGATION

An experimental investigation allows for the verification of the previously attained theoretical results and operation of the device. The experimental investigation was thus completed in two main phases. First, an experimental reconstruction of the theoretical investigation, as completed in Section 5, was required. This allowed for the verification of both the theoretical results and satisfactory operation of transducer. Second, the wheel force transducer was subject to operating conditions that tested the wheel force transducer in its entirety (i.e. the transducer, telemetry, angular transformation, strain compliance etc.).

In this section the experimental procedure and setup are discussed for both these phases of the investigation. The results of the investigation and discussions thereof will only be addressed in Section 7 of this report.

6.1. REQUIRED EXPERIMENTAL INVESTIGATIONS

6.1.1. CALIBRATION AND VERIFICATION OF THEORETICAL INVESTIGATION

During the theoretical investigation the transducer was fully characterized by the strain compliance matrix $[C]$ that was produced for both the mathematical and FE model. The cross-sensitivity coefficient matrix $[CSC]$ could be determined from the strain compliance matrix directly. It was therefore necessary to develop/design an experimental investigation that was able to determine the strain compliance matrix of the transducer. After this experimental strain compliance had been obtained it could be compared to that of the theoretical investigation. In completing such an investigation we are able to determine the accuracy and applicability of the theoretical investigation as completed in Section 5. Additionally the satisfactory operation of the transducer, with all the strain gauges, can be verified.

In order to reconstruct the strain compliance matrix experimentally we turn to the literature addressed in Section 3.7. Reconstruction of the strain compliance matrix is also known as calibration. The procedure to calibrate a transducer has therefore been addressed in Section 3.7.1 and is applicable to the transducer at hand. To avoid completely reiterating some points the procedure will only be briefly mentioned below:

- Fabricate a transducer as designed and incorporate strain gauges as presented in Figure 22. Create the six Wheatstone bridges such that the configuration as used in Equation (5.49) is achieved.

- Incorporate the telemetry system such that the strain signal from each Wheatstone bridge $(S_1; S_2; \dots S_5; S_6)$ can be recorded.

- Using the telemetry obtain the strain signals at zero loading. Incorporate these zero loading strain signals as offsets such that zero signal is produced at zero loading.

- Apply the maximum design loads statically to the transducer (or a fraction of the maximum loads) individually in each axis and note the strain signals generated by the six Wheatstone bridges.

- Reconstruct the strain compliance matrix $[C]$ using Equation (5.49) while accounting for the load reduction factor used during loading.

Upon completion of the calibration process the strain compliance matrix can be used to determine the cross-sensitivity coefficient matrix $[CSC]$. The theoretical results as produced in Section 5.2.6 can then be used for direct comparison.

6.1.2. GENERAL WHEEL FORCE TRANSDUCER TESTING

Developing an experimental strain compliance matrix, as addressed previously, may in theory fully describe the wheel force transducer in its operation. However during operation the wheel force transducer will be dependent on all the strain gauges, bridge configurations, telemetry system, angular monitoring and angular transformation. Calibration alone will not test all these various systems as it is completed statically. In order to ensure the angular position is correctly monitored and angular transformation correctly executed we require dynamic testing.

Dynamic testing can be completed in two manners. The first is by the utilization of a tyre tester to complete the general wheel force transducer testing as explained in Section 3.8.1. A tyre tester can be used to mimic dynamic operating conditions on the wheel force transducer while monitoring the input forces. The input forces as compiled by the wheel force transducer can then be compared to the input forces as measured by the tyre tester. The alternate method is to implement the wheel force transducer to the vehicle and run dynamic tests that will specifically

70

load certain axes. For instance, accelerating and braking tests should load the driving torque axis of the wheel force transducer.

The major advantage of utilizing the tyre tester is that it creates two sets of comparable data, thus the actual measurements may be verified. However, a tyre tester does not expose a wheel force transducer to the vehicle's operating conditions. Implementing the wheel force transducer to the vehicle has this advantage rather, but direct comparable data is not created.

The original plan for MSC 422 was to implement both these testing procedures; however, due to time constraints only one of the aforementioned two testing procedures could be completed. It was decided that implementing the wheel force transducer to the Baja vehicle and running field tests would provide more meaningful data since it would not only test the general operation of the device, but also the effectiveness of the design. In other words, this testing procedure would place the wheel force transducer in the position and conditions it was ultimately designed for.

An additional argument for the selected general testing procedure is that the calibration (Section 6.1.1) was completed for the transducer as a whole: The transducer is fabricated from a single piece of aluminium rather than comprising of several separate load cells in an assembly. The tyre tester may in effect therefore have created a redundancy, thus it was decided to implement the wheel force transducer to the Baja vehicle under the given time constraints.

The wheel force transducer was therefore installed and tested on the Baja itself. Specific tests were completed to load specific axes ($F_X'; F_Y'; F_Z'; M_X'; M_Y'; M_Z'$): It may be important to review Figure 1 for the load axes. For instance acceleration and braking tests produced high loads in F_X' and M_Z'. Additionally, driving the Baja in a tight constant radius produced high loads in F_Z' and M_X'. Other tests included a jump and towing test but will be further addressed later in Section 6.

At this point it is important to notice that three strain compliance matrixes exist that can be used in the wheel force transducer: That from the mathematical model, FE model and from calibration. The strain compliance as compiled during calibration should be used as it would most accurately characterize the specific transducer: The calibration strain compliance matrix will account for all defects in the transducer, strain gauges and in their misalignments. In addition the varying strain field under each strain gauge would not be approximated as being linear as done in the mathematical and FE model. Despite utilizing the calibration strain

71

compliance matrix on account of its higher applicability to the specific transducer, the three compliance matrixes should still correspond strongly.

6.2.   FABRICATION OF THE WHEEL FORCE TRANSDUCER

Before any experimental investigations could commence the wheel force transducer first had to be fabricated and assembled. Fabrication was completed over a much longer time span than expected resulting in the time constraints mentioned in Section 6.1.2. However, no major unexpected problems were encountered during fabrication as a result of the well completed design phase during the MOX 410 Design project. The following figure displays the center-piece of the design (transducer) with the selected KYOWA KFG-5-350-C1-23 aluminium strain gauges:
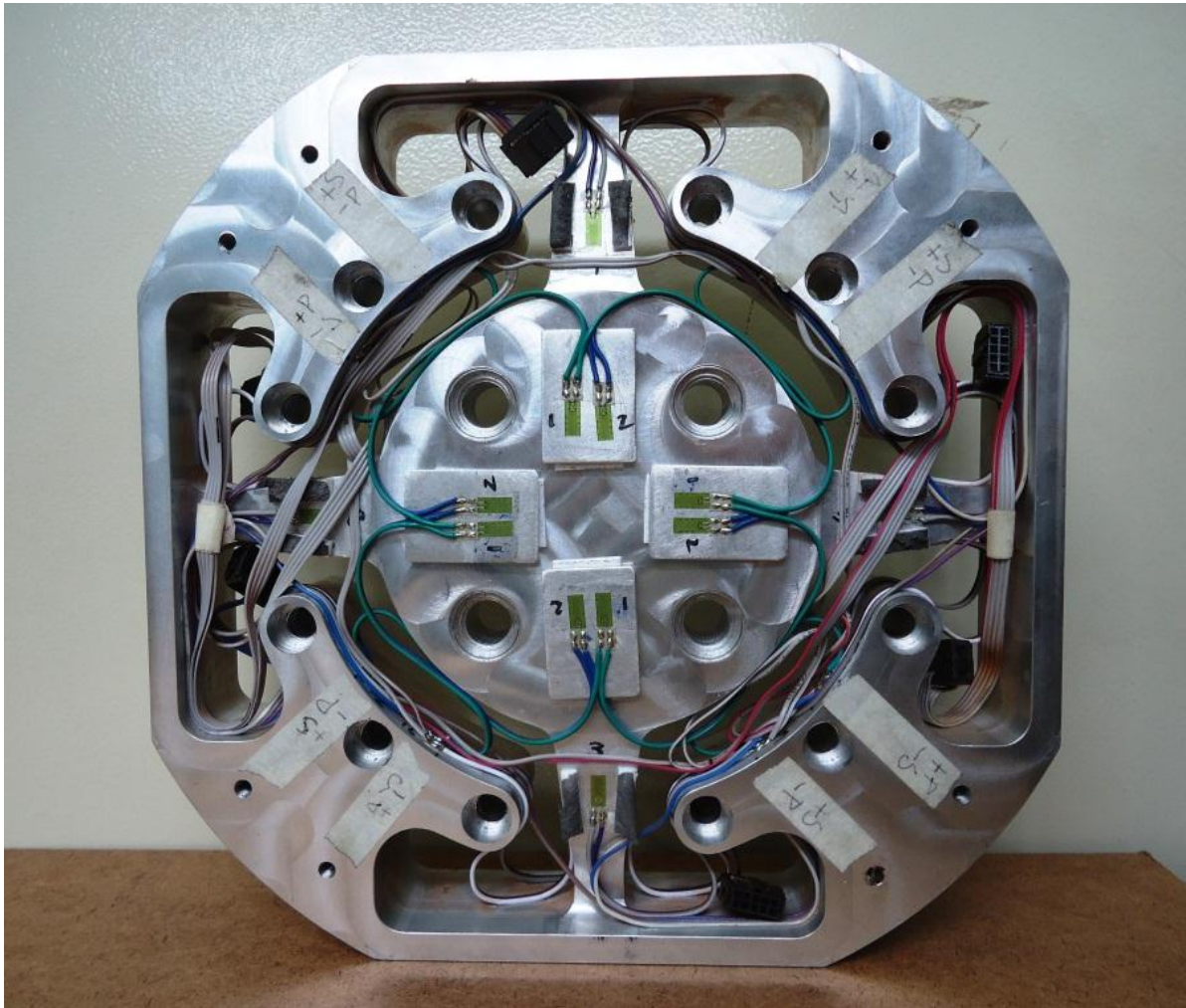
Figure 27: Fabricated transducer with strain gauges

The specific strain gauges were selected since they provided practical base dimensions of $9.4mm \times 4.2mm$ and a commonly used 350Ω resistance. It should be noted that the design is not perfect since the fabrication did reveal several small issues that can simply be avoided if another wheel force transducer were to be manufactured. Insights such as this can only be developed during fabrication and assembly and should constitute the second phase of the design process (prototype phase). The design could simply be improved as follows:

- Incorporation of electronic circuit boards to preserve space and reduce excessive wiring for the Wheatstone bridges.
- Increase the clearances during machining of the transducer such that larger ($\geq 10mm$) end mill machining bits can be used. This would reduce the cantilever deflection effect encountered during deep cuts as is required in the machining of the transducer.
- Increase the clearance at the strain gauges placed on the sides of the cantilever spokes. This refers to the strain gauges ε_9 to ε_{16} in Figure 22. Increasing the clearance would provide more working space while sticking the strain gauges.
- Provide sufficient space for the placement of dummy gauges.

These improvements do not fundamentally change the design or operation of the wheel force transducer. They would simply make the fabrication and assembly much easier.

6.3. EXPERIMENTAL EQUIPMENT FOR DATA TRANSMISSION

The wheel force transducer with its Wheatstone bridges forms only one part of the entire experimental setup. Equipment is still required to measure, amplify, convert, transmit and record the signals from the bridges and angular transducer. To create the necessary perspective a flow chart is included in the following figure to demonstrate the use of the communications equipment:
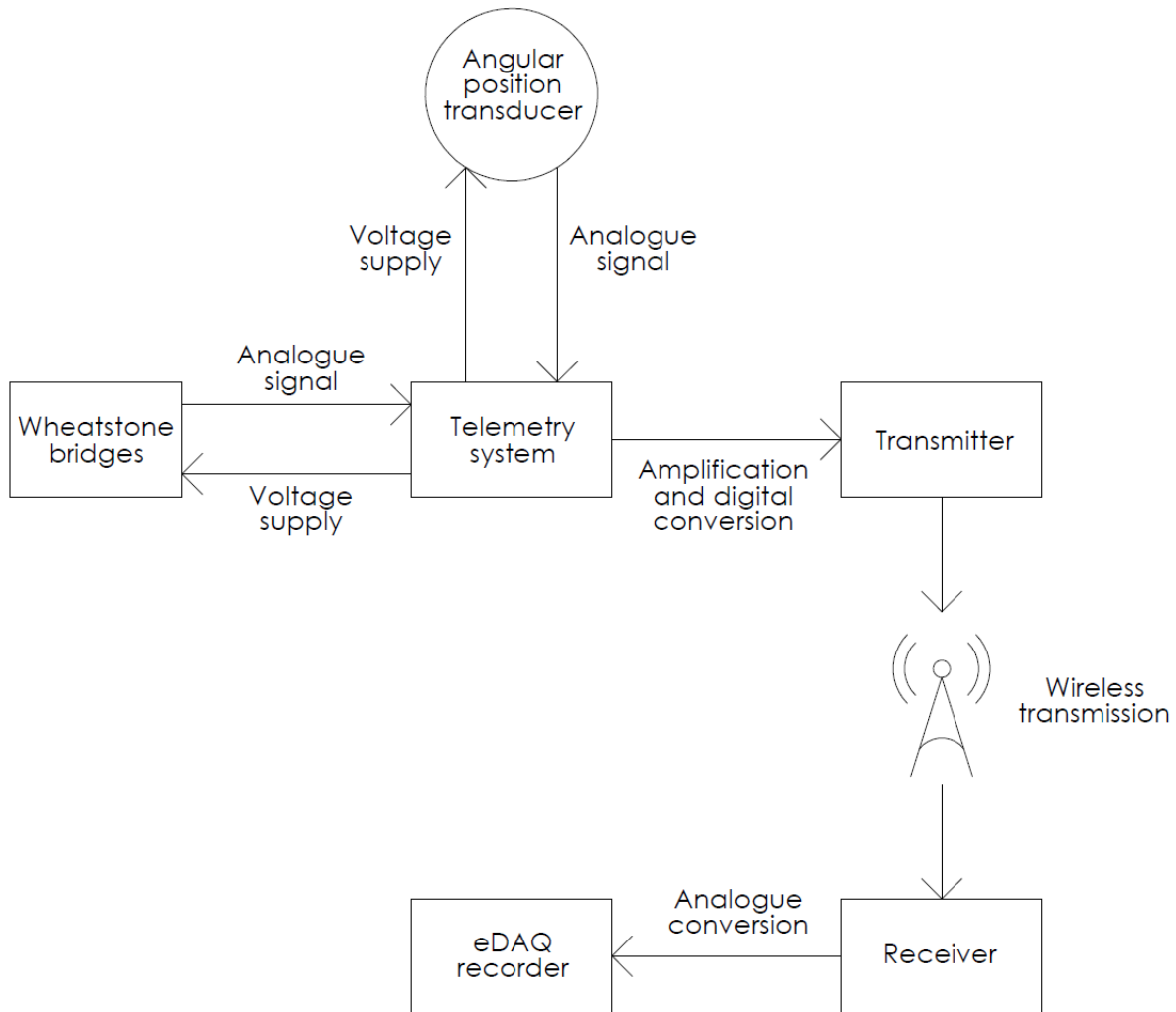
Figure 28: Communications equipment

With reference to the Figure 28 data is created and recorded as follows: The telemetry first creates a voltage supply of 4 Volts to the Wheatstone bridges on the transducer and potentiometers in the angular position transducer. Based on the position of the wheel and transmitted forces certain analogue voltage signals are received back from the transducers in each channel. These voltage signals are very small in magnitude thus are amplified by a factor of 1000 in the telemetry system. The amplified signal is then converted to a digital format for wireless transmission to the receiver. Finally the receiver converts the signal back to an analogue format for transmission to the eDAQ recording system. Data can then be recovered digitally from the eDAQ after yet again another digital conversion.

The wireless system is extremely beneficial as it eliminates the need for slip ring, thus reducing noise in the data. Unfortunately wireless systems are associated with low data transmission rates but even at high data frequencies the system could easily cope during the entire experimental investigation.

6.4.   DATA PROCESSING

The telemetry and eDAQ are responsible for initial low-pass filtering, however, data is still recorded with substantial noise. Post-processing of the data is required, on the software level, to reduce the effect of noise and improve the quality of the data.

Data is uploaded from the eDAQ recording system using SoMat TCE software and may be viewed with SoMat INFIELD analysis software. The field analysis software has limited capabilities thus data can be saved in text format and uploaded to a programming language with higher processing abilities. The student incorporated GNU Octave 3.6.2 for the post processing and analysis of data.

All data from the experimental investigation was required to undergo additional low-pass filtering to attenuate high frequency noise. The methodology incorporated was to transform to data to the frequency domain using a Fourier series. The data was then visible as the sum of simple oscillating functions with varying frequencies and magnitudes. A low-pass filter could be used to withdraw all functions with a frequency higher than a specified cut-off frequency. Generally a $20Hz$ cut off frequency was used as it conserved all important data while effectively reducing the noise. The data, now filtered, could be transformed back to the time domain and used to formulate results.

Due to the static manner in which calibration was completed, filtering was not required. Additionally data did not have to be transformed through the rotation matrix from Equation (3.1). The only processing for calibration was to relate the voltage signals through the applied static loads and to form the calibration matrix.

The Baja testing required extensive post processing: The data first had to be filtered (as explained above), multiplied through the calibration matrix (known at this stage) and then finally transformed through the rotation matrix to the static co-ordinate system of the vehicle. The

angular position of the wheel was first required before the data could be rotated. The position had to be determined from the two sequential potentiometers' voltage signal in the angular transducer. The two signals, offset in phase, changed linearly with the angular position of the wheel from and to a minimum to maximum voltage, or maximum to minimum voltage depending on the direction of rotation. The signal would rapidly drop from/to the maximum signal to/from the minimum signal when a full rotation had been completed. The angular position could be determined through the calibration of the potentiometers and by using the sequential voltage signals in the usable range of the potentiometers. The sine and cosine components of rotation could then be determined for the rotation matrix in Equation (3.1).

6.5. CALIBRATION EXPERIMENTAL SETUP AND PROCEDURE

The ideal procedure for the calibration of the transducer bas been outlined in Section 3.7.1 and briefly again in Section 6.1.1, thus will not be reiterated.

6.5.1. CALIBRATION EXPERIMENTAL SETUP

With the procedure and theory of calibration known, all that was left to establish was the means of applying known static loads to the wheel force transducer. At this point it may be important to review Figure 1 and Figure 2 for the load axes.

Before loads could be applied to the wheel force transducer a mounting rig had to be created that insured the transducer was stable and secure when placed under load. The rig is shown in the following figure with the transducer's coordinate system:
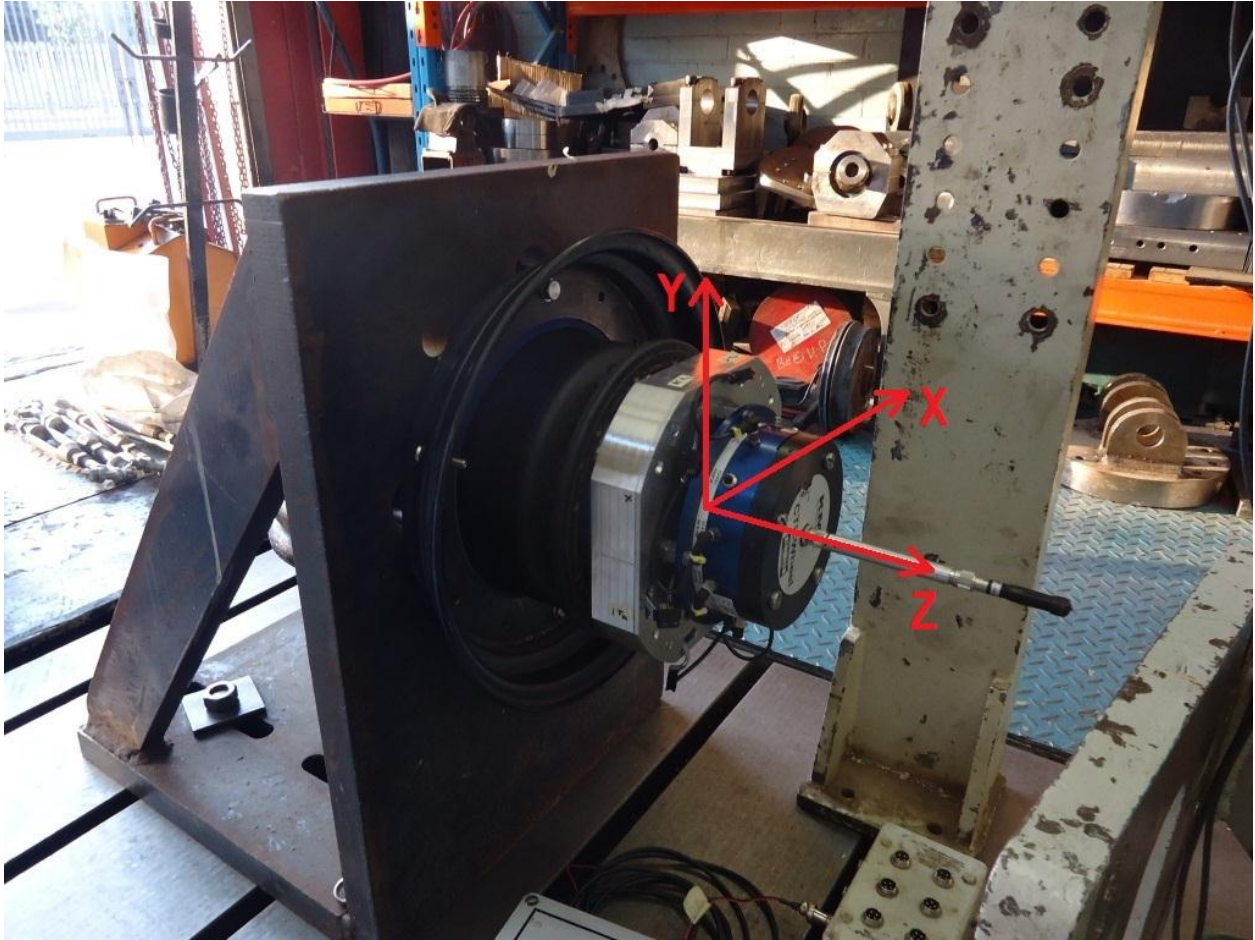
Figure 29: Calibration rig with transducer coordinate system

Here the rim (with the implemented transducer and telemetry) is seen clamped to a secure mounting rig. The rear-side of the rig (not shown) exposes the wheel hub for the application of loads to be transmitted through the hub, transducer, rim and finally to the mounting rig (all loads pass through the transducer as required).

In the ideal calibration process pure loads are applied to the transducer (F_X; F_Y; F_Z; M_X; M_Y; M_Z). Applying a pure static axial torque was simple to accomplish. The torque M_Z was applied using two universal couplings and a moment arm. The couplings insured only an axial torque was transmitted through to the wheel hub, and therefore transducer, as seen in the following figure:
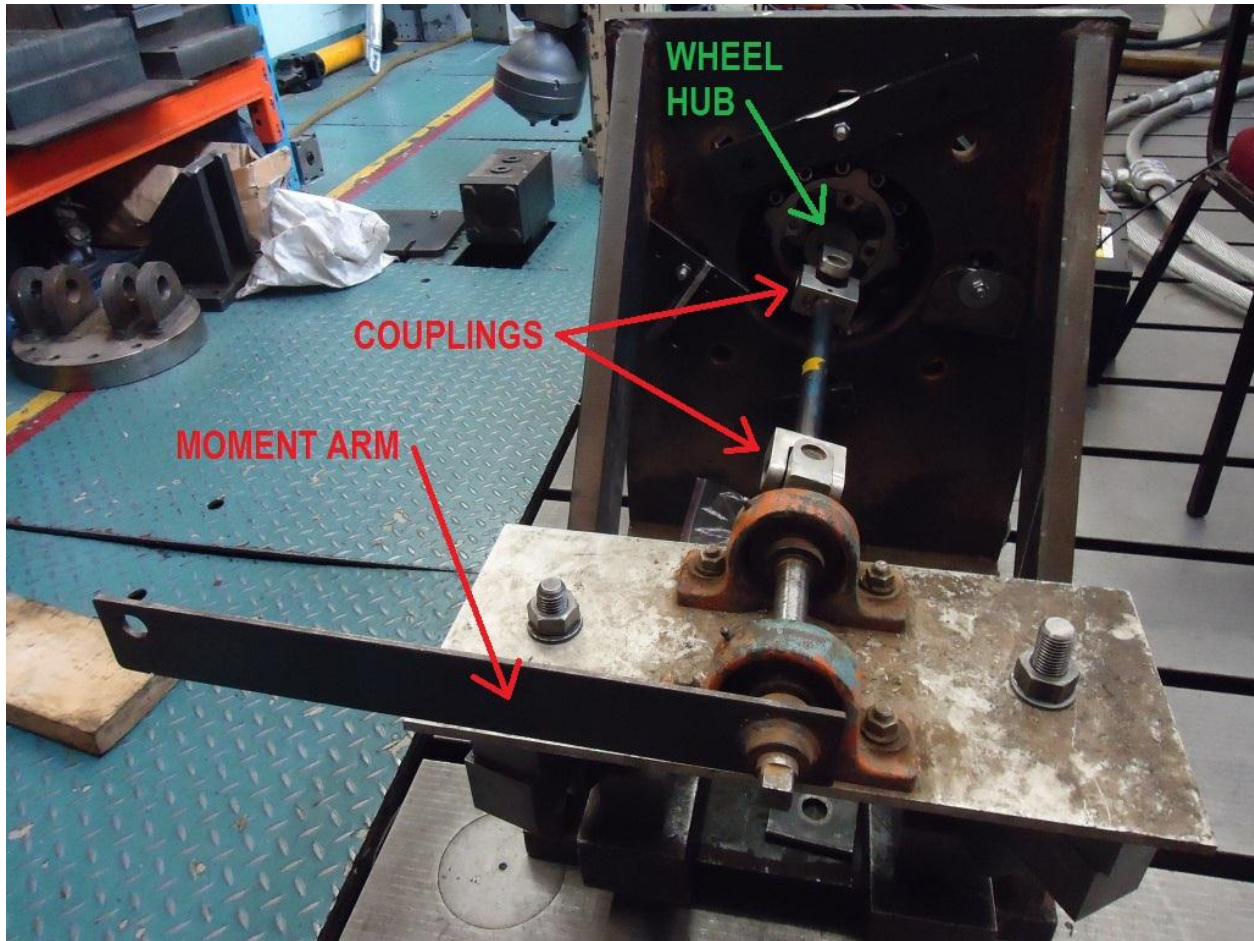
Figure 30: Torque applicator for calibration

The end of the moment arm with had an effective and sufficient cantilever length of $435mm$. Weights could simply be applied at this location to create the desired moment load. The loads F_X, F_Y, M_X and M_Y could not be applied purely to the system. It was decided to use a cantilever beam with weights to apply loads F_X and M_Y simultaneously to the system. By altering the cantilever length but maintaining the applied weights, the load F_X would remain constant while M_Y would vary. The effects on the strain sensors due to F_X and M_Y could be separately resolved for provided at least two different cantilever lengths were used. The same applies to the loads F_Y and M_X. The following figure illustrates the use of weights on an adjustable cantilever:
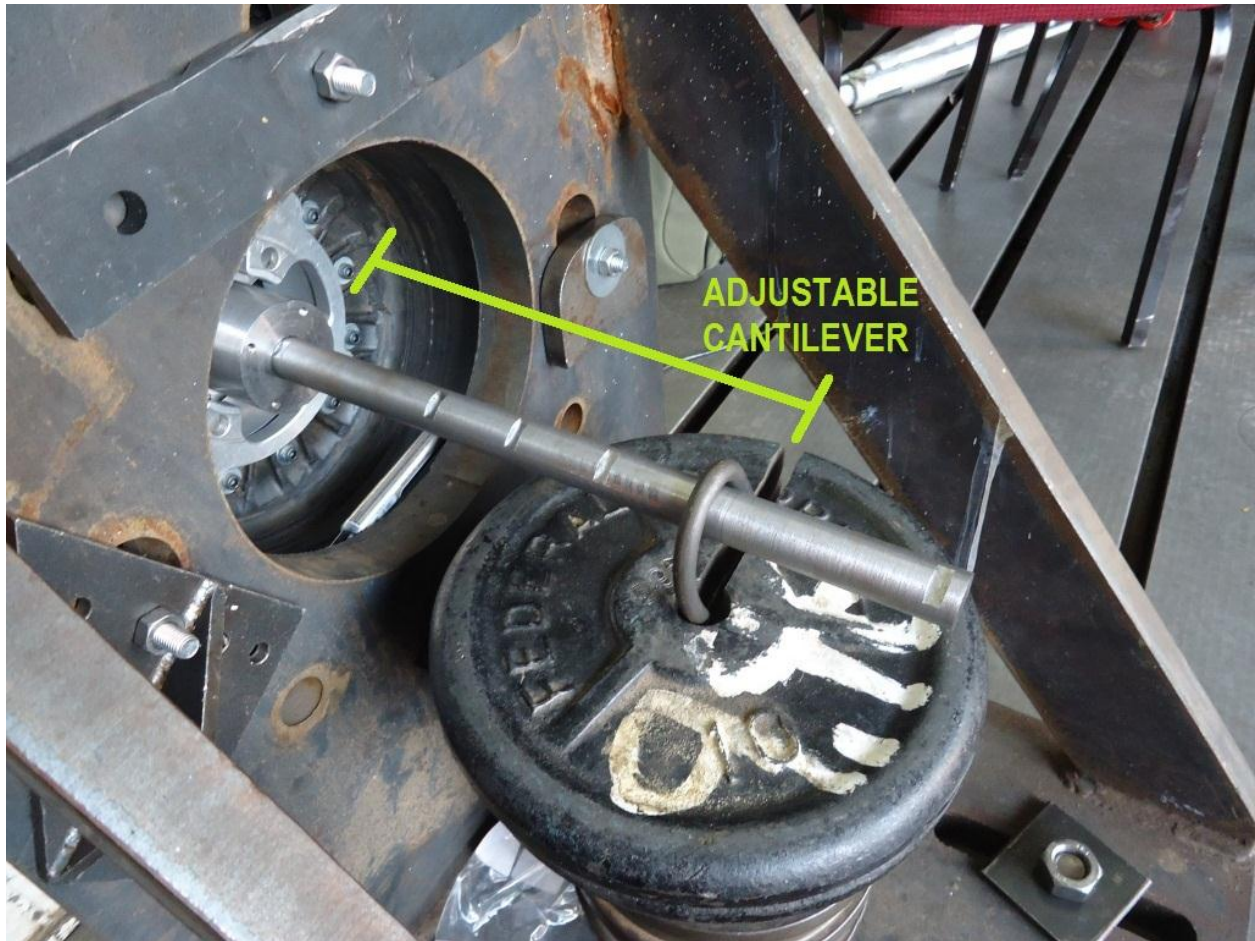
Figure 31: Force and moment applicator for calibration

A spirit level was used to insure the wheel force transducer was level such that the loads were applied purely on the axes in question. Finally the mounting rig could be rotated through 90° such that weights could be hung through the central axis of the transducer to apply the pure load F_Z. This is illustrated in the following figure:

Figure 32: Axial force applicator for calibration

6.5.2. CALIBRATION EXPERIMENTAL PROCEDURE

The loads were applied to the system as outlined in Section 6.5.1. The loads F_X, F_Y, M_X, M_Y and M_Z could be completely reversed (applied in the opposite direction) using the existing setup. Collecting data for the loads applied in both directions would insure the Wheatstone bridges operated as expected provided the forward and reverse effects differed only in direction and not magnitude of the signal.

The design loads of the system could not be reached using the experimental setup presented. As explained before, a fraction of the design loads may be used for calibration due to the linearity of the transducer under deformation. Higher loads would provide more accurate calibration data, thus loading was still maintained as high as possible while complying with the given space restrictions of the experimental setup. The following table summarizes the loading used during calibration:

Table 3: Summarized calibration loading

Test No.	Load Axis	Force (N)	Load Axis	Moment (Nm)
1	F_X	∓600.3	M_Y	±290.2
2	F_X	∓600.3	M_Y	±230.1
3	F_Y	±600.3	M_X	±290.2
4	F_Y	±600.3	M_X	±230.1
5	F_Z	-588.6		
6			M_Z	±175.8

The loads were slowly applied to the system and then allowed to fully stabilize before the loads were removed. Prior to loading, the axes were zeroed using the telemetry system, however, exactly zeroing the system was not necessary. Rather the voltage signals before and after loading were noted, thus the pure effect due to the loading could be determined. Zeroing the system only insured the Wheatstone bridges operated within the working range of the telemetry system.

The voltage signals before and after loading provided an 'average base' from which the signals were measured during loading. This provided a means of accounting for the hysteresis during loading, however, was not entirely necessary since the signals before and after loading did not have appreciable variations during calibration. Additionally, it was found that when the loads were reversed, the magnitude of the generated did not vary significantly. Despite this, the average signal was still used. This demonstrated that the Wheatstone bridges operated correctly during calibration. The calibration data has been included in Appendix D and not in the main report to maintain coherency.

At this point the effect of various pure loads on the system could be determined from the collected data. A strain compliance matrix could therefore be directly assembled according to the previously addressed theory, however, it described the system in terms of $mV/design\ load$. The strain compliance matrix in this format would be used for the remaining experimental investigation as it did not require conversion of the data received from the eDAQ.

For direct comparison to the theoretical results we required the compliance matrix to describe the system in terms of $strain/design\ load$. Thus it was necessary to convert the voltage signal to strain. This could simply be accomplished by considering the theory addressed in Section 3.4 and Equation (3.16):

$$V_{out} \cong \frac{1}{4} K_s \, \varepsilon V_{in} \qquad (6.1)$$

Equation (6.1) describes the input-output voltage relation for a quarter Wheatstone bridge. In consideration of the half and full Wheatstone bridges utilized in the transducer we have:

$$V_{out} \cong \frac{1}{2} K_s \, \varepsilon V_{in} \; \rightarrow Half\ bridge$$
$$V_{out} \cong K_s \, \varepsilon V_{in} \; \rightarrow Full\ bridge \qquad (6.2)$$

Where ε is the effective measured strain described by Equation (5.49). By accounting for the gain and excitation voltage of the telemetry system we can simply solve for the measured effective strain:

$$\varepsilon \cong \frac{2 \times V_{out} \times (Telemetry\ Gain)}{K_s \times V_{in}} \; \rightarrow Half\ bridge$$
$$\varepsilon \cong \frac{V_{out} \times (Telemetry\ Gain)}{K_s \times V_{in}} \; \rightarrow Full\ bridge \qquad (6.3)$$

Where $V_{in} = 4V$, $K_s = 2.11$ for the implemented strain gauges and $Telemetry\ Gain = 1000$. It should be noted that the half and full bridge distinction is required since the 'dummy gauges' do not contribute toward the effective measured strain ε. Thus in considering Equation (5.49) the Wheatstone bridges C_{3i} and C_{6i} will required the full bridge conversion and the remaining bridges the half bridge conversion in Equation (6.3).

With this the compliance matrix could be determined in terms of micro-strain as done in the theoretical investigation allowing for direct comparison. This is the scope of Section 7.

82

6.6. BAJA TESTING EXPERIMENTAL SETUP AND PROCEDURE

General testing of the wheel force transducer in its entirety is required for a complete experimental investigation. Additionally it would provide evidence that the device meets all design specifications as imposed by the Baja vehicle.

6.6.1. BAJA TESTING EXPERIMENTAL SETUP

Prior to the field testing the wheel force transducer was assembled to the Baja vehicle. The following figure illustrates the wheel force transducer on the Baja without the telemetry system:

Figure 33: Wheel force transducer on the Baja without the telemetry system

In Figure 33 we see the wheel force transducer attached to the rear left tyre. Finally the following figure illustrates the assembly of the wheel force transducer with the telemetry and angular positioning equipment:

Figure 34: Wheel force transducer with the telemetry and angular positioning equipment

The blue piping in Figure 34 maintained the position of the angular transducer as the wheel rotated. All the equipment as was required on the wheel is illustrated in this figure. The remaining equipment (eDAQ, receiver, power distribution box and wiring) was fastened to the roof of the vehicle. This is illustrated in the following figure:

Figure 35: Communications equipment on the Baja

6.6.2. BAJA TESTING EXPERIMENTAL PROCEDURE

With the fabrication and assembly completed, all that remained was to complete a series of tests that would specifically load certain axes of the wheel. The following table summarizes the completed tests and the associated targeted axes that were loaded:

Table 4: Baja test maneuvers

Maneuver/Test Name	Targeted Axis/Axes
Accelerating and braking	• Driving torque M_Z' • Longitudinal/tractive force F_X'
Tight constant radius turns (both directions)	• Over turning moment M_X' • Lateral force F_Z'
Towing	• Longitudinal/tractive force F_X' • Vertical load F_Y' • Driving torque M_Z'
Jump	• General all-round heavy loading

Before the maneuvers were executed a zeroing test was completed. The wheel with the transducer was held in mid-air and rotated such that sinusoid signals were generated by the transducer's active strain sensors. In that manner the center of oscillation (zero-point) could be determined for each channel. This test was also completed after the maneuvers were completed to reevaluate the zeros and insure that they had not drastically changed.

Since each test would last several minutes, triggers were placed at the critical points of the experiment. This created distinct points in the data indicating the time at which a maneuver would be completed (e.g. just a second before the vehicle jumped to avoid having to analyse the run-up).

Each maneuver is briefly explained in the following subsections.

6.6.2.1.   ACCELERATING AND BRAKING

The Baja was accelerated to top speed as fast as possible and then braked such that all four wheels locked up. The following figure displays the drastic braking maneuver:

Figure 36: Baja braking maneuver

6.6.2.2.   TIGHT CONSTANT RADIUS TURNS

The Baja was driven as quickly as possible around a $4m$ radius on the inner wheels in both the clockwise and anticlockwise directions. Several rotations were completed in every direction over level yet rough terrain.

6.6.2.3. TOWING

The Baja was used to tow a vehicle with the tow rope fastened as follows:

Figure 37: Baja towing maneuver

The tow rope was fastened high above the center of the rear wheels to create a pitching effect that lifted the front wheels off the surface. This combined with the absence and a slip differential meant all loads were being carried equally by the rear wheels. This was necessary since the tow rope was linked to a separate load cell measuring the tension that would provide data for further verification of the wheel force transducer i.e. the tension in the tow rope could be compared to the tractive force measured by the wheel force transducer.

The Baja would initially accelerate the towed vehicle but would eventually be slowed to standstill as the brakes in the towed vehicle were gradually applied. The maximum towing ability of the Baja could then be determined.

6.6.2.4. JUMP

To mimic the driving conditions of the Baja during a competition a small jump was completed to create high loading in the wheel force transducer. The following figure illustrates the Baja lifting off the ground as it hit the ramp:

Figure 38: Baja jumping maneuver

6.7.   EXPERIMENTAL INVESTIGATION SUMMARY

The experimental procedure and setup has been described for the calibration and general testing of the wheel force transducer. The results obtained by these investigations will be the scope of Section 7.

6.8. BUDGET AND EXPENDITURE

6.8.1. OVERVIEW

If the wheel force transducer, as research in this project, were implemented independently it would not have been possible. This is due to the extremely high expenses associated with telemetry and data recording systems. Since similar research was already being undertaken in the Vehicle Dynamics Lab at the University of Pretoria all these facilities were readily available to the student for use on the project. Additionally, external labour and machining costs were avoided since all fabrication was completed internally.

Another major advantage to the selected research project was the University of Pretoria Baja Team association. The student received invaluable assistance from both members of the Baja Team and Vehicle Dynamics Research Group. All equipment necessary for the fabrication and assembly of the wheel force transducer was made freely available to the student through these research groups. In many cases the student was able to utilize existing stock from the workshops made available to them. It was only necessary to purchase the high grade aluminium for the transducer itself. This combined with the strain gauges and adhesive formed the only major expenses of the wheel force transducer.

6.8.2. COST SUMMARY

The following major costs were incurred in the research project:

Table 5: Major project costs

Aluminium stock for the transducer	R2750
Strain gauges with required adhesive	R3100
Total	**R5850**

These notable costs are related to the transducer which forms the major component in the project. No other major costs were incurred. A strict budget was not put in place for the research project; however, the total expenditure was not expected to exceed R8000. As seen in the total cost this limit was not exceeded.

7. RESULTS

With the experimental investigation completed as outlined in Section 6, results were obtained to verify the operation of the wheel force transducer and theoretical modeling. In this section the calibration results will be discussed followed by the results obtained during the Baja tests. The calibration results are discussed in a quantitative manner while the Baja test results have been approached more qualitatively (explained by reason).

7.1. CALIBRATION RESULTS

The data from the calibration procedure has been included in Appendix D. The strain compliance matrix was very easily assembled from this data according to the theory addressed in Section 3.5.2 (simple substitution into the strain compliance matrix).

The following experimental strain compliance matrix was obtained:

$$C_{ij}(10^6) = \begin{bmatrix} 361.1 & -13.9 & 7.2 & 6.3 & -16.9 & 0.3 \\ 5.1 & 369.0 & 10.6 & 18.4 & -12.0 & -10.1 \\ -16.4 & 10.4 & 310.2 & -4.8 & -6.7 & -0.6 \\ 1.7 & -0.5 & 37.7 & 1623 & 7.1 & 11.7 \\ -19.4 & -1.0 & -26.8 & -7.4 & 1617 & 53.4 \\ 1.2 & -8.5 & 0.1 & -9.9 & 0.7 & 918.4 \end{bmatrix}$$

The results are presented in micro-strain per maximum/design load. The design loads were presented in Section 5. For convenience the compliance matrixes as obtained during the theoretical investigation are provided again for direct comparison.

According to the mathematical model we had the following strain compliance matrix:

$$C_{ij}(10^6) = \begin{bmatrix} 359.1 & 0 & 0 & 0 & 0 & 0 \\ 0 & 359.1 & 0 & 0 & 0 & 0 \\ -12.9 & 12.9 & 301.3 & 0 & 0 & 0 \\ 0 & 0 & 0 & 1562 & 0 & 0 \\ 0 & 0 & 0 & 0 & 1562 & 0 \\ 12.9 & -12.9 & 0 & 0 & 0 & 769.7 \end{bmatrix}$$

And according to the FE model we had the following strain compliance matrix:

$$C_{ij}(10^6) = \begin{bmatrix} 341.6 & 0 & 3.1 & 34.0 & 0.9 & -1.6 \\ 0 & 340.9 & 2.5 & -0.7 & 24.5 & 6.7 \\ -13.7 & 13.9 & 306.1 & -0.9 & 1.0 & -12.4 \\ 4.7 & 0 & 0 & 1581 & 0 & 0 \\ 0 & -0.1 & 0 & -0.1 & 1583 & 11.1 \\ 14.4 & -15.3 & -0.2 & -1.9 & 9.7 & 803.7 \end{bmatrix}$$

The cross-sensitivity coefficient matrix $[CSC]$ (from Section 3.5.2) for the experimental compliance matrix is also given:

$$CSC_{ij}(\%) = \begin{bmatrix} 89.2 & 1.27 & -4.6 & 0.1 & -1.2 & 0.1 \\ -3.4 & 91.5 & 2.6 & 0.0 & -0.1 & 0.9 \\ 1.8 & 2.6 & 79.0 & 2.3 & -1.6 & 0.0 \\ 1.6 & 4.6 & -1.2 & 97.2 & -0.5 & -1.0 \\ -4.2 & -3.0 & -1.7 & 0.4 & 97.4 & 0.1 \\ 0.1 & -2.5 & -0.2 & 0.7 & 3.2 & 92.34 \end{bmatrix}$$

7.2. DISCUSSION OF CALIBRATION RESULTS

The diagonal elements of experimental strain compliance matrix corresponded well to the experimental results. When considering the diagonal elements i.e. C_{ii} we see the experimental and FE model deviate as follows using the FE model as the reference:

Table 6: Experimental and theoretical calibration results and errors

	C_{11}	C_{22}	C_{33}	C_{44}	C_{55}	C_{66}
Axis	F_X	F_Y	F_Z	M_X	M_Y	M_Z
Experimental ($\mu\varepsilon$)	361.1	369.0	310.2	1623	1617	918.4
FE ($\mu\varepsilon$)	341.6	340.9	306.1	1581	1583	803.7
Error (%)	5.7	8.2	1.3	2.7	2.1	14.3

All the diagonal elements (except C_{66}) correspond well within 10%. The torque axis, which deviates by 14.3%, presents the only significant deviation.

The coupling experienced in the experimental strain compliance matrix (non-diagonal elements) has no strong correlation to either the mathematical or FE model. This may be a result of many factors such as:

- Strain gauge misalignments from the intended angle

- Strain gauge off-sets from intended position

- Strain gauge defects

- Defects/stress concentrations in the transducer from fabrication

The coupling in the transducer will be much more sensitive to these defects since decoupling the system relies heavily on perfect fabrication and application of strain gauges. However, since this is extremely difficult to accomplish we have an experimental strain compliance that fully describes the system with all defects included. The experimental cross-sensitivity coefficient matrix does therefore not produce any comparable/meaningful data.

Thus regardless of the deviations from the theoretical model, the forces and moments may be resolved for using the experimental strain compliance. However, we know the transducer operates as expected since the main diagonal elements correspond very well to the theoretical results. At the same time the mathematical model has been verified thus the optimization of the transducer as done during the theoretical investigation was effective.

7.3.   BAJA TESTING RESULTS AND DISCUSSION OF RESULTS

The experimental investigation was completed as outlined in Section 6, unfortunately it was found that the channel representing the driving and braking torque M_Z' did not function as expected. This was only detected upon completion of the tests, thus was not rectified for the experimental testing on the Baja.

An investigation was completed to determine the cause of the malfunctioning channel. When the test data was examined more closely it was found that the M_Z' channel (channel 6) had offset twice from the original zero position. It was found that the port connecting the channel 6 Wheatstone bridge to the telemetry had faulty pins (the pins were loose in the port). During the post-experimental investigation these pins were deliberately removed and it was found that aforementioned examined offsets could be recreated. This confirmed that it was the faulty port/connections that had caused the malfunctioning channel (the transducer and strain compliance theory were not at fault).

The remaining five channels were securely connected and did produce the expected results as will be illustrated. Since the M_Z' produced meaningless data it will not be presented in the results.

The results are presented and discussed according to the performed maneuver in the subsections to follow. Additionally it should be noted that the standard vehicle dynamics sign convention and axis system, as recommended by Thomas D. Gillespie, has been used (D, Gillespie Thomas, 1992). However, the overturning moment and aligning torque are measured at the center of the transducer rather than the tyre contact patch since the wheel force transducer is being verified rather than the dynamics of the Baja vehicle.

To summarize the measured forces and moments in conjunction with Figure 1, the table is presented:

Table 7: Active axes during Baja tests

Force/Moment as presented in Figure 1	Standard terminology	Active in Test
F_X'	Tractive force	Yes
F_Y'	Vertical force	Yes
F_Z'	Lateral force	Yes
M_X'	Overturning moment	Yes
M_Y'	Aligning torque	Yes
M_Z'	Driving/braking torque	No

7.3.1.   ACCELERATION AND BRAKING
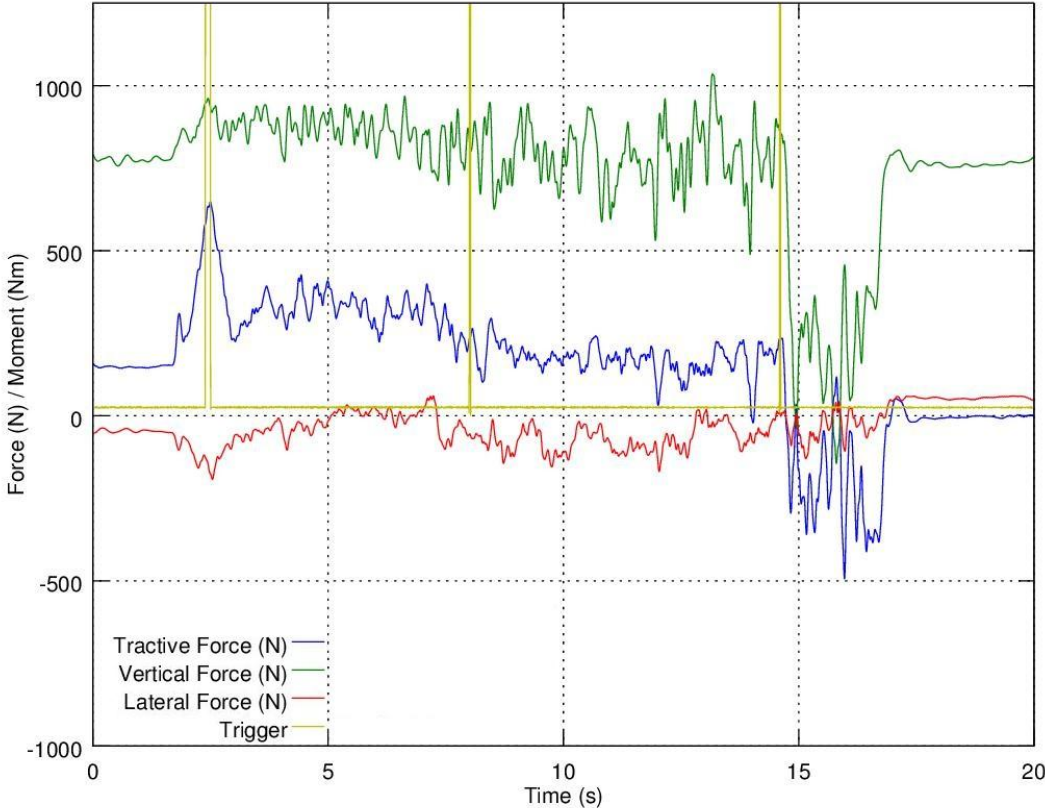
Figure 39: Acceleration and braking maneuver Baja test results (1)
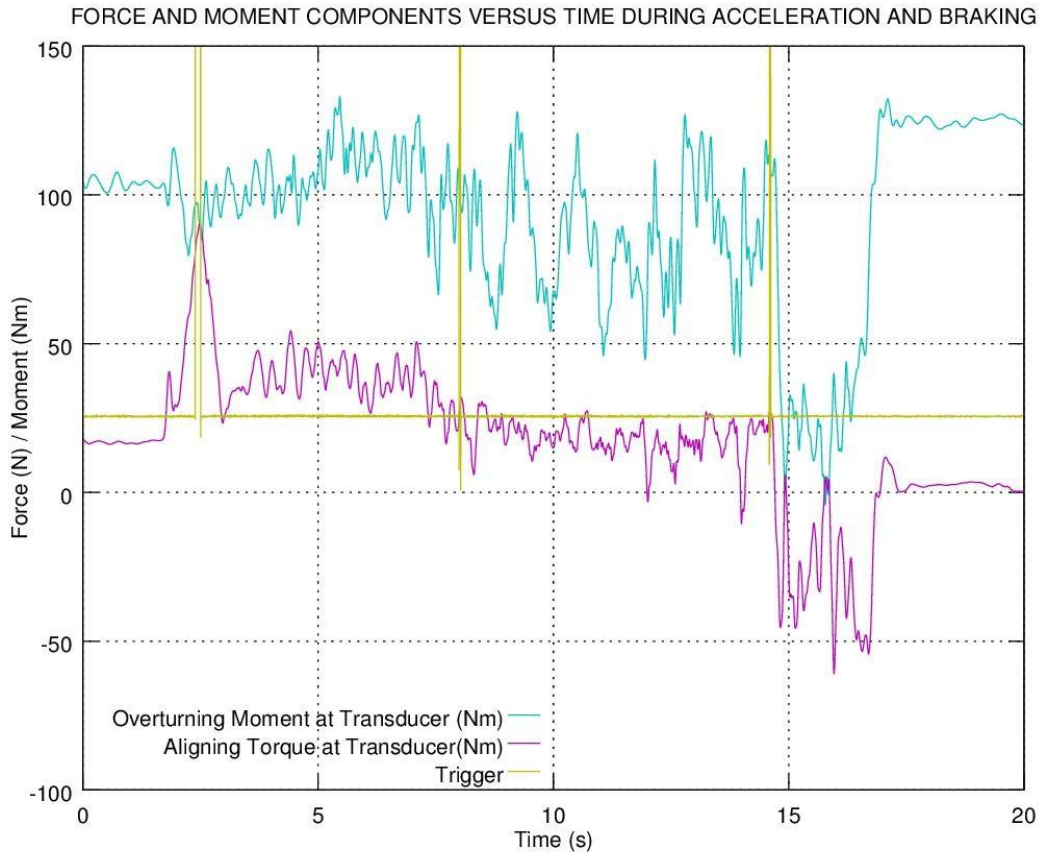
Figure 40: Acceleration and braking maneuver Baja test results (2)

The plots presented signify the forces and moments generated at the transducer as the Baja is fully accelerated from standstill to a maximum speed and then braked with full lock-up. The trigger is activated at three points: First at initial pull away, then at top speed and finally at the point where braking commences.

The plots contains a significant amount of data, however, we start by explaining the static loads before the vehicle has set off. The vertical loading of approximately $830N$ corresponds well to the expected normal loading per rear wheel. Additionally a constant offset in overturning moment is expected due to the normal loading and cantilever effect of the transducer on the outside of the wheel. Initially slight off-sets are seen in the tractive force and aligning torque due to the negative slope the Baja accelerated from. These force and moment components return to zero after braking and returning to standstill on a level surface (at a time of 18 seconds).

96

During acceleration a positive tractive force is expected to create a net positive accelerating force. This is clearly seen in the plots with a maximum tractive force upon pull-away. The tractive force decays as the Baja reaches its maximum speed, but never returns to zero. This signifies the non-zero demand forces from drag, rolling resistance, friction in the front wheels etc.

Upon braking a negative tractive force is experienced as expected. The deceleration causes a drastic weight transfer to the front wheels due to the height of the center of gravity, and thus the vertical loading on the rear wheels decrease as expected. This in turn reduces the maximum braking force that can be applied to the surface (from the dry friction rule), thus a major dependence is seen between the vertical loading and tractive force.

The sudden decrease in vertical loading reduces the overturning moment as seen in the plots. The initial positive overturning moment was induced by the vertical loading itself, thus decreasing the vertical loading will decrease the overturning moment. The aligning torque is similarly effected by the tractive force due to the same cantilever, thus the dependence of the aligning on the tractive force can be clearly noted on the plots.

No significant lateral forces were generated as expected in an acceleration and braking test. It was found that the generated data was noisy (had large oscillations). This, however, is expected since the tests were completed off-road (over rough terrain). Additionally the thread pattern on the tyres were typical of all-terrain-vehicles, thus were very coarse and would contribute to the noise. This presence of noise was seen across all the completed tests.

7.3.2. CONSTANT RADIUS TURNING

7.3.2.1. OUTER WHEEL MEASUREMENTS

FORCE AND MOMENT COMPONENTS VERSUS TIME DURING CONSTANT RADIUS TURNS: OUTER WHEEL
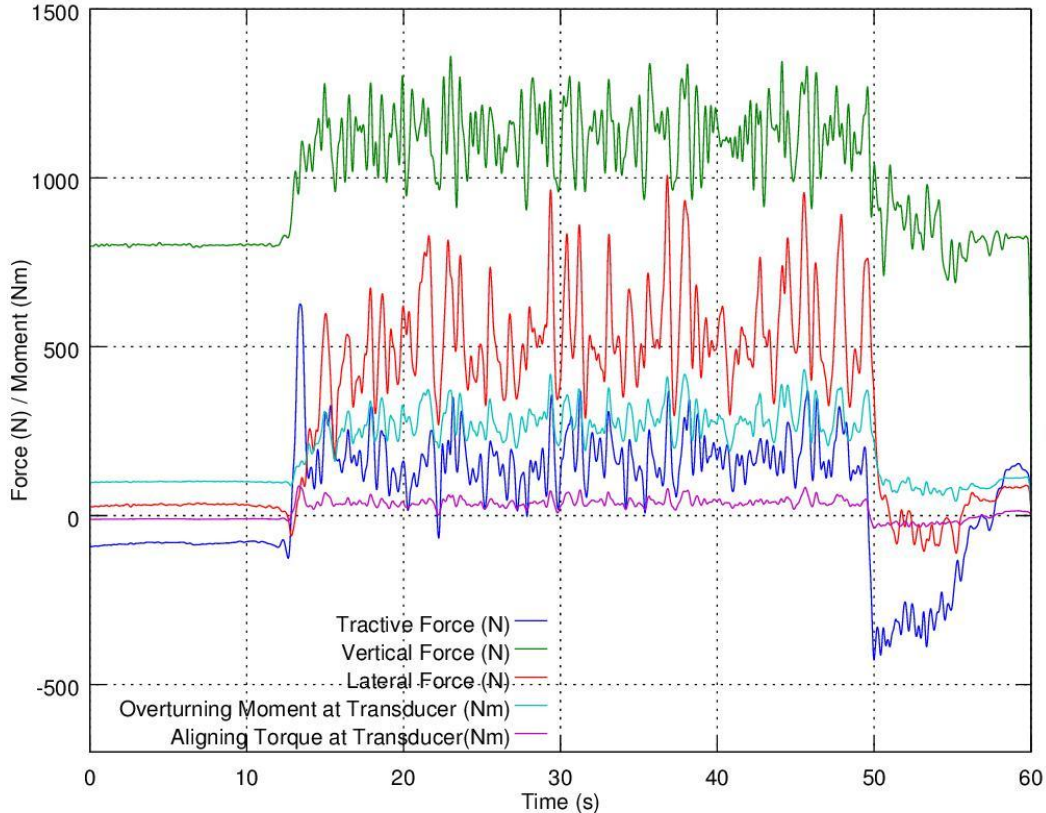
Figure 41: Constant radius turning maneuver Baja test results (outer wheel)

The plot illustrates steady state cornering that was accomplished between approximately 15 and 50 seconds. In this time approximately five circulations were completed such that the inner wheels rotated about a 4 meter radius. The results presented are the forces and moments experienced on the transducer placed on the outer wheel. Large oscillations are seen in the data due to the rough terrain over which the turns were completed.

Due to the centripetal acceleration and high center of gravity, load was transferred to the outer wheels. This is evident in the increased vertical loading which it turn increases the overturning moment as it did in the accelerating and braking test. However another positive contributor to the increased overturning moment is the increased lateral loading through the rolling radius of the wheel. It should be remembered that the lateral and vertical loads will both positively effect the

98

overturning moment since the transducer lies outside the wheel. If the transducer was placed toward the inside of the wheel the cantilever would be reversed on the vertical load thus would effect the overturning moment oppositely to the lateral force (the lateral force would still maintain its cantilever through the rolling radius).

Of major importance in the constant radius turns is the lateral force generation. The lateral force increased greatly to oscillate about $550N$ signifying the centripetal acceleration of the Baja around the 4 meter radius.

7.3.2.2.   INNER WHEEL MEASUREMENTS
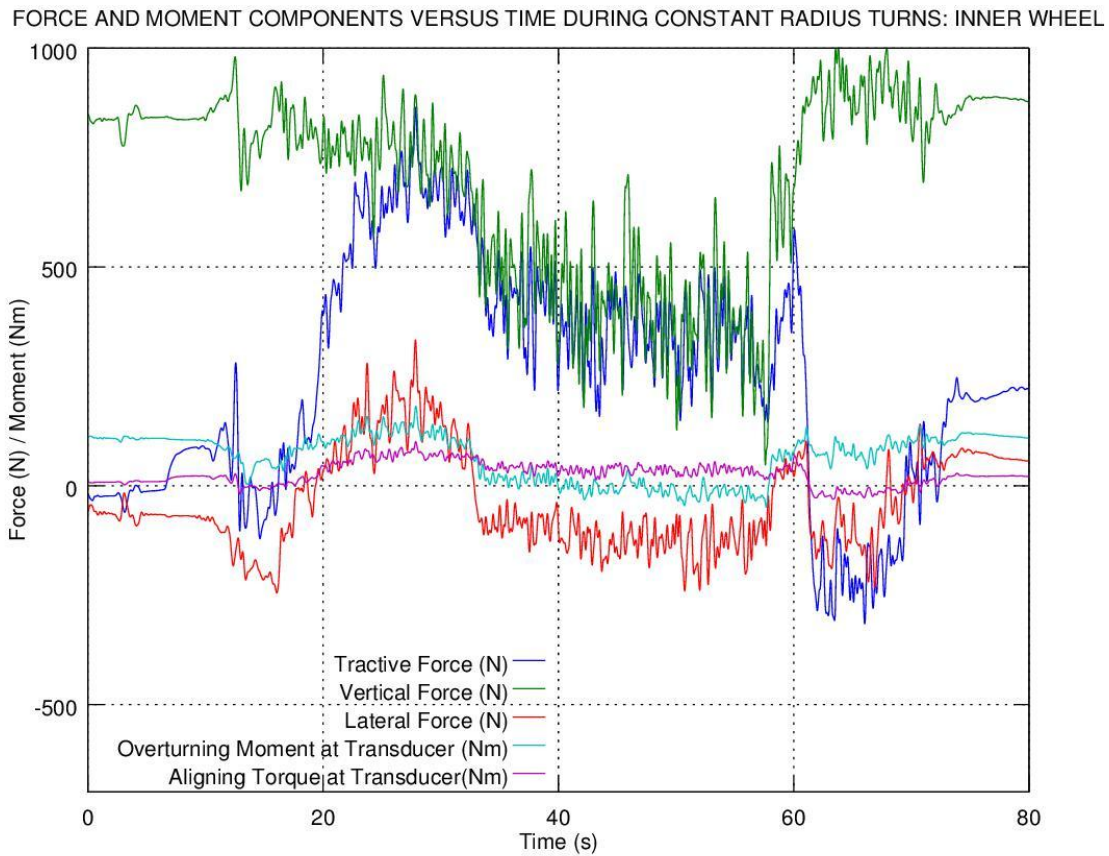
Figure 42: Constant radius turning maneuver Baja test results (inner wheel)

The plot illustrates steady state cornering that was accomplished between approximately 35 and 55 seconds. In this time approximately four circulations were completed such that the inner wheels rotated about a 4 meter radius. The results presented are the forces experienced on the transducer placed on the inner wheel.

The forces and moments are in agreement to that presented on the outer wheel measurements. Since load is transferred to the outer wheels, the vertical loading must be reduced on the inner wheels. This is evident in the presented data. Additionally the lateral force is reversed as expected, however, differs greatly in magnitude compared to the outer wheel measurements. This reduction is due to the wheels inability to generate additional lateral load when the vertical loading is reduced. From the data it is clear that the outer wheels are mainly responsible for lateral force generation during such turning maneuvers. The inner wheels only marginally contribute.

Another point of interest is the tractive force generated on the outer and inner wheels: Since the Baja has no slip differential the inner rear wheel transfers a higher tractive force than the outer rear wheel.

7.3.3. TOWING
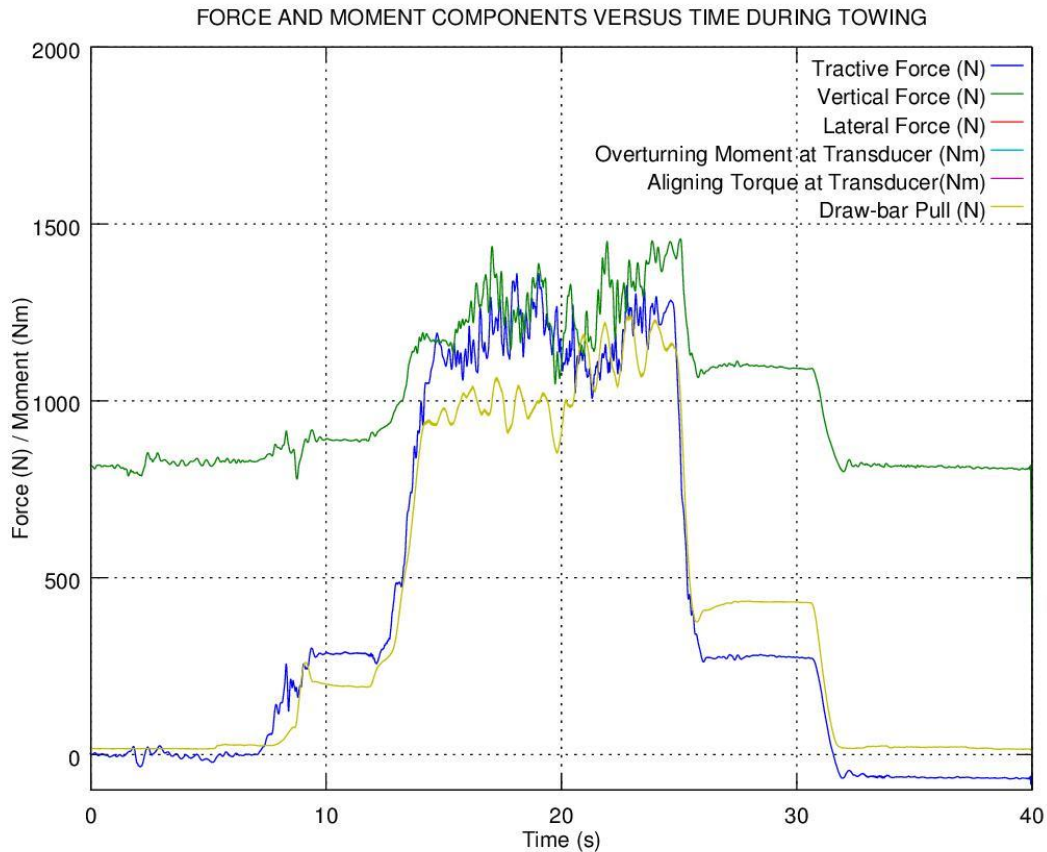
Figure 43: Towing maneuver Baja test results

A plot is shown illustrating the forces and corrected draw bar pull generated during the towing test. The moment components have been excluded from the results since they did not generate any significant data and were not the targeted axes of this test.

The generated data behaves exactly as expected. Initially the Baja is at standstill with no draw bar pull, however, as the towing commences the tractive force and draw bar pull increase considerably. Initially the tractive force exceeds the draw bar pull signifying a resultant positive acceleration of both the Baja and vehicle being towed. The draw bar pull eventually converges to the tractive force as the two vehicles reach standstill due to increased braking in the towed vehicle. The vertical load increases notably due to the load transfer of the system as the weight is completely removed from the front tyres. A maximum vertical load on both rear wheel of approximately $1450N \times 2 = 295kg$ compares very well with the tested mass of the Baja.

101

7.3.4.   JUMP
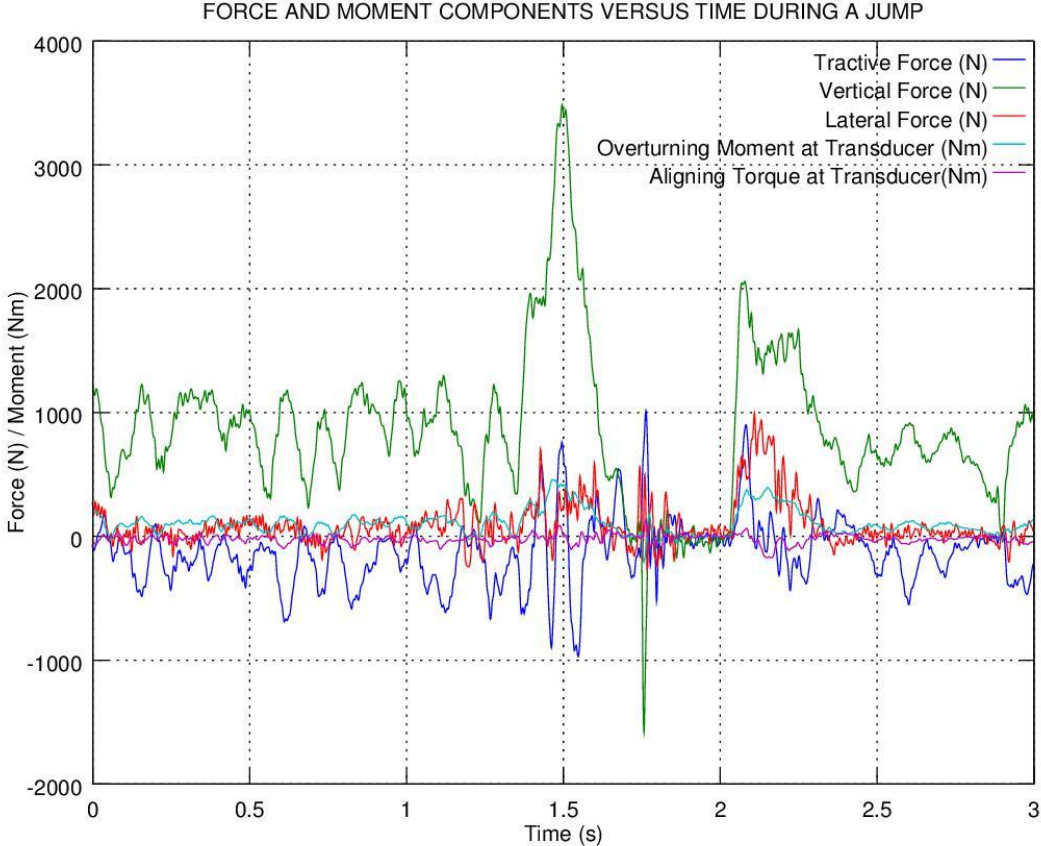
Figure 44: Jumping maneuver Baja test results

The jumping maneuver was intended to generate high loading in the wheel force transducer. The presented data confirms the operation of the transducer under server conditions. The Baja's rear wheels hit the ramp at approximately 1.5 seconds at which an extremely high vertical loading of $3500N$ is produced. A point of great interest is the section between 1.75 and 2 seconds where the rear wheel is essentially free falling back to the ground. Under free falling conditions no loading should be experienced on the transducer which is exactly what happens: all the loads turn to zero during the fall. When the wheel strikes the ground high forces are generated in all the axis except the aligning torque. A very high lateral force is generated due to the Baja's rear suspension configuration: The rear wheels 'kick-out' as the suspension is compressed. This causes high axial loading under heavy vertical loading as during the landing.

7.4.   UNCERTAINTY ANALYSIS

No assumptions or simplifications were made during the completed experimental investigation. However, during the dynamic testing the channel representing the driving torque encountered a faulty connection, thus the specific channel was never tested. This does and will introduce a degree of uncertainty in the operation of the wheel force transducer until the channel is finally tested dynamically.

It should be noted that the driving torque channel is independent in its operation (does not rely on the angular position of the wheel during rotation) and proved to be effective during the calibration process. The likelihood of this channel malfunctioning during a dynamic test is very small.

Ideally the wheel force transducer should have been undergone additional experimental testing on the tyre tester to quantitatively verify its operation under dynamic conditions. Nonetheless, this does not introduce a significant uncertainty since a calibration procedure was completed for the transducer as a whole i.e. the transducer did not require additional assembly after calibration (it is a one piece transducer).

7.5.   CONCLUSION BASED ON THE RESULTS

The experimental calibration corresponded well to the theoretical modeling of the transducer. The deviations were accounted for by incorporating the experimental strain compliance matrix in the Baja testing. Additionally all future testing on the Baja will incorporate the experimental strain compliance.

The results from the Baja testing were consistent with expectations based on vehicle dynamics across all the completed maneuvers. It would be ideal to quantitatively test the wheel force transducer in its entirety on a tyre tester; however, it can be concluded with confidence that the wheel force transducer is operational and has effectively met the design specifications as imposed by the Baja vehicle.

8.   CONCLUSIONS

The modeling, fabrication, calibration and testing of a six axis wheel force transducer was successfully completed. During the modeling phase the transducer was optimized according to the design parameters imposed by a Baja vehicle using a mathematical model. Upon completion of the optimization phase a finite element model was used to verify the design and mathematical modeling of the transducer. It was found that the two models correlated extremely well allowing the fabrication of the optimized transducer to commence.

The design of the wheel force transducer assembly was completed in a separate design project entitled *DETAIL DESIGN OF A SIX-AXIS WHEEL FORCE TRANSDUCER.* The well-executed design phase allowed for seamless fabrication and assembly of the wheel force transducer.

During the theoretical investigation, a strain compliance was established for the transducer. The strain compliance allowed for the full characterization of the transducer relating the signals in the Wheatstone bridge strain sensors to the forces transmitted through the transducer. It was of utmost importance to verify the theoretical strain compliance by means of an experimental calibration phase. During the experimental investigation it was found that the stain compliance as predicted by the theoretical model correlated sufficiently well to the experimentally determined strain compliance. This verified both the operation of the transducer and model used for the optimization process.

Finally an additional experimental investigation was completed to verify the general operation of the wheel force transducer on the Baja vehicle it was ultimately designed for. The strain compliance as determined during calibration was utilized to insure all fabrication defects were accounted for. The wheel force transducer was exposed to dynamic loading conditions as experienced by the Baja during operation. It was found that the data received from the transducer correlated very well to the expected results for various driving maneuvers.

It can be concluded that a wheel force transducer has been successfully modeled, fabricated, calibrated and tested thus producing a working piece of equipment that will aid in the future development of the Baja vehicles at the University of Pretoria.

9.   RECOMMENDATIONS

Despite the success of the research project, recommendations can be made to aid in any future development of the wheel force transducer. The transducer was optimized to be as sensitive in all the axes as possible while complying with the design requirements. As observed in the obtained strain compliance matrixes the sensitivities are relatively low and should preferably be higher. These low sensitivities are a direct result of the high maximum specified design loads which were assumed to act simultaneously due to a shortage of information. In order to improve the performance of the wheel force transducer it is then recommended that these maximum loads be reexamined (the current wheel force transducer may be utilized to accomplish this task). The second transducer (first iteration) should be based on these reexamined loading characteristics for higher sensitivity and performance.

Further recommendations have previously been made in Section 6.2 regarding the fabrication of the wheel force transducer. It was noted that electronic circuit boards should be utilized to preserve space and reduce excessive wiring for the Wheatstone bridges. Additionally greater clearances should be made for machining and applying the strain gauges.

The calibration procedure was correctly executed; however, the applied loads were low relative to the design loads of the transducer. It is recommended that higher loads be used to calibrate the transducer for increased accuracy. A tyre tester was not used to dynamically test the wheel force transducer; rather it was tested on the Baja vehicle. The Baja tests exposed the wheel force transducer to the operating conditions it was ultimately designed for, thus providing invaluable feedback on the design and operational ability of the wheel force transducer in its entirety. Strictly speaking the calibration and Baja tests provide a sufficient experimental investigation; however, it is recommended that a tyre tester be utilized in addition. The tyre tester can provide directly comparable data for further and definite experimental verification of the wheel force transducer.

10. REFERENCES

ASM Aerospace. [online]. [Accessed 3 March 2013]. Available from World Wide Web: <http://asm.matweb.com/search/SpecificMaterial.asp?bassnum=MA7075T6>

BUDYNAS, Richard G. and J. Keith NISBETT. 2011. *Shigley's Mechanical Engineering Design -9th ed*. McGraw-Hill.

CENTKOWSKI, Karol and Alfred ULRICH. 2012. Portable tyre test rig for investigation of physical parameters of agricultural and construction machinery tyres under critical on-road conditions. *In*: *International Society for Terrain Vehicle Systems*. Pretoria, pp.1-4.

CHAO, Lu-Ping and Kuen-Tzong CHEN. 1997. Shape optimal design and force sensitivity evaluation of six-axis force sensors. *Sensors and Actuators A Physical*. **63**, pp.105-112.

CHAO, Lu-Ping and Ching-Yan YIN. 1999. The six-component force sensor for measuring the loading of the feet in locomotion. *Materials and Design*. **20**, pp.237-244.

CHELI, F, F BRAGHIN, M BRUSAROSCO et al. 2011. Design and testing of an innovative measurement device for tyre-road contact forces. *Mechanical Systems and Signal Processing*. **25**, pp.1956-1972.

D, Gillespie Thomas. 1992. *In*: *Fundamentals of Vehicle Dynamics*, SAE, p.350.

GOBBI, M, G PREVIATI, and G MASTINU. 2011. Refined design of a measuring wheel. *In*: *International Design Engineering Technical Conferences & Computers and Information in Engineering Conference*. Washington: American Society of Mechanical Engineers, pp.1-10.

KMT Telemetry. [online]. [Accessed 10 October 2013]. Available from World Wide Web: <http://www.kmt-telemetry.com/fileadmin/media/DS_UM_AP/engl_rotierend/CT4-8-Wheel-UM-e.pdf>

Kyowa. [online]. [Accessed 15 February 2013]. Available from World Wide Web: <http://www.kyowa-ei.co.jp/eng>

LIU, Sheng A and Hung L TZO. 2002. A novel six-component force sensor of good measurement isotropy and sensitivities. *Sensors and Actuators A*. **100**, pp.223-230.

MIDDLE, Tersius. 2007. *Development and Testing of an Inner Wheel Load Cell*.

NOUWENS, Oscar. 2013. *Detail Design of a Six-Axis Wheel Force Transducer*.

PANAS, Robert.M. 2009. *Design, Fabrication and Mechanical Optimization of a Flexural High Speed Nanopositioning Imaging Stage*.

PARK, Joong-Jo and Gab-Soon KIM. 2005. Development of the 6-axis force/moment sensor for an intelligent robo't gripper. *Sensors and Actuators A*. **118**, pp.127-134.

PENNY, W.C.W. 2012. *Rear suspension optimization of the Baja vehicle*.

RADOVITZKY, Raul. 2012. *16.20 Techniques of Structural Analysis and Design*.

SLOCUM, A.H. 1992. *In*: *Precision Machine Design*, Prentice Hall, pp.61-64.

STEFANESCU, Dan M and Mirela A ANGHEL. 2012. Electrical methods for force measurement - A brief survey. *Measurement*. **43**, pp.949-959.

APPENDICES

APPENDICES

APPENDIX A: FIRST PROGRESS REPORT

MSC 412/422: First Progress Report

OMM Nouwens: 10389467

Supervisor: Prof. PS Els

The modeling, fabrication, calibration and testing of a six axis wheel force transducer.

Introduction

This report discusses the current progress thus far completed by the student on the research project regarding the modeling, fabrication, calibration and testing of a six axis wheel force transducer. Implications of the current progress will be discussed with regard to the project plan and future progress.

Current Project Status

The current status of the project is overall positive. The student is currently on schedule in terms of the original project progress plan and no changes to the Project Protocol are thus far necessary.

The student has thus far completed the greater deal of literature review and has gained a widespread knowledge in the modeling and calibration of various wheel force transducers. The design of the wheel force transducer is to be completed by the student in the MOX 410 Design Project which is currently ahead of schedule: The concept generation is currently being undertaken and all possible concepts have already been analysed in terms of modeling, implementation and calibration.

Project Planning

Planning for the project is based on a predefined schedule, comprising of deadlines, as stated in the MSC 412/422 Study Guide. The resultant schedule with all activities is presented on a Gantt chart included in this report.

The critical deadlines are as follows:

- Handing in of protocol   18-02-2013
- First progress report   04-03-2013
- Half year report   27-05-2013
- Half year evaluation   14-06-2013
- Second progress report   12-08-2013
- Closure of workshops, and all computer facilities   14-10-2013
- Handing in of final report   28-10-2013
- Presentation and oral examination   15-11-2013
- Poster exhibition during final year function   28-11-2013

The required tasks as listed in the Gantt chart are as follows:

- *Literature study of wheel force transducer implementation*: The outcomes of this task are explained in part a) of the *Project Scope* section.
- *Design of the transducer for fabrication (MOX 410):* This task represents the MOX 410 design project of the wheel force transducer. It has been included to outline an appropriate timescale till the design is available to the research project.
- *Functional modeling of the transducer:* The student is to model the force transducer such that applied loads can be predicted based on information from the strain gauges, load cells etc.
- *Selection of the transducer communication system:* As explained, the appropriate equipment is made available to the project for data recording; however the student will be required to select the system and the correct interface medium.
- *Design of the calibration procedure and setup*: A procedure and setup is to be designed to effectively calibrate the wheel force transducer while utilizing existing equipment.

- *Design of a procedure to validate theoretical predictions*: The student is to validate the models by compiling a procedure to compare the experimental data from calibration to the theoretical predictions.

- *Design of a test procedure using the tyre tester*: A procedure is to be designed that will allow the wheel force transducer to be tested in the tyre tester after calibration. This will insure the transducer is operational.

- *Fabrication of the transducer and accessories for assembly*: This task represents all fabrication required for the wheel force transducer assembly and implementation into the Baja with the communications system.

- *Fabrication of the calibration setup*: If applicable, this task represents all fabrication required for calibration according to the calibration setup as previously designed.

- *Installation of the transducer into the Baja*: The wheel force transducer is to be installed into the Baja with all required communication systems. Only completed after calibration and testing.

- *Calibration of the transducer*: The wheel force transducer is to be calibrated according to the calibration procedure as previously compiled.

- *Experimental verification of theoretical predictions*: The theoretical predictions are to be verified using the experimental verification procedure as previously compiled.

- *Initial testing of the transducer in the tyre tester*: The wheel force transducer is to be tested in the tyre tester according to the procedure, as previously compiled, prior to the installation in the Baja.

- *Testing of the transducer in the Baja*: The wheel force transducer is to be installed and tested in the Baja.

The student plans to complete all deliverables and reports more or less a week before the time to ensure the critical deadlines are met with a safety margin. This safety margin is presented on the Gantt chart.

Important points to note on the Gantt diagram is that the design of the wheel force transducer for fabrication coincides with the MOX 410 project initiation and deadline dates, thus it extends over the whole first semester. In addition the fabrication of various components extends over a large period of time to account for the overlap with examinations and the half year report and

evaluation deliverables. The student plans to fabricate various components in the workshop made available to them during the June-July recess period in order to remain on a safe schedule.

The Gantt diagram is included on the following page:

Gantt chart — Project schedule (weeks by month)

Header (months and weeks):

Month	Weeks (date ranges)
February	Week 6 (4 – 10), Week 7 (11 – 17), Week 8 (18 – 24), Week 9 (25 – 3)
March	Week 10 (4 – 10), Week 11 (11 – 17), Week 12 (18 – 24), Week 13 (25 – 31)
April	Week 14 (1 – 7), Week 15 (8 – 14), Week 16 (15 – 21), Week 17 (22 – 28)
May	Week 18 (29 – 5), Week 19 (6 – 12), Week 20 (13 – 19), Week 21 (20 – 26), Week 22 (27 – 2)
June	Week 23 (3 – 9), Week 24 (10 – 16), Week 25 (17 – 23), Week 26 (24 – 30)
July	Week 27 (1 – 7), Week 28 (8 – 14), Week 29 (15 – 21), Week 30 (22 – 28)
August	Week 31 (29 – 4), Week 32 (5 – 11), Week 33 (12 – 18), Week 34 (19 – 25), Week 35 (26 – 1)
September	Week 36 (2 – 8), Week 37 (9 – 15), Week 38 (16 – 22), Week 39 (23 – 29)
October	Week 40 (30 – 6), Week 41 (7 – 13), Week 42 (14 – 20), Week 43 (21 – 27), Week 44 (28 – 3)
November	Week 45 (4 – 10), Week 46 (11 – 17), Week 47 (18 – 24), Week 48 (25 – 1)

Tasks (by category):

Category	Task
Literature survey	Literature study of wheel force transducer implementation
Transducer design and modeling	Design of the transducer for fabrication (MOX 410)
Transducer design and modeling	Functional modeling of the transducer
Transducer design and modeling	Selection of the transducer communication system
Procedures for the transducer	Design of the calibration procedure and setup
Procedures for the transducer	Design of a procedure to validate theoretical predictions
Procedures for the transducer	Design of a test procedure using the tyre tester
Fabrication and installation	Fabrication of the transducer and accessories for assembly
Fabrication and installation	Fabrication of the calibration setup
Fabrication and installation	Installation of the transducer into the Baja
Analysis and testing	Calibration of the transducer
Analysis and testing	Experimental verification of theoretical predictions
Analysis and testing	Initial testing of the transducer in the tyre tester
Analysis and testing	Testing of the transducer in the Baja
Deliverables and reports	Project protocol
Deliverables and reports	First progress report
Deliverables and reports	Half year report
Deliverables and reports	Half year evaluation
Deliverables and reports	Second progress report
Deliverables and reports	Handing in of final report
Deliverables and reports	Presentation and oral examination
Deliverables and reports	Poster exhibition during final year function

Personal Opinion

It can be seen form the Gantt diagram on the previous page that the student is currently on schedule as the literature review has essentially been completed. The student is to start modeling the wheel force transducer in mid-March; however, the concept selection phase must first be completed in MOX 410 Design Project. As the concept selection phase is expected to be completed in early March, it can be concluded that the current project status is in accordance with future planning.

The literature survey completed thus far indicates that no major technical complications beyond the capability of the student are expected. The presented project is thus far well understood by the student and, as a result, knows what is expected of them. A major advantage to the project is that telemetry systems are readily available for data recording and processing. The student will therefore have more time to focus on the design and modeling of the wheel force transducer.

Project Budget

At this stage an accurate budget cannot be forecasted since a design concept has not yet been selected. Upon selection of the concept and the design phase the student will be able to compile a meaningful forecasted budget for the duration of the research project based on the required items and components.

The research project in question has allocated funding from the University of Pretoria which will be utilized by the student. Since all components of major expense such as the telemetry system are already available to the research project no foreseeable budget problems are expected.

Fabrication costs are expected to be relatively low: Other than the costs incurred during the acquisition of materials, the student is to utilize a workshop readily available to them. The workshop will provide all, or at least most of the necessary machinery to the student at no direct cost. A major advantage of this is that the student can complete a large amount of fabrication during recess periods such as in the June-July holidays.

MSC 422: Research Project

Second Progress Report

The Modeling, Fabrication, Calibration and Testing of a Six-Axis Wheel Force Transducer

---

Student: OMM Nouwens

                    10389467

Supervisor: Prof. PS Els

Date: 12 August 2013

INTRODUCTION

This report discusses the current progress thus far completed by the student on the research project regarding the modeling, fabrication, calibration and testing of a six axis wheel force transducer. Implications of the current progress will be discussed with regard to the project plan and future progress.

CURRENT PROJECT STATUS

The student is currently fabricating all components necessary for the wheel force transducer. The majority of the fabricating process has thus far been completed, however, according to the original project schedule the student should already have completed this phase entirely.

The student estimates that the project has fallen approximately one and a half weeks behind schedule. However, the student feels that the time allocated to calibration and testing phase is plentiful and will bring the project back up to schedule.

Additionally, when considering the original project schedule it should be noted that an entire month of flexibility is available in October. This means that while the original schedule will be challenging to comply with, the deadlines will still be easily met.

Due to the favourable budget and progress made in the fabrication of the wheel force transducer and various additional components, the student feels overall positive regarding the current project status.

PROJECT PLANNING

Planning for the project is based on a predefined schedule, comprising of deadlines, as stated in the MSC 412/422 Study Guide. The resultant schedule with all activities is presented on a Gantt chart included in this report.

The critical deadlines are as follows:

- Handing in of protocol   (Completed)
- First progress report   (Completed)
- Half year report   (Completed)
- Half year evaluation   (Completed)
- Second progress report   (Submitted)
- Closure of workshops, and all computer facilities   14-10-2013
- Handing in of final report   28-10-2013
- Presentation and oral examination   15-11-2013
- Poster exhibition during final year function   28-11-2013

The required tasks as listed in the Gantt chart are as follows:

- *Literature study of wheel force transducer implementation*: The outcomes of this task are explained in part a) of the *Project Scope* section.
- *Design of the transducer for fabrication (MOX 410):* This task represents the MOX 410 design project of the wheel force transducer. It has been included to outline an appropriate timescale till the design is available to the research project.
- *Functional modeling of the transducer:* The student is to model the force transducer such that applied loads can be predicted based on information from the strain gauges, load cells etc.
- *Selection of the transducer communication system:* As explained, the appropriate equipment is made available to the project for data recording; however the student will be required to select the system and the correct interface medium.
- *Design of the calibration procedure and setup*: A procedure and setup is to be designed to effectively calibrate the wheel force transducer while utilizing existing equipment.

- *Design of a procedure to validate theoretical predictions*: The student is to validate the models by compiling a procedure to compare the experimental data from calibration to the theoretical predictions.

- *Design of a test procedure using the tyre tester*: A procedure is to be designed that will allow the wheel force transducer to be tested in the tyre tester after calibration. This will insure the transducer is operational.

- *Fabrication of the transducer and accessories for assembly*: This task represents all fabrication required for the wheel force transducer assembly and implementation into the Baja with the communications system.

- *Fabrication of the calibration setup*: If applicable, this task represents all fabrication required for calibration according to the calibration setup as previously designed.

- *Installation of the transducer into the Baja*: The wheel force transducer is to be installed into the Baja with all required communication systems. Only completed after calibration and testing.

- *Calibration of the transducer*: The wheel force transducer is to be calibrated according to the calibration procedure as previously compiled.

- *Experimental verification of theoretical predictions*: The theoretical predictions are to be verified using the experimental verification procedure as previously compiled.

- *Initial testing of the transducer in the tyre tester*: The wheel force transducer is to be tested in the tyre tester according to the procedure, as previously compiled, prior to the installation in the Baja.

- *Testing of the transducer in the Baja*: The wheel force transducer is to be installed and tested in the Baja.

The student plans to complete all deliverables and reports more or less a week before the time to ensure the critical deadlines are met with a safety margin. This safety margin is presented on the Gantt chart.

The Gantt diagram is included on the following page:

Project schedule (Gantt chart)

Week/date header:

Month	Weeks (date ranges)
February	Week 6 (4–10), Week 7 (11–17), Week 8 (18–24), Week 9 (25–3)
March	Week 10 (4–10), Week 11 (11–17), Week 12 (18–24), Week 13 (25–31)
April	Week 14 (1–7), Week 15 (8–14), Week 16 (15–21), Week 17 (22–28)
May	Week 18 (29–5), Week 19 (6–12), Week 20 (13–19), Week 21 (20–26), Week 22 (27–2)
June	Week 23 (3–9), Week 24 (10–16), Week 25 (17–23), Week 26 (24–30)
July	Week 27 (1–7), Week 28 (8–14), Week 29 (15–21), Week 30 (22–28)
August	Week 31 (29–4), Week 32 (5–11), Week 33 (12–18), Week 34 (19–25), Week 35 (26–1)
September	Week 36 (2–8), Week 37 (9–15), Week 38 (16–22), Week 39 (23–29)
October	Week 40 (30–6), Week 41 (7–13), Week 42 (14–20), Week 43 (21–27), Week 44 (28–3)
November	Week 45 (4–10), Week 46 (11–17), Week 47 (18–24), Week 48 (25–1)

Tasks by category:

Category	Task
Literature survey	Literature study of wheel force transducer implementation
Transducer design and modeling	Design of the transducer for fabrication (MOX 410)
	Functional modeling of the transducer
	Selection of the transducer communication system
Procedures for the transducer	Design of the calibration procedure and setup
	Design of a procedure to validate theoretical predictions
	Design of a test procedure using the tyre tester
Fabrication and installation	Fabrication of the transducer and accessories for assembly
	Fabrication of the calibration setup
	Installation of the transducer into the Baja
Analysis and testing	Calibration of the transducer
	Experimental verification of theoretical predictions
	Initial testing of the transducer in the tyre tester
	Testing of the transducer in the Baja
Deliverables and reports	Project protocol
	First progress report
	Half year report
	Half year evaluation
	Second progress report
	Handing in of final report
	Presentation and oral examination
	Poster exhibition during final year function

PERSONAL OPINION AND AREAS OF CONCERN

The student has fallen slightly behind the very conservative original project schedule; however, feel they will be able to catch this time up again. The reason for falling behind is that the fabrication process is more extensive than expected.

The student currently only has two areas of concern which are:

1. Functionality of the implemented strain-gauge Wheatstone bridges. If they do not function properly (are faulty) then a great amount of extra time will be required to rectify the errors. The student addresses this concern with the leeway presented in the project schedule in the month of October.
2. Availability of testing equipment. There is great demand for the required equipment needed to calibrate and test the wheel force transducer. The student plans to address this area of concern by notifying the project supervisor as soon as possible and booking the required equipment.

However, the student reflects positively on the research project as a whole. To date, no major errors in the design, modeling or testing procedure have been found, thus the project is being executed as was planned. Additionally, as will be seen in the budget section of this progress report, the research project is within budget.

BUDGET

OVERVIEW

A large budget is not necessary for the research project due to the nature in which it is planned to be undertaken: Since similar research is already being undertaken in the Vehicle Dynamics Lab at the University of Pretoria many facilities are readily available to the project and the wheel force transducer has been designed with this in mind. A major example includes the telemetry system which would ordinarily be extremely expensive to purchase, but instead the current design facilitates the existing telemetry systems available to the project.

Another major cost advantage is that all machining of components will have been completed internally avoiding labour and machining costs. Additionally, some stock (for various components) was made readily available to the student from the workshops available to them. All these perks have greatly assisted the research project thus far.

COST SUMMARY

Despite all the aforementioned cost savings some purchases have had to be made. The following major costs have thus far been incurred in the research project:

Aluminium stock for the transducer	R2750
Strain gauges with required adhesive	R3100
Total	**R5850**

These notable costs are related to the transducer which forms the major component in the project. No major additional costs are anticipated for the research project; however, small costs are still expected for the nuts, bolts and studs.

It has been previously suggested that the project budget not exceed R8000 by the project supervisor. Based on the current project status and incurred costs thus far, the budget of R8000 will not be exceeded.

CONCLUSION

The design project is currently in accordance with future planning, the budget and the original design, fabrication and testing procedures.

RESEARCH REPORT

Since the Half Year Report was submitted for MSC 412 no major additions/alterations have been made to the report. All efforts have been focused on the fabrication of the wheel force transducer and necessary additional components. However, the report is available upon request.

APPENDIX C: REPORT CARD

REPORT CARD FOR THESIS MSC 412 and 422   20......13....
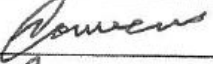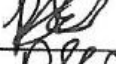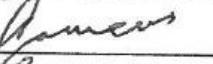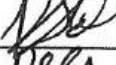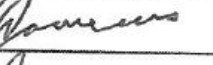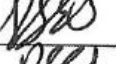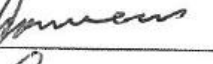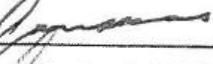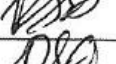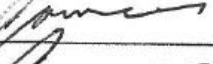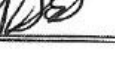
Name OMM Nouwens   Reg. no. 10389467

Topic Wheel Force Transducer

Supervisor Prof PS Els

Commencement date: 12/02/2013

Date	Signature (Supervisor)	Signature (Student)	Comments
12/02/2013		Nouwens	Initial discussion
14/02/2013		Nouwens	Protocol discussion
21/02/2013		Nouwens	General discussion
4/04/2013		Nouwens	General discussion
10/05/2013		Nouwens	General discussion
14/05/2013		Nouwens	General discussion
20/09/2013		Nouwens	Protocol change
3/10/2013		Nouwens	General discussion
22/10/2013		Nouwens	Final report

The protocol was adjusted on the 20 September 2013: It was decided that under the given time constraints the tyre tester section of the experimental investigation would not form part of the required outcomes. This has been further discussed in Section 6.1.2.

APPENDIX D: CALIBRATION DATA

The calibration data is included below sorted according to the applied loads. The signals are sorted according to the load axes on the transducer (a designated Wheatstone bridge per axis).

Applied Loads				mV Signals from Wheatstone Bridges						
	N		Nm		Fx	Fy	Fz	Mx	My	Mz
FxNeg	600.2739	MyPos	290.1724	Initial	13.58978	-10.36735	26.3736	2.143399	-21.4973	-7.904825
				Peak	-170.9763	-31.02076	27.59421	8.985427	1401.999	-11.55946
				Final	21.61039	-10.15634	26.75807	0.191876	-20.21453	-16.61154
FxNeg	600.2739	MyPos	230.145	Initial	21.65565	-10.12821	26.78464	0.185636	-20.29744	-16.56309
				Peak	-164.8282	-27.17111	32.35631	5.72665	1110.623	-10.61844
				Final	21.342	-10.58304	26.62835	-0.482031	-20.24582	-17.38374
FxPos	600.2739	MyNeg	290.1724	Initial	47.20144	-3.812145	19.69385	1.04518	-78.39427	-15.71117
				Peak	236.4036	0.758053	12.52336	-1.967122	-1503.641	-15.47357
				Final	40.12958	-5.245411	19.92516	0.912582	-78.09705	-16.13635
FxPos	600.2739	MyNeg	230.145	Initial	40.32775	-5.329813	19.86264	0.900103	-78.03134	-16.21294
				Peak	229.0914	-0.572056	12.40458	-1.361854	-1210.252	-9.616468
				Final	40.08588	-5.568951	20.01737	1.01242	-78.38019	-16.29422
FyNeg	600.2739	MxNeg	290.1724	Initial	30.47052	-17.2117	22.9212	-31.34292	-44.84366	-14.49661
				Peak	36.87764	-210.9856	13.97996	-1451.095	-41.37236	10.89356
				Final	28.32648	-11.95379	19.17029	-32.1853	-46.56131	-12.82404
FyNeg	600.2739	MxNeg	230.145	Initial	28.31712	-11.93816	19.36408	-32.2243	-46.52846	-12.88188
				Peak	35.74477	-204.707	13.086	-1157.406	-42.89761	9.13502
				Final	27.8646	-12.51803	19.36408	-32.42554	-46.83507	-12.95378
FyPos	600.2739	MxPos	290.1724	Initial	18.33037	15.91442	21.54587	20.38101	-42.3579	-18.4201
				Peak	25.14789	207.9127	19.37346	1440.874	-51.93173	-46.91311
				Final	21.81949	9.402978	23.93238	21.6477	-42.24527	-22.14508
FyPos	600.2739	MxPos	230.145	Initial	21.73523	9.457683	24.01209	21.68358	-42.30785	-22.24043
				Peak	24.72501	201.8217	24.9967	1148.503	-49.75572	-44.28859
				Final	21.80857	9.124765	24.25903	21.97374	-42.21398	-22.43738
		MzNeg	175.7721	Initial	26.19338	-16.35362	15.10993	-25.61783	-52.79368	-27.51761
				Peak	28.79929	-13.67933	48.63839	-13.47502	-72.49198	-1012.136
				Final	30.49548	-16.44271	17.12291	-25.26527	-52.85157	-47.88226
		MzPos	175.7721	Initial	16.48126	-5.090675	53.67087	0.672347	-39.48576	4.258007
				Peak	14.25141	-14.70622	77.05468	25.75978	-1.26243	981.5816
				Final	10.44396	-8.430795	38.10145	2.09816	-36.96246	14.83112
FzNeg	588.6			Initial	-8.315531	36.55064	-1.475359	20.26557	-37.52876	23.23303
				Peak	-11.66733	31.71004	-298.0147	2.113759	-24.54465	23.20958
				Final	-8.140763	36.98984	-1.786372	19.95514	-37.20963	23.40028

APPENDIX E: MODELING AND OPTIMIZATION CODE

Appendix A includes all the code that was used during the mathematical modeling and optimization.

MAIN SCRIPT

```matlab
clear all
close all

% Initialization
    n = 600; % Number of finite beams over diameter. Must be even and >=2
    l = 0.225/2; % Length of half a full beam (radius of the transducer to the boundaries)
    rhub = 0.120/2; % Hub radius
% w and h describe the width and height respectively for 2*l (full beam)
    w = zeros(1,n);
    h = zeros(1,n);

% Read previously optimized geometry
    MyFile = dlmread('wnx.txt',',');
    w = MyFile(1:n,1).*(2)./1000;
    MyFile = dlmread('hnx.txt',',');
    h = MyFile(1:n,3).*(2)./1000;

% Boundary stiffness with axial direction in y (as optimized)
    kx = 8.3469E8;
    ky = 1.7675E7;
    kz = 4.7852E8;
    kmx = 5.4176E3;
    kmy = 6.5105E5;
    kmz = 2.4048E4;
    KA = [kx ky kz kmx kmy kmz];

% Optimized boundary geometry
    hbndy = 0.04;
    bbndy = 0.0076876;
    lbndy = 0.12;

% Run convergence/optimization
for I = 1:10
    % Solve for new transducer geometry
        [NewHeight, NewWidth, R, SGstrains] = Forces(n, w, h, l, rhub, KA, 0, [1:6]);
        w(1:n/2) = NewWidth;
        h(1:n/2) = NewHeight;
        for J = 1:(n/2)
            w(n/2 + J) = NewWidth(n/2-(J-1));
            h(n/2 + J) = NewHeight(n/2-(J-1));
        end
    % Solve for new boundary geometry and stiffness
        [kx ky kz kmx kmy kmz lbndynew bbndynew hbndynew] = Boundaries(R, lbndy, bbndy, hbndy, w(1));
    % To display in iteration
        KA = [kx ky kz kmx kmy kmz]
        R
        I
    % Redefine variable to new data and display results
        hbndy = hbndynew;
        bbndy = bbndynew;
        lbndy = lbndynew;
        figure(2)
        K = 1:(n/2);
        plot(K/(n/2)*l*1000,h(K)/2*1000,'r-.',K/(n/2)*l*1000,w(K)/2*1000,'b',K/(n/2)*l*1000,-h(K)/2*1000,'r-
.',K/(n/2)*l*1000,-w(K)/2*1000,'b');
        axis([0,225/2,-60,60],'square')
        grid on
        title('GEOMERTY OF THE TRANSDUCER [ONE SPOKE PRESENTED]')
        legend('Height in Z axis','Width in X or Y axis','location','north');
        xlabel('Axial position (mm)')
        ylabel('Height/Width (mm)')
end

% Strain compliance
C = zeros(6,6);
Strains = zeros(16,6);
```

```matlab
% Compiling of compliance matrix
% Loading in Fx
    [NewHeight, NewWidth, R, SGstrains] = Forces(n, w, h, l, rhub, KA, 1, [5200 0 0 0 0 0]);
        C(1,1) = (SGstrains(2,8) + SGstrains(1,8))/2;
        C(2,1) = (SGstrains(3,8) + SGstrains(4,8))/2;
        C(3,1) = (SGstrains(1,2) + SGstrains(4,2) - SGstrains(3,5) - SGstrains(2,5))/4;
        C(4,1) = (SGstrains(2,2) + SGstrains(1,5))/2;
        C(5,1) = (SGstrains(3,2) + SGstrains(4,5))/2;
        C(6,1) = (SGstrains(2,11) - SGstrains(1,11) + SGstrains(3,11) - SGstrains(4,11))/4;
            STRAINS(1:16,1) = [SGstrains(2,2),SGstrains(2,11),SGstrains(2,5),SGstrains(2,8),...
                               SGstrains(1,2),SGstrains(1,8),SGstrains(1,5),SGstrains(1,11),...
                               SGstrains(4,2),SGstrains(4,8),SGstrains(4,5),SGstrains(4,11),...
                               SGstrains(3,2),SGstrains(3,11),SGstrains(3,5),SGstrains(3,8)];
% Loading in Fy
    [NewHeight, NewWidth, R, SGstrains] = Forces(n, w, h, l, rhub, KA, 1, [0 5200 0 0 0 0]);
        C(1,2) = (SGstrains(2,8) + SGstrains(1,8))/2;
        C(2,2) = (SGstrains(3,8) + SGstrains(4,8))/2;
        C(3,2) = (SGstrains(1,2) + SGstrains(4,2) - SGstrains(3,5) - SGstrains(2,5))/4;
        C(4,2) = (SGstrains(2,2) + SGstrains(1,5))/2;
        C(5,2) = (SGstrains(3,2) + SGstrains(4,5))/2;
        C(6,2) = (SGstrains(2,11) - SGstrains(1,11) + SGstrains(3,11) - SGstrains(4,11))/4;
            STRAINS(1:16,2) = [SGstrains(2,2),SGstrains(2,11),SGstrains(2,5),SGstrains(2,8),...
                               SGstrains(1,2),SGstrains(1,8),SGstrains(1,5),SGstrains(1,11),...
                               SGstrains(4,2),SGstrains(4,8),SGstrains(4,5),SGstrains(4,11),...
                               SGstrains(3,2),SGstrains(3,11),SGstrains(3,5),SGstrains(3,8)];

% Loading in Fz
    [NewHeight, NewWidth, R, SGstrains] = Forces(n, w, h, l, rhub, KA, 1, [0 0 5200 0 0 0]);
        C(1,3) = (SGstrains(2,8) + SGstrains(1,8))/2;
        C(2,3) = (SGstrains(3,8) + SGstrains(4,8))/2;
        C(3,3) = (SGstrains(1,2) + SGstrains(4,2) - SGstrains(3,5) - SGstrains(2,5))/4;
        C(4,3) = (SGstrains(2,2) + SGstrains(1,5))/2;
        C(5,3) = (SGstrains(3,2) + SGstrains(4,5))/2;
        C(6,3) = (SGstrains(2,11) - SGstrains(1,11) + SGstrains(3,11) - SGstrains(4,11))/4;
            STRAINS(1:16,3) = [SGstrains(2,2),SGstrains(2,11),SGstrains(2,5),SGstrains(2,8),...
                               SGstrains(1,2),SGstrains(1,8),SGstrains(1,5),SGstrains(1,11),...
                               SGstrains(4,2),SGstrains(4,8),SGstrains(4,5),SGstrains(4,11),...
                               SGstrains(3,2),SGstrains(3,11),SGstrains(3,5),SGstrains(3,8)];

% Loading in Mx
    [NewHeight, NewWidth, R, SGstrains] = Forces(n, w, h, l, rhub, KA, 1, [0 0 0 1400 0 0]);
        C(1,4) = (SGstrains(2,8) + SGstrains(1,8))/2;
        C(2,4) = (SGstrains(3,8) + SGstrains(4,8))/2;
        C(3,4) = (SGstrains(1,2) + SGstrains(4,2) - SGstrains(3,5) - SGstrains(2,5))/4;
        C(4,4) = (SGstrains(2,2) + SGstrains(1,5))/2;
        C(5,4) = (SGstrains(3,2) + SGstrains(4,5))/2;
        C(6,4) = (SGstrains(2,11) - SGstrains(1,11) + SGstrains(3,11) - SGstrains(4,11))/4;
            STRAINS(1:16,4) = [SGstrains(2,2),SGstrains(2,11),SGstrains(2,5),SGstrains(2,8),...
                               SGstrains(1,2),SGstrains(1,8),SGstrains(1,5),SGstrains(1,11),...
                               SGstrains(4,2),SGstrains(4,8),SGstrains(4,5),SGstrains(4,11),...
                               SGstrains(3,2),SGstrains(3,11),SGstrains(3,5),SGstrains(3,8)];

% Loading in My
    [NewHeight, NewWidth, R, SGstrains] = Forces(n, w, h, l, rhub, KA, 1, [0 0 0 0 1400 0]);
        C(1,5) = (SGstrains(2,8) + SGstrains(1,8))/2;
        C(2,5) = (SGstrains(3,8) + SGstrains(4,8))/2;
        C(3,5) = (SGstrains(1,2) + SGstrains(4,2) - SGstrains(3,5) - SGstrains(2,5))/4;
        C(4,5) = (SGstrains(2,2) + SGstrains(1,5))/2;
        C(5,5) = (SGstrains(3,2) + SGstrains(4,5))/2;
        C(6,5) = (SGstrains(2,11) - SGstrains(1,11) + SGstrains(3,11) - SGstrains(4,11))/4;
            STRAINS(1:16,5) = [SGstrains(2,2),SGstrains(2,11),SGstrains(2,5),SGstrains(2,8),...
                               SGstrains(1,2),SGstrains(1,8),SGstrains(1,5),SGstrains(1,11),...
                               SGstrains(4,2),SGstrains(4,8),SGstrains(4,5),SGstrains(4,11),...
                               SGstrains(3,2),SGstrains(3,11),SGstrains(3,5),SGstrains(3,8)];

% Loading in Mz
    [NewHeight, NewWidth, R, SGstrains] = Forces(n, w, h, l, rhub, KA, 1, [0 0 0 0 0 1400]);
        C(1,6) = (SGstrains(2,8) + SGstrains(1,8))/2;
        C(2,6) = (SGstrains(3,8) + SGstrains(4,8))/2;
        C(3,6) = (SGstrains(1,2) + SGstrains(4,2) - SGstrains(3,5) - SGstrains(2,5))/4;
        C(4,6) = (SGstrains(2,2) + SGstrains(1,5))/2;
        C(5,6) = (SGstrains(3,2) + SGstrains(4,5))/2;
        C(6,6) = (SGstrains(2,11) - SGstrains(1,11) + SGstrains(3,11) - SGstrains(4,11))/4;
            STRAINS(1:16,6) = [SGstrains(2,2),SGstrains(2,11),SGstrains(2,5),SGstrains(2,8),...
                               SGstrains(1,2),SGstrains(1,8),SGstrains(1,5),SGstrains(1,11),...
                               SGstrains(4,2),SGstrains(4,8),SGstrains(4,5),SGstrains(4,11),...
                               SGstrains(3,2),SGstrains(3,11),SGstrains(3,5),SGstrains(3,8)];

% Display Compliance and Calibration
    CC = round(C*1E7);
```

```
        CC = CC./10
        B = C^-1;
        BB = round(B*1E6)
        Ess = zeros(6,1);
        dlmwrite('strains.txt',STRAINS,',');
```

TRANSDUCER SOLVING AND OPTIMIZATION SCRIPT

```matlab
function [NewHeight, NewWidth, R, SGstrains] = Forces(n, w, h, l, rhub, KA, StrainAnalysis, StrainF)

% All units in SI

% Geometrical and material properties of spokes
    % We know each spoke will be identical with rectangular cross sections:
    % Hc** = Centroidal Bending Stiffness about **
    % E = modulus of elasticity
    % v = Poisson's ratio
    % G = shear modulus

    E = 71.7E9;
    v = 0.33;
    G = E/(2*(1+v));

    Hcxx = (E/12).*((h).^3).*(w);
    Hcyy = (E/12).*((h).^3).*(w); % Note: Hcxx = Hcyy
    Hczz = (E/12).*((w).^3).*(h);

    dl = 2*l/n; % Length of each finite beam

% Boundary stiffness, center stiffness and applied loads
    % The boundaries are identical, however are differently orientated
    % SF = Safety factor

    SF = 1.1;

    Fx = 5200*SF;
    Fy = 5200*SF;
    Fz = 5200*SF; %Fz > 0
    Mx = 1400*SF;
    My = 1400*SF;
    Mz = 1400*SF; %Mz > 0

if StrainAnalysis == 1
    Fx = StrainF(1);
    Fy = StrainF(2);
    Fz = StrainF(3) + 0.00001; %Fz >= 0
    Mx = StrainF(4);
    My = StrainF(5);
    Mz = StrainF(6) + 0.00001; %Mz > 0
end

    kxA = KA(1);
    kyA = KA(2);
    kzA = KA(3);
    kxmA = KA(4);
    kymA = KA(5);
    kzmA = KA(6);

    kxB = KA(1);
    kyB = KA(2);
    kzB = KA(3);
    kxmB = KA(4);
    kymB = KA(5);
    kzmB = KA(6);

    kxC = KA(2);
    kyC = KA(1);
    kzC = KA(3);
    kxmC = KA(5);
    kymC = KA(4);
    kzmC = KA(6);

    kxD = KA(2);
    kyD = KA(1);
    kzD = KA(3);
    kxmD = KA(5);
    kymD = KA(4);
    kzmD = KA(6);
```

```
        kxE = 2*KA(2);
        kyE = 2*KA(2);

% Coupled torque due to spokes
        Beta = [0.141 0.196 0.214 0.228 0.249 0.263 0.281 0.299 0.307 0.313];
        SideRatio = [1 1.5 1.75 2 2.5 3 4 6 8 10];
        Coeffs = polyfit(SideRatio, Beta,5);
        F = @(SideRatio) polyval(Coeffs, SideRatio);
        Summation = 0;
        for I = 1:(n/2)
            if h(I) >= w(I)
                Summation = Summation + (F(h(I)./w(I)).*h(I).*(w(I)^3).*G./dl)^-1;
            else
                Summation = Summation + (F(w(I)./h(I)).*w(I).*(h(I)^3).*G./dl)^-1;
            end
        end
        kxmE = 2/Summation;
        kymE = 2/Summation;

% Assemblage of matrix for beam AB in xz plane and CD in yz plane (Coupled system)
        % Order: [(u'zo1 uzo1 u'zo2 uzo2 ... u'zon uzon u'zo(n+1) uzo(n+1))AB (u'zo1 uzo1 u'zo2 uzo2 ... u'zon uzon
u'zo(n+1) uzo(n+1))CD RzA RxmA RzB RxmB RxmE Alpha RzC RymC RzD RymD RymE Beta A B C D E F G H]
        % M = coefficient matrix Co = Constant matrix
        % Displacements = 1 to 4*n+4
        % RzA = 4*n+4 +1
        % RxmA = 4*n+4 +2
        % RzB = 4*n+4 +3
        % RxmB = 4*n+4 +4
        % RxmE = 4*n+4 +5
        % Alpha = 4*n+4 +6
        % RzC = 4*n+4 +7
        % RymC = 4*n+4 +8
        % RzD = 4*n+4 +9
        % RymD = 4*n+4 +10
        % RymE = 4*n+4 +11
        % Beta = 4*n+4 +12
        % A = 4*n+4 +13
        % B = 4*n+4 +14
        % C = 4*n+4 +15
        % D = 4*n+4 +16
        % E = 4*n+4 +17
        % F = 4*n+4 +18
        % G = 4*n+4 +19
        % H = 4*n+4 +20

        M = zeros(16+8+4*n, 16+8+4*n);
        Co1 = zeros(16+8+4*n,1);

% Define A-H in terms of reaction forces. A-H describe the bending moment. A-D for beam AB and E-H for beam CD
%   A - RzA = 0
        M(1,4*n+4 +13) = 1;
        M(1,4*n+4 +1) = -1;
%   B + RxmA = 0
        M(2,4*n+4 +14) = 1;
        M(2,4*n+4 +2) = 1;
%   C + RzB = 0
        M(3,4*n+4 +15) = 1;
        M(3,4*n+4 +3) = 1;
%   D - 2*l*RzB - RxmB = 0
        M(4,4*n+4 +16) = 1;
        M(4,4*n+4 +3) = -2*l;
        M(4,4*n+4 +4) = -1;
%   E - RzC = 0;
        M(5,4*n+4 +17) = 1;
        M(5,4*n+4 +7) = -1;
%   F - RymC = 0
        M(6,4*n+4 +18) = 1;
        M(6,4*n+4 +8) = -1;
%   G + RzD = 0
        M(7,4*n+4 +19) = 1;
        M(7,4*n+4 +9) = 1;
%   H - 2*l*RzD + RymD = 0
        M(8,4*n+4 +20) = 1;
        M(8,4*n+4 +9) = -2*l;
        M(8,4*n+4 +10) = 1;

% Define force and moment equilibrium
%   RzA + RzB + Alpha*Fz = 0
        M(9,4*n+4 +1) = 1;
        M(9,4*n+4 +3) = 1;
        M(9,4*n+4 +6) = Fz;
```

```matlab
%   RxmA + RxmB + RxmE + l*Alpha*Fz + 2*l*RzB = -Mx
    M(10,4*n+4 +2) = 1;
    M(10,4*n+4 +4) = 1;
    M(10,4*n+4 +5) = 1;
    M(10,4*n+4 +6) = l*Fz;
    M(10,4*n+4 +3) = 2*l;
    Col(10,1) = -Mx;
%   RzC + RzD + Beta*Fz = 0
    M(11,4*n+4 +7) = 1;
    M(11,4*n+4 +9) = 1;
    M(11,4*n+4 +12) = Fz;
%   -RymC - RymD - RymE + l*Beta*Fz + 2*l*RzD = My
    M(12,4*n+4 +8) = -1;
    M(12,4*n+4 +10) = -1;
    M(12,4*n+4 +11) = -1;
    M(12,4*n+4 +12) = l*Fz;
    M(12,4*n+4 +9) = 2*l;
    Col(12,1) = My;

% Define boundary condition equations
%   (u'zo1)AB + RxmA/kxmA = 0
    M(13,1) = 1;
    M(13,4*n+4 +2) = 1/kxmA;
%   (uzo1)AB + RzA/kzA = 0;
    M(14,2) = 1;
    M(14,4*n+4 +1) = 1/kzA;
%   (u'zo(n+1))AB + RxmB/kxmB = 0
    M(15,2*n+1) = 1;
    M(15,4*n+4 +4) = 1/kxmB;
%   (uzo(n+1))AB + RzB/kzB = 0
    M(16,2*n+2) = 1;
    M(16,4*n+4 +3) = 1/kzB;
%   (u'zo1)CD - RymC/kymC = 0
    M(17,2*n+3) = 1;
    M(17,4*n+4 +8) = -1/kymC;
%   (uzo1)CD + RzC/kzC = 0;
    M(18,2*n+4) = 1;
    M(18,4*n+4 +7) = 1/kzC;
%   (u'zo(n+1))CD - RymD/kymD = 0
    M(19,4*n+3) = 1;
    M(19,4*n+4 +10) = -1/kymD;
%   (uzo(n+1))CD + RzD/kzD = 0
    M(20,4*n+4) = 1;
    M(20,4*n+4 +9) = 1/kzD;
%   RxmE/kxmE + u'zo(n/2+1)AB = 0
    M(21,4*n+4 +5) = 1/kxmE;
    M(21,n+1) = 1;
%   - RymE/kymE + u'zo(n/2+1)CD = 0
    M(22,4*n+4 +11) = -1/kymE;
    M(22,2*n+2 + n+1) = 1;

% Define coupling equations
%   Alpha + Beta = 1
    M(23,4*n+4 + 6) = 1;
    M(23,4*n+4 + 12) = 1;
    Col(23,1) = 1;
%   (uzo(n+1))AB - (uzo(n+1))CD = 0
    M(24,n+2) = 1;
    M(24,2*n+2 + n+2) = -1;

% Define finite beam bending equations
    for K = 1:(n/2)
        % u'zoi - u'zo(i+1) + [(dl^2)/(2*Hc) + (dl^2)*(i-1)/(Hc)]*A + (dl)/(Hc)*B = 0
        M(24+2*K-1,2*K-1) = 1;
        M(24+2*K-1,2*K+1) = -1;
        M(24+2*K-1,4*n+4 +13) = (dl^2)/(2*Hcxx(K)) + (dl^2)*(K-1)/(Hcxx(K));
        M(24+2*K-1,4*n+4 +14) = (dl)/(Hcxx(K));
        % dl*u'zoi + uzoi - uzo(i+1) + [(dl^3)/(6*Hc) + (dl^3)*(i-1)/(2*Hc)]*A + (dl^2)/(2*Hc)*B = 0
        M(24+2*K,2*K-1) = dl;
        M(24+2*K,2*K) = 1;
        M(24+2*K,2*K+2) = -1;
        M(24+2*K,4*n+4 +13) = (dl^3)/(6*Hcxx(K)) + (dl^3)*(K-1)/(2*Hcxx(K));
        M(24+2*K,4*n+4 +14) = (dl^2)/(2*Hcxx(K));
    end
    for K = (n/2 + 1):n
        % u'zoi - u'zo(i+1) + [(dl^2)/(2*Hc) + (dl^2)*(i-1)/(Hc)]*C + (dl)/(Hc)*D = 0
        M(24+2*K-1,2*K-1) = 1;
        M(24+2*K-1,2*K+1) = -1;
        M(24+2*K-1,4*n+4 +15) = (dl^2)/(2*Hcxx(K)) + (dl^2)*(K-1)/(Hcxx(K));
        M(24+2*K-1,4*n+4 +16) = (dl)/(Hcxx(K));
        % dl*u'zoi + uzoi - uzo(i+1) + [(dl^3)/(6*Hc) + (dl^3)*(i-1)/(2*Hc)]*C + (dl^2)/(2*Hc)*D = 0
```

```
            M(24+2*K,2*K-1) = dl;
            M(24+2*K,2*K) = 1;
            M(24+2*K,2*K+2) = -1;
            M(24+2*K,4*n+4 +15) = (dl^3)/(6*Hcxx(K)) + (dl^3)*(K-1)/(2*Hcxx(K));
            M(24+2*K,4*n+4 +16) = (dl^2)/(2*Hcxx(K));
        end

        for K = 1:(n/2)
            % u'zoi - u'zo(i+1) + [(dl^2)/(2*Hc) + (dl^2)*(i-1)/(Hc)]*E + (dl)/(Hc)*F = 0
            M(24+2*n+2*K-1,2*n+2 +2*K-1) = 1;
            M(24+2*n+2*K-1,2*n+2 +2*K+1) = -1;
            M(24+2*n+2*K-1,4*n+4 +17) = (dl^2)/(2*Hcyy(K)) + (dl^2)*(K-1)/(Hcyy(K));
            M(24+2*n+2*K-1,4*n+4 +18) = (dl)/(Hcyy(K));
            % dl*u'zoi + uzoi - uzo(i+1) + [(dl^3)/(6*Hc) + (dl^3)*(i-1)/(2*Hc)]*E + (dl^2)/(2*Hc)*F = 0
            M(24+2*n+2*K,2*n+2 +2*K-1) = dl;
            M(24+2*n+2*K,2*n+2 +2*K) = 1;
            M(24+2*n+2*K,2*n+2 +2*K+2) = -1;
            M(24+2*n+2*K,4*n+4 +17) = (dl^3)/(6*Hcyy(K)) + (dl^3)*(K-1)/(2*Hcyy(K));
            M(24+2*n+2*K,4*n+4 +18) = (dl^2)/(2*Hcyy(K));
        end
        for K = (n/2 + 1):n
            % u'zoi - u'zo(i+1) + [(dl^2)/(2*Hc) + (dl^2)*(i-1)/(Hc)]*G + (dl)/(Hc)*H = 0
            M(24+2*n+2*K-1,2*n+2 +2*K-1) = 1;
            M(24+2*n+2*K-1,2*n+2 +2*K+1) = -1;
            M(24+2*n+2*K-1,4*n+4 +19) = (dl^2)/(2*Hcyy(K)) + (dl^2)*(K-1)/(Hcyy(K));
            M(24+2*n+2*K-1,4*n+4 +20) = (dl)/(Hcyy(K));
            % dl*u'zoi + uzoi - uzo(i+1) + [(dl^3)/(6*Hc) + (dl^3)*(i-1)/(2*Hc)]*G + (dl^2)/(2*Hc)*H = 0
            M(24+2*n+2*K,2*n+2 +2*K-1) = dl;
            M(24+2*n+2*K,2*n+2 +2*K) = 1;
            M(24+2*n+2*K,2*n+2 +2*K+2) = -1;
            M(24+2*n+2*K,4*n+4 +19) = (dl^3)/(6*Hcyy(K)) + (dl^3)*(K-1)/(2*Hcyy(K));
            M(24+2*n+2*K,4*n+4 +20) = (dl^2)/(2*Hcyy(K));
        end

% Assemblage of matrix for beam AB in xy plane and CD in xy plane (Coupled system)
    % Order: [(u'xo1 uxo1 u'xo2 uxo2 ... u'xon uxon u'xo(n+1) uxo(n+1))AB (u'yo1 uyo1 u'yo2 uyo2 ... u'yon uyon
u'yo(n+1) uyo(n+1))CD RxA RzmA RxB RzmB RxE Gamma RyC RzmC RyD RzmD RyE Zeta A B C D E F G H]
    % N = coefficient matrix Co2 = Constant matrix
    % Displacements = 1 to 4*n+4
    % RxA = 4*n+4 +1
    % RzmA = 4*n+4 +2
    % RxB = 4*n+4 +3
    % RzmB = 4*n+4 +4
    % RxE = 4*n+4 +5
    % Gamma = 4*n+4 +6
    % RyC = 4*n+4 +7
    % RzmC = 4*n+4 +8
    % RyD = 4*n+4 +9
    % RzmD = 4*n+4 +10
    % RyE = 4*n+4 +11
    % Zeta = 4*n+4 +12
    % A = 4*n+4 +13
    % B = 4*n+4 +14
    % C = 4*n+4 +15
    % D = 4*n+4 +16
    % E = 4*n+4 +17
    % F = 4*n+4 +18
    % G = 4*n+4 +19
    % H = 4*n+4 +20

    N = zeros(16+8+4*n, 16+8+4*n);
    Co2 = zeros(16+8+4*n,1);

% Define A-H in terms of reaction forces. A-H describe the bending moment. A-D for beam AB and E-H for beam CD
%   A + RxA = 0
    N(1,4*n+4 +13) = 1;
    N(1,4*n+4 +1) = 1;
%   B + RzmA = 0
    N(2,4*n+4 +14) = 1;
    N(2,4*n+4 +2) = 1;
%   C - RxB = 0
    N(3,4*n+4 +15) = 1;
    N(3,4*n+4 +3) = -1;
%   D + 2*l*RxB - RzmB = 0
    N(4,4*n+4 +16) = 1;
    N(4,4*n+4 +3) = 2*l;
    N(4,4*n+4 +4) = -1;
%   E - RyC = 0;
    N(5,4*n+4 +17) = 1;
    N(5,4*n+4 +7) = -1;
%   F + RzmC = 0
```

```
    N(6,4*n+4 +18) = 1;
    N(6,4*n+4 +8) = 1;
%   G + RyD = 0
    N(7,4*n+4 +19) = 1;
    N(7,4*n+4 +9) = 1;
%   H - 2*l*RyD - RzmD = 0
    N(8,4*n+4 +20) = 1;
    N(8,4*n+4 +9) = -2*l;
    N(8,4*n+4 +10) = -1;

% Define force and moment equilibrium
%   RxA + RxB + RxE = -Fx
    N(9,4*n+4 +1) = 1;
    N(9,4*n+4 +3) = 1;
    N(9,4*n+4 +5) = 1;
    Co2(9,1) = -Fx;
%   RzmA + RzmB + Gamma*Mz - l*RxE - 2*l*RxB = l*Fx
    N(10,4*n+4 +2) = 1;
    N(10,4*n+4 +4) = 1;
    N(10,4*n+4 +6) = Mz;
    N(10,4*n+4 +5) = -l;
    N(10,4*n+4 +3) = -2*l;
    Co2(10,1) = l*Fx;
%   -RyC - RyD - RyE = Fy
    N(11,4*n+4 +7) = -1;
    N(11,4*n+4 +9) = -1;
    N(11,4*n+4 +11) = -1;
    Co2(11,1) = Fy;
%   RzmC + RzmD + Zeta*Mz + l*RyE + 2*l*RyD = -l*Fy
    N(12,4*n+4 +8) = 1;
    N(12,4*n+4 +10) = 1;
    N(12,4*n+4 +12) = Mz;
    N(12,4*n+4 +11) = l;
    N(12,4*n+4 +9) = 2*l;
    Co2(12,1) = -l*Fy;

% Define boundary condition equations
%   (u'xo1)AB + RzmA/kzmA = 0
    N(13,1) = 1;
    N(13,4*n+4 +2) = 1/kzmA;
%   (uxo1)AB + RxA/kxA = 0;
    N(14,2) = 1;
    N(14,4*n+4 +1) = 1/kxA;
%   (u'xo(n+1))AB + RzmB/kzmB = 0
    N(15,2*n+1) = 1;
    N(15,4*n+4 +4) = 1/kzmB;
%   (uxo(n+1))AB + RxB/kxB = 0
    N(16,2*n+2) = 1;
    N(16,4*n+4 +3) = 1/kxB;
%   (u'yo1)CD + RzmC/kzmC = 0
    N(17,2*n+3) = 1;
    N(17,4*n+4 +8) = 1/kzmC;
%   (uyo1)CD + RyC/kyC = 0;
    N(18,2*n+4) = 1;
    N(18,4*n+4 +7) = 1/kyC;
%   (u'yo(n+1))CD + RzmD/kzmD = 0
    N(19,4*n+3) = 1;
    N(19,4*n+4 +10) = 1/kzmD;
%   (uyo(n+1))CD + RyD/kyD = 0
    N(20,4*n+4) = 1;
    N(20,4*n+4 +9) = 1/kyD;
%   RxE/kxE + uxo(n/2+1)AB = 0
    N(21,4*n+4 +5) = 1/kxE;
    N(21,n+2) = 1;
%   RyE/kyE + uyo(n/2+1)CD = 0
    N(22,4*n+4 +11) = 1/kyE;
    N(22,2*n+2 + n+2) = 1;

% Define coupling equations
%   Gamma + Zeta = 1
    N(23,4*n+4 + 6) = 1;
    N(23,4*n+4 + 12) = 1;
    Co2(23,1) = 1;
%   (u'xo(n+1))AB - (u'yo(n+1))CD = 0
    N(24,n+1) = 1;
    N(24,2*n+2 + n+1) = -1;

% Define finite beam bending equations
    for K = 1:(n/2)
        % u'xoi - u'xo(i+1) + [(dl^2)/(2*Hc) + (dl^2)*(i-1)/(Hc)]*A + (dl)/(Hc)*B = 0
        N(24+2*K-1,2*K-1) = 1;
```

E-7

```
            N(24+2*K-1,2*K+1) = -1;
            N(24+2*K-1,4*n+4 +13) = (dl^2)/(2*Hczz(K)) + (dl^2)*(K-1)/(Hczz(K));
            N(24+2*K-1,4*n+4 +14) = (dl)/(Hczz(K));
            % dl*u'xoi + uxoi - uxo(i+1) + [(dl^3)/(6*Hc) + (dl^3)*(i-1)/(2*Hc)]*A + (dl^2)/(2*Hc)*B = 0
            N(24+2*K,2*K-1) = dl;
            % N(24+2*K,2*K) = 1;
            % N(24+2*K,2*K+2) = -1;
            N(24+2*K,2*K) = -1;
            N(24+2*K,2*K+2) = 1;
            N(24+2*K,4*n+4 +13) = (dl^3)/(6*Hczz(K)) + (dl^3)*(K-1)/(2*Hczz(K));
            N(24+2*K,4*n+4 +14) = (dl^2)/(2*Hczz(K));
        end
        for K = (n/2 + 1):n
            % u'xoi - u'xo(i+1) + [(dl^2)/(2*Hc) + (dl^2)*(i-1)/(Hc)]*C + (dl)/(Hc)*D = 0
            N(24+2*K-1,2*K-1) = 1;
            N(24+2*K-1,2*K+1) = -1;
            N(24+2*K-1,4*n+4 +15) = (dl^2)/(2*Hczz(K)) + (dl^2)*(K-1)/(Hczz(K));
            N(24+2*K-1,4*n+4 +16) = (dl)/(Hczz(K));
            % dl*u'xoi + uxoi - uzo(i+1) + [(dl^3)/(6*Hc) + (dl^3)*(i-1)/(2*Hc)]*C + (dl^2)/(2*Hc)*D = 0
            N(24+2*K,2*K-1) = dl;
            % N(24+2*K,2*K) = 1;
            % N(24+2*K,2*K+2) = -1;
            N(24+2*K,2*K) = -1;
            N(24+2*K,2*K+2) = 1;
            N(24+2*K,4*n+4 +15) = (dl^3)/(6*Hczz(K)) + (dl^3)*(K-1)/(2*Hczz(K));
            N(24+2*K,4*n+4 +16) = (dl^2)/(2*Hczz(K));
        end

        for K = 1:(n/2)
            % u'yoi - u'yo(i+1) + [(dl^2)/(2*Hc) + (dl^2)*(i-1)/(Hc)]*E + (dl)/(Hc)*F = 0
            N(24+2*n+2*K-1,2*n+2 +2*K-1) = 1;
            N(24+2*n+2*K-1,2*n+2 +2*K+1) = -1;
            N(24+2*n+2*K-1,4*n+4 +17) = (dl^2)/(2*Hczz(K)) + (dl^2)*(K-1)/(Hczz(K));
            N(24+2*n+2*K-1,4*n+4 +18) = (dl)/(Hczz(K));
            % dl*u'yoi + uyoi - uyo(i+1) + [(dl^3)/(6*Hc) + (dl^3)*(i-1)/(2*Hc)]*E + (dl^2)/(2*Hc)*F = 0
            N(24+2*n+2*K,2*n+2 +2*K-1) = dl;
            N(24+2*n+2*K,2*n+2 +2*K) = 1;
            N(24+2*n+2*K,2*n+2 +2*K+2) = -1;
            N(24+2*n+2*K,4*n+4 +17) = (dl^3)/(6*Hczz(K)) + (dl^3)*(K-1)/(2*Hczz(K));
            N(24+2*n+2*K,4*n+4 +18) = (dl^2)/(2*Hczz(K));
        end
        for K = (n/2 + 1):n
            % u'yoi - u'yo(i+1) + [(dl^2)/(2*Hc) + (dl^2)*(i-1)/(Hc)]*G + (dl)/(Hc)*H = 0
            N(24+2*n+2*K-1,2*n+2 +2*K-1) = 1;
            N(24+2*n+2*K-1,2*n+2 +2*K+1) = -1;
            N(24+2*n+2*K-1,4*n+4 +19) = (dl^2)/(2*Hczz(K)) + (dl^2)*(K-1)/(Hczz(K));
            N(24+2*n+2*K-1,4*n+4 +20) = (dl)/(Hczz(K));
            % dl*u'yoi + uyoi - uyo(i+1) + [(dl^3)/(6*Hc) + (dl^3)*(i-1)/(2*Hc)]*G + (dl^2)/(2*Hc)*H = 0
            N(24+2*n+2*K,2*n+2 +2*K-1) = dl;
            N(24+2*n+2*K,2*n+2 +2*K) = 1;
            N(24+2*n+2*K,2*n+2 +2*K+2) = -1;
            N(24+2*n+2*K,4*n+4 +19) = (dl^3)/(6*Hczz(K)) + (dl^3)*(K-1)/(2*Hczz(K));
            N(24+2*n+2*K,4*n+4 +20) = (dl^2)/(2*Hczz(K));
        end

    V1 = (M^-1)*Co1;
    V2 = (N^-1)*Co2;

% Reactions at boundaries

%   RA = RxA RyA RzA RxmA RymA RzmA
    RA = [V2(4*n+4 +1), -V2(4*n+4 +11)/2, V1(4*n+4 +1), V1(4*n+4 +2), -V1(4*n+4 +11)/2, V2(4*n+4 +2)];
%   RB = RxB RyB RzB RxmB RymB RzmB
    RB = [V2(4*n+4 +3), V2(4*n+4 +11)/2, V1(4*n+4 +3), V1(4*n+4 +4), V1(4*n+4 +11)/2, V2(4*n+4 +4)];
%   RC = RxC RyC RzC RxmC RymC RzmC
    RC = [-V2(4*n+4 +5)/2, V2(4*n+4 +7), V1(4*n+4 +7), -V1(4*n+4 +5)/2, V1(4*n+4 +8), V2(4*n+4 +8)];
%   RD = RxD RyD RzD RxmD RymD RzmD
    RD = [V2(4*n+4 +5)/2, V2(4*n+4 +9), V1(4*n+4 +9), V1(4*n+4 +5)/2, V1(4*n+4 +10), V2(4*n+4 +10)];

% Moment, shear and torque equations for each spoke (measured from the boundaries)
% nl = normalized length (y/l)
%   Spoke A (0<=nl<=1)
%       Vx = -RxA
%       Vz = RzA
%       Mx = RzA(y) - RxmA
%       Mz = -RxA(y) - RzmA
%       Ty = RymE/2
%       Fy = RyE/2 (Tension = +ve)
    VxA = @ (nl) -RA(1)*(nl.^0);
    VzA = @ (nl) RA(3)*(nl.^0);
    MxA = @ (nl) RA(3)*(nl*l) - RA(4);
```

E-8

```matlab
    MzA = @ (nl) -RA(1)*(nl*l) - RA(6);
    TyA = @ (nl) RA(5)*(nl.^0);
    FyA = @ (nl) RA(2)*(nl.^0);

%   Spoke B (0<=nl<=1)
%       Vx = RxB
%       Vz = -RzB
%       Mx = RzB(y) + RxmB
%       Mz = -RxB(y) + RzmB
%       Ty = RymE/2
%       Fy = RyE/2 (Tension = +ve)
    VxB = @ (nl) RB(1)*(nl.^0);
    VzB = @ (nl) -RB(3)*(nl.^0);
    MxB = @ (nl) RB(3)*(nl*l) + RB(4);
    MzB = @ (nl) -RB(1)*(nl*l) + RB(6);
    TyB = @ (nl) RB(5)*(nl.^0);
    FyB = @ (nl) RB(2)*(nl.^0);

%   Spoke C (0<=nl<=1)
%       Vy = RyC
%       Vz = RzC
%       My = RzC(x) + RymC
%       Mz = RyC(x) - RzmC
%       Tx = RxmE/2
%       Fx = RxE/2 (Tension = +ve)
    VyC = @ (nl) RC(2)*(nl.^0);
    VzC = @ (nl) RC(3)*(nl.^0);
    MyC = @ (nl) RC(3)*(nl*l) + RC(5);
    MzC = @ (nl) RC(2)*(nl*l) - RC(6);
    TxC = @ (nl) RC(4)*(nl.^0);
    FxC = @ (nl) RC(1)*(nl.^0);

%   Spoke D (0<=nl<=1)
%       Vy = -RyD
%       Vz = -RzD
%       My = RzD(x) - RymD
%       Mz = RyD(x) + RzmD
%       Tx = RxmE/2
%       Fx = RxE/2 (Tension = +ve)
    VyD = @ (nl) -RD(2)*(nl.^0);
    VzD = @ (nl) -RD(3)*(nl.^0);
    MyD = @ (nl) RD(3)*(nl*l) - RD(5);
    MzD = @ (nl) RD(2)*(nl*l) + RD(6);
    TxD = @ (nl) RD(4)*(nl.^0);
    FxD = @ (nl) RD(1)*(nl.^0);

% Display Moment, shear and torque diagrams
    figure(1)
    nl = linspace(0,1,100);
    subplot(3,2,1)
    plot(nl, MxA(nl),'g');
    hold on
    plot(nl, MzA(nl), 'r');
    hold on
    plot(-nl+2, MxB(nl),'g'); % Reflect about vertical axis and move 2 to the right
    hold on
    plot(-nl+2, MzB(nl),'r');
    grid on
    title('Beam AB')
    ylabel('Bending moment (Nm)')
    xlabel('y/l')
    legend('Mx','Mz')
    hold off
    subplot(3,2,2)
    plot(nl, MyC(nl), 'b');
    hold on
    plot(nl, MzC(nl), 'r');
    hold on
    plot(-nl+2, MyD(nl),'b');
    hold on
    plot(-nl+2, MzD(nl),'r');
    grid on
    title('Beam CD')
    ylabel('Bending moment (Nm)')
    xlabel('y/l')
    legend('My','Mz')
    hold off

    subplot(3,2,3)
    plot(nl, VxA(nl),'r');
    hold on
```

E-9

```matlab
    plot(nl, VzA(nl), 'g');
    hold on
    plot(-nl+2, VxB(nl),'r'); % Reflect about vertical axis and move 2 to the right
    hold on
    plot(-nl+2, VzB(nl),'g');
    grid on
    title('Beam AB')
    ylabel('Shear force (N)')
    xlabel('y/l')
    legend('Vx','Vz')
    hold off
    subplot(3,2,4)
    plot(nl, VyC(nl), 'r');
    hold on
    plot(nl, VzC(nl), 'b');
    hold on
    plot(-nl+2, VyD(nl),'r');
    hold on
    plot(-nl+2, VzD(nl),'b');
    grid on
    title('Beam CD')
    ylabel('Shear force (N)')
    xlabel('y/l')
    legend('Vy','Vz')
    hold off

    subplot(3,2,5)
    plot(nl, TyA(nl),'b');
    hold on
    plot(nl, TyB(nl), 'r');
    hold on
    plot(nl, TxC(nl),'g');
    hold on
    plot(nl, TxD(nl),'c');
    grid on
    title('Torque in each spoke')
    ylabel('Torque (Nm)')
    xlabel('y/l')
    legend('A','B','C','D')
    hold off
    subplot(3,2,6)
    plot(nl, FyA(nl),'b');
    hold on
    plot(nl, FyB(nl), 'r');
    hold on
    plot(nl, FxC(nl),'g');
    hold on
    plot(nl, FxD(nl),'c');
    grid on
    title('Tension/Compression in each spoke (N)')
    ylabel('Tension[Positive] (N)')
    xlabel('y/l')
    legend('A','B','C','D')
    hold off

% Optimization
if StrainAnalysis ~= 1
    %   SigMax = Maximum allowable stress anywhere
    SigMax = 240E6;
    MaxHeight = 0.4;
    MaxWidth = 0.4;

    % Max stress formulation
    %   xyn, zn are normalized positions: xyn(K) = x/w(K) or y/w(K) zn = z/h(K)
    %    K is the discrete position from 1 to n/2: x or y(normalized) = K/(n/2)

    MxyMax = @(K) max([abs(MxA(K/(n/2))), abs(MxB(K/(n/2))), abs(MyC(K/(n/2))), abs(MyD(K/(n/2)))]);
    MzMax = @(K) max([abs(MzA(K/(n/2))), abs(MzB(K/(n/2))), abs(MzC(K/(n/2))), abs(MzD(K/(n/2)))]);
    VxyMax = @(K) max([abs(VxA(K/(n/2))), abs(VxB(K/(n/2))), abs(VyC(K/(n/2))), abs(VyD(K/(n/2)))]);
    VzMax = @(K) max([abs(VzA(K/(n/2))), abs(VzB(K/(n/2))), abs(VzC(K/(n/2))), abs(VzD(K/(n/2)))]);
    TxyMax = @(K) max([abs(TyA(K/(n/2))), abs(TyB(K/(n/2))), abs(TxC(K/(n/2))), abs(TxD(K/(n/2)))]);
    FxyMax = @(K) max([abs(FyA(K/(n/2))), abs(FyB(K/(n/2))), abs(FxC(K/(n/2))), abs(FxD(K/(n/2)))]);

    % Maximum reaction force at boundary with axial direction in y-axis. Compatible with Boundaries.m
        R = [VxyMax(0), FxyMax(0), VzMax(0), MxyMax(0), TxyMax(0), MzMax(0)];

    Sigxxyy = @(xyn, zn, K) MxyMax(K).*(zn.*h(K))./(1/12*(h(K).^3).*w(K)) + ...
MzMax(K).*(xyn.*w(K))./(1/12*(w(K).^3).*h(K)) + FxyMax(K)./(w(K).*h(K)*0.85);
    if h(K) >= w(K)
        TauMaxTorque = @(K) TxyMax(K).*(3 + 1.8*w(K)./(h(K)))./(h(K).*(w(K).^2));
    else
```

```matlab
            TauMaxTorque = @(K) TxyMax(K).*(3 + 1.8*h(K)./(w(K)))./(w(K).*(h(K).^2));
        end
        Sigyz = @(zn, K) 3*VzMax(K).*(1 - 4*((zn.*h(K)).^2)./(h(K).^2))./(2*h(K).*w(K)) + TauMaxTorque(K);
        Sigxyyx = @(xyn, K) 3*VxyMax(K).*(1 - 4*((xyn.*w(K)).^2)./(w(K).^2))./(2*h(K).*w(K)) + TauMaxTorque(K);
        NewHeight = zeros(1,n/2);
        NewWidth = zeros(1,n/2);

        bool = 1; % Boolean operator

        for K = 1:(n/2);
            % NegSigVM is the negative Von Mises stress at a specific cross section to optimize
            % xn = x(1) and zn = x(2)
            NegSigVM = @(x) (-1)*(2^-0.5)*((2*(Sigxxyy(x(1), x(2), K)).^2 + 6*((Sigyz(x(2), K)).^2 + (Sigxyyx(x(1),
K)).^2))).^0.5;

            [xynzn, NegSigMax] = sqp([0,0],NegSigVM,[],[],[-0.5,-0.5],[0.5,0.5]);
            xyn = xynzn(1);
            zn = xynzn(2);

            Sigxxyyhw = @(h, w) MxyMax(K).*(zn.*h)./(1/12*(h.^3).*w) + MzMax(K).*(xyn.*w)./(1/12*(w.^3).*h) +
FxyMax(K)./(w.*h*0.85);
            TauMaxTorquehw = @(h, w) (TxyMax(K).*(3 + 1.8*w./(h))./(h.*(w.^2))).*(h>w) + (TxyMax(K).*(3 +
1.8*h./(w))./(w.*(h.^2))).*(w>=h);
            Sigyzhw = @(h, w) 3*VzMax(K).*(1 - 4*((zn.*h).^2)./(h.^2))./(2*h.*w) + TauMaxTorquehw(h, w);
            Sigxyyxhw = @(h, w) 3*VxyMax(K).*(1 - 4*((xyn.*w).^2)./(w.^2))./(2*h.*w) + TauMaxTorquehw(h, w);
            SigVMhw = @(h, w) (2^-0.5)*((2*(Sigxxyyhw(h, w)).^2 + 6*((Sigyzhw(h, w)).^2 + (Sigxyyxhw(h,
w)).^2))).^0.5;

            Area = @(x) 0*(x(1).*x(2)) + 1*(x(1).^2 + x(2).^2) + 0*(x(1) - x(2)).^2;
            H = @(x) -1*SigVMhw(x(1), x(2)) + SigMax;

            [hw] = sqp([h(K),w(K)],Area,[],H,[0.001, 0.001],[MaxHeight, MaxWidth],20);

            % Adjust for hub radius
            if (K/(n/2)*l) > (l-rhub)
                y = 2*(rhub^2 - (K/(n/2)*l - l)^2)^0.5;
                if (y) > hw(2)
                    if bool == 1
                        hhub = hw(1);
                        bool = 0;
                    end
                    hw(2) = y;
                    hw(1) = hhub;
                    if (H([hw(1), hw(2)])) < -1E6
                     error = K/(n/2)*l
                    end
                end
            end

            NewHeight(K) = hw(1);
            NewWidth(K) = hw(2);
        end
end

if StrainAnalysis == 1
% Spoke A
%   K is the discrete position from 1 to n/2: y(normalized) = K/(n/2)
%   xn, zn are normalized positions: Positive surface = 0.5, Centre = 0, Negative surface = -0.5
        SigyyA = @(xn, zn, K) -1*MxA(K/(n/2)).*(zn.*h(K))./(1/12*(h(K).^3).*w(K)) +
MzA(K/(n/2)).*(xn.*w(K))./(1/12*(w(K).^3).*h(K)) + FyA(K/(n/2))./(w(K).*h(K));
% Spoke B
        SigyyB = @(xn, zn, K) -1*MxB(K/(n/2)).*(zn.*h(K))./(1/12*(h(K).^3).*w(K)) +
MzB(K/(n/2)).*(xn.*w(K))./(1/12*(w(K).^3).*h(K)) + FyB(K/(n/2))./(w(K).*h(K));
% Spoke C
        SigxxC = @(yn, zn, K) -1*MyC(K/(n/2)).*(zn.*h(K))./(1/12*(h(K).^3).*w(K)) -
MzC(K/(n/2)).*(yn.*w(K))./(1/12*(w(K).^3).*h(K)) + FxC(K/(n/2))./(w(K).*h(K));
% Spoke D
        SigxxD = @(yn, zn, K) -1*MyD(K/(n/2)).*(zn.*h(K))./(1/12*(h(K).^3).*w(K)) -
MzD(K/(n/2)).*(yn.*w(K))./(1/12*(w(K).^3).*h(K)) + FxD(K/(n/2))./(w(K).*h(K));

% Strain gauge readings
%   Placement of strain gauges (SG)
%       nlSG is the normalized inward axial position of all the gauges to l
%       Kn = the nth position where nlSG is Kn = f(n,nlSG)
%       oSG is the offset position of the offset gauges
%       noSG is the normalized offset position with h or w (0 < noSG < 0.5)
%   For up to 48 gauges
        nlSG = 0.3333333; %(l-rub-15)/l
        Kn = round(nlSG*n/2);
        oSG = 0.005;
        noSGh = oSG./h(Kn);
```

```
        noSGw = oSG./w(Kn);

%    Plot Strain
    % if Fx ~= 0
        % K = [1:(n/2)];
        % figure(5)
        % plot(K/(n/2)*l*1000,SigyyA(0.5,0,K')./E.*1E6,'b')
        % grid on
        % title('SURFACE STRAIN UNDER Fx LOAD')
        % xlabel('Axial position (mm)')
        % ylabel('Axial strain (micro-strain)')
        % print plot.jpg -djpeg
    % end
    % hold on
    % plot(K,SigyyB(0.5,0,K')./E.*1E6,'r')
    % hold on
    % plot(K,SigxxC(0.5,0,K')./E.*1E6,'b')
    % hold on
    % plot(K,SigxxD(0.5,0,K')./E.*1E6,'r')

% Strain gauge readings
%    Convention Ei*#
%    # is the spoke A, B, C or D
%    i is the face 1=Positive Z; 2 = Negative Z; 3 = Positive X or Y; 4 = Negative X or Y
%    * is the offset with respect to global coordinate system a = positive offset; '' is no offset; b = negative
offset

%    Spoke A
    E1aA = SigyyA(noSGw, 0.5, Kn)/E;
    E1A = SigyyA(0, 0.5, Kn)/E
    E1bA = SigyyA(-noSGw, 0.5, Kn)/E;

    E2aA = SigyyA(noSGw, -0.5, Kn)/E;
    E2A = SigyyA(0, -0.5, Kn)/E
    E2bA = SigyyA(-noSGw, -0.5, Kn)/E;

    E3aA = SigyyA(0.5, noSGh, Kn)/E;
    E3A = SigyyA(0.5, 0, Kn)/E
    E3bA = SigyyA(0.5, -noSGh, Kn)/E;

    E4aA = SigyyA(-0.5, noSGh, Kn)/E;
    E4A = SigyyA(-0.5, 0, Kn)/E
    E4bA = SigyyA(-0.5, -noSGh, Kn)/E;

%    Spoke B
    E1aB = SigyyB(noSGw, 0.5, Kn)/E;
    E1B = SigyyB(0, 0.5, Kn)/E
    E1bB = SigyyB(-noSGw, 0.5, Kn)/E;

    E2aB = SigyyB(noSGw, -0.5, Kn)/E;
    E2B = SigyyB(0, -0.5, Kn)/E
    E2bB = SigyyB(-noSGw, -0.5, Kn)/E;

    E3aB = SigyyB(0.5, noSGh, Kn)/E;
    E3B = SigyyB(0.5, 0, Kn)/E
    E3bB = SigyyB(0.5, -noSGh, Kn)/E;

    E4aB = SigyyB(-0.5, noSGh, Kn)/E;
    E4B = SigyyB(-0.5, 0, Kn)/E
    E4bB = SigyyB(-0.5, -noSGh, Kn)/E;

%    Spoke C
    E1aC = SigxxC(noSGw, 0.5, Kn)/E;
    E1C = SigxxC(0, 0.5, Kn)/E
    E1bC = SigxxC(-noSGw, 0.5, Kn)/E;

    E2aC = SigxxC(noSGw, -0.5, Kn)/E;
    E2C = SigxxC(0, -0.5, Kn)/E
    E2bC = SigxxC(-noSGw, -0.5, Kn)/E;

    E3aC = SigxxC(0.5, noSGh, Kn)/E;
    E3C = SigxxC(0.5, 0, Kn)/E
    E3bC = SigxxC(0.5, -noSGh, Kn)/E;

    E4aC = SigxxC(-0.5, noSGh, Kn)/E;
    E4C = SigxxC(-0.5, 0, Kn)/E
    E4bC = SigxxC(-0.5, -noSGh, Kn)/E;

%    Spoke D
    E1aD = SigxxD(noSGw, 0.5, Kn)/E;
    E1D = SigxxD(0, 0.5, Kn)/E
```

E-12

```
    E1bD = SigxxD(-noSGw, 0.5, Kn)/E;

    E2aD = SigxxD(noSGw, -0.5, Kn)/E;
    E2D = SigxxD(0, -0.5, Kn)/E
    E2bD = SigxxD(-noSGw, -0.5, Kn)/E;

    E3aD = SigxxD(0.5, noSGh, Kn)/E;
    E3D = SigxxD(0.5, 0, Kn)/E
    E3bD = SigxxD(0.5, -noSGh, Kn)/E;

    E4aD = SigxxD(-0.5, noSGh, Kn)/E;
    E4D = SigxxD(-0.5, 0, Kn)/E
    E4bD = SigxxD(-0.5, -noSGh, Kn)/E;

SGstrains = [E1aA,E1A,E1bA,E2aA,E2A,E2bA,E3aA,E3A,E3bA,E4aA,E4A,E4bA;...
             E1aB,E1B,E1bB,E2aB,E2B,E2bB,E3aB,E3B,E3bB,E4aB,E4B,E4bB;...
             E1aC,E1C,E1bC,E2aC,E2C,E2bC,E3aC,E3C,E3bC,E4aC,E4C,E4bC;...
             E1aD,E1D,E1bD,E2aD,E2D,E2bD,E3aD,E3D,E3bD,E4aD,E4D,E4bD];

end

end
```

BOUNDARY SOLVING AND OPTIMIZATION SCRIPT

```
function [kx ky kz kmx kmy kmz lnew bnew hnew] = Boundaries(R, l, b, h, wo)

% R = [Fx Fy Fz Mx My Mz] for boundary with axial direction of spoke in y-axis
% l = length of flexure beam in x
% b = width of flexure beam in y
% h = height of flexure beam in z
% wo = width of spoke in x at the boundary

function [KoptSigVM kx ky kz kmx kmy kmz] = Stiffness(R, l, b, h, wo, SelectOpt)

    % If SelectOpt = 1 then KoptSigVM = Kopt
    % If SelectOpt = 2 then KoptSigVM = SigVM

    % Geometrical and material properties of spokes

    E = 71.7E9;
    v = 0.33;
    G = E/(2*(1+v));

    Hczz = (E/12)*(b^3)*h;
    Hcyy = (E/12)*(h^3)*b;

    M = zeros(12,12);
    N = zeros(12,12);
    Co1 = zeros(12,1);
    Co2 = zeros(12,1);

    % Assemblage of matrix for boundary AB in xy plane
    %   Order [u'yo2 uyo2 u'yo3 uyo3 RyA RyB MzA MzB A B C D]

    % Define A-D in terms of reaction forces
    % A - RyA = 0
    M(1,9) = 1;
    M(1,5) = -1;
    % B + MzA = 0
    M(2,10) = 1;
    M(2,7) = 1;
    % C + RyB = 0;
    M(3,11) = 1;
    M(3,6) = 1;
    % D - l*RyB - MzB = 0
    M(4,12) = 1;
    M(4,6) = -1*l;
    M(4,8) = -1;

    % Define governing equations
    % RyA + RyB = -Fy;
    M(5,5) = 1;
    M(5,6) = 1;
    Co1(5,1) = -1*R(2);
    % MzA + MzB + l*RyB = -(1/2)*Fy - Mz
    M(6,7) = 1;
    M(6,8) = 1;
    M(6,6) = l;
```

E-13

```
Co1(6,1) = -(1/2)*R(2) - R(6);
% u'yo2 - (1/Hczz)*{A*[((l-wo)^2)/8] + B*[(l-wo)/2]} = 0
M(7,1) = 1;
M(7,9) = -1*((l-wo)^2)/(8*Hczz);
M(7,10) = -1*(l-wo)/(2*Hczz);
% uyo2 - (1/Hczz)*{A*[((l-wo)^3)/48] + B*[((l-wo)^2)/8]} = 0
M(8,2) = 1;
M(8,9) = -1*((l-wo)^3)/(48*Hczz);
M(8,10) = -1*((l-wo)^2)/(8*Hczz);
% u'yo3 - u'yo2 = 0
M(9,3) = 1;
M(9,1) = -1;
% uyo3 - wo*u'yo2 - uyo2 = 0
M(10,4) = 1;
M(10,1) = -1*wo;
M(10,2) = -1;
% u'yo3 + (1/Hczz)*{C*[((l-wo)^2)/8 + (l/2 + wo/2)*(l-wo)/2] + D*[(l-wo)/2]} = 0
M(11,3) = 1;
M(11,11) = (((l-wo)^2)/8 + (l/2 + wo/2)*(l-wo)/2)/(Hczz);
M(11,12) = (l-wo)/(2*Hczz);
% uyo3 + u'yo3*(l-wo)/2 + (1/Hczz)*{C*[((l-wo)^3)/48 + (l/2 + wo/2)*((l-wo)^2)/8] + D*[((l-wo)^2)/8]} = 0
M(12,4) = 1;
M(12,3) = (l-wo)/2;
M(12,11) = (((l-wo)^3)/48 + (l/2 + wo/2)*((l-wo)^2)/8)/(Hczz);
M(12,12) = ((l-wo)^2)/(8*Hczz);


V1 = (M^-1)*Co1;

% Assemblage of matrix for boundary AB in xz plane
%   Order [u'zo2 uzo2 u'zo3 uzo3 RzA RzB MyA MyB A B C D]

% Define A-D in terms of reaction forces
% A - RzA = 0
N(1,9) = 1;
N(1,5) = -1;
% B + MyA = 0
N(2,10) = 1;
N(2,7) = 1;
% C + RzB = 0;
N(3,11) = 1;
N(3,6) = 1;
% D - l*RzB - MyB = 0
N(4,12) = 1;
N(4,6) = -1*l;
N(4,8) = -1;

% Define governing equations
% RzA + RzB = -Fz;
N(5,5) = 1;
N(5,6) = 1;
Co2(5,1) = -1*R(3);
% MyA + MyB + l*RzB = -(1/2)*Fz - My
N(6,7) = 1;
N(6,8) = 1;
N(6,6) = l;
Co2(6,1) = -(1/2)*R(3) - R(5);
% u'zo2 - (1/Hcyy)*{A*[((l-wo)^2)/8] + B*[(l-wo)/2]} = 0
N(7,1) = 1;
N(7,9) = -1*((l-wo)^2)/(8*Hcyy);
N(7,10) = -1*(l-wo)/(2*Hcyy);
% uzo2 - (1/Hcyy)*{A*[((l-wo)^3)/48] + B*[((l-wo)^2)/8]} = 0
N(8,2) = 1;
N(8,9) = -1*((l-wo)^3)/(48*Hcyy);
N(8,10) = -1*((l-wo)^2)/(8*Hcyy);
% u'zo3 - u'zo2 = 0
N(9,3) = 1;
N(9,1) = -1;
% uzo3 - wo*u'zo2 - uzo2 = 0
N(10,4) = 1;
N(10,1) = -1*wo;
N(10,2) = -1;
% u'zo3 + (1/Hcyy)*{C*[((l-wo)^2)/8 + (l/2 + wo/2)*(l-wo)/2] + D*[(l-wo)/2]} = 0
N(11,3) = 1;
N(11,11) = (((l-wo)^2)/8 + (l/2 + wo/2)*(l-wo)/2)/(Hcyy);
N(11,12) = (l-wo)/(2*Hcyy);
% uzo3 + u'zo3*(l-wo)/2 + (1/Hcyy)*{C*[((l-wo)^3)/48 + (l/2 + wo/2)*((l-wo)^2)/8] + D*[((l-wo)^2)/8]} = 0
N(12,4) = 1;
N(12,3) = (l-wo)/2;
N(12,11) = (((l-wo)^3)/48 + (l/2 + wo/2)*((l-wo)^2)/8)/(Hcyy);
N(12,12) = ((l-wo)^2)/(8*Hcyy);
```

E-14

```matlab
    V2 = (N^-1)*Co2;

    % Determine stiffness
        ky = R(2)/(V1(1)*wo/2 + V1(2));
        kmz = R(6)/(V1(1));
        kz = R(3)/(V2(1)*wo/2 + V2(2));
        kmy = R(5)/(V2(1));

    % Boundary AB in x direction
        kx = 4*b*h*E/(l-wo);

    % Boundary AB about x
        Beta = [0.141 0.196 0.214 0.228 0.249 0.263 0.281 0.299 0.307 0.313];
        SideRatio = [1 1.5 1.75 2 2.5 3 4 6 8 10];
        Coeffs = polyfit(SideRatio, Beta,5);
        F = @(SideRatio) polyval(Coeffs, SideRatio);
        if h >= b
            kmx = 4*F(h/b)*h*(b^3)*G./(l-wo);
        else
            kmx = 4*F(b/h)*b*(h^3)*G./(l-wo);
        end

    % Function to minimize in SQL
        Kopt = (ky + kmx/(l^2) + kmz/(l^2));

    % Stress formulation

    % Shear forces, bending moments, tensions/compression and torque
    %    Normalized to nl=x/(l/2) therefore 0<=nl<=1

    Vy1 = @(nl) abs(V1(5).*(nl*l/2).^0);
    Mz1 = @(nl) abs(V1(5).*(nl*l/2) - V1(7));
    Vy2 = @(nl) abs(-V1(6).*(nl*l/2).^0);
    Mz2 = @(nl) abs(V1(6).*(nl*l/2) + V1(8));

    Vz1 = @(nl) abs(V2(5).*(nl*l/2).^0);
    My1 = @(nl) abs(V2(5).*(nl*l/2) - V2(7));
    Vz2 = @(nl) abs(-V2(6).*(nl*l/2).^0);
    My2 = @(nl) abs(V2(6).*(nl*l/2) + V2(8));

    Fx = @(nl) abs((R(1)/2).*(nl*l/2).^0);
    Tx = @(nl) abs((R(4)/2).*(nl*l/2).^0);

    % Max stress formulation
    %    yn, zn are normalized positions: yn = y/b zn = z/h
    %    Normalized to nl=x/(l/2) therefore 0<=nl<=1 for 0<=x<(l/2)
    %    x is the position from 0-l

    % For 0=<x<(l/2)
    Sigxx1 = @(yn, zn, nl) My1(nl)*(zn*h)/(1/12*(h^3)*b) + Mz1(nl)*(yn*b)/(1/12*(b^3)*h) + Fx(nl)/(b*h*0.85);
    TauMaxTorque1 = @(nl) max(Tx(nl)*(3 + 1.8*b/h)/(h*(b^2)), Tx(nl)*(3 + 1.8*h/b)/(b*(h^2)));
    Sigxz1 = @(zn, nl) 3*Vz1(nl)*(1 - 4*((zn*h)^2)/(h^2))/(2*h*b) + TauMaxTorque1(nl);
    Sigxy1 = @(yn, nl) 3*Vy1(nl)*(1 - 4*((yn*b)^2)/(b^2))/(2*h*b) + TauMaxTorque1(nl);
    % For (l/2)<x<=l
    Sigxx2 = @(yn, zn, nl) My2(nl)*(zn*h)/(1/12*(h^3)*b) + Mz2(nl)*(yn*b)/(1/12*(b^3)*h) + Fx(nl)/(b*h*0.85);
    TauMaxTorque2 = @(nl) max(Tx(nl)*(3 + 1.8*b/h)/(h*(b^2)), Tx(nl)*(3 + 1.8*h/b)/(b*(h^2)));
    Sigxz2 = @(zn, nl) 3*Vz2(nl)*(1 - 4*((zn*h)^2)/(h^2))/(2*h*b) + TauMaxTorque2(nl);
    Sigxy2 = @(yn, nl) 3*Vy2(nl)*(1 - 4*((yn*b)^2)/(b^2))/(2*h*b) + TauMaxTorque2(nl);

    % Von Mises stress
    % x = yn zn nl
    SigVM1 = @(x) (2^-0.5)*((2*(Sigxx1(x(1), x(2), x(3))).^2 + 6*((Sigxz1(x(2), x(3))).^2 + (Sigxy1(x(1),
x(3))).^2))).^0.5;
    SigVM2 = @(x) (2^-0.5)*((2*(Sigxx2(x(1), x(2), x(3))).^2 + 6*((Sigxz2(x(2), x(3))).^2 + (Sigxy2(x(1),
x(3))).^2))).^0.5;
    MaxSigVm = 0;
    % K as discretized nl from 0-1
    % Check stress at all corners and side centers (9 points in total)
    for K = 0:0.1:1
        [TempMaxSigVM1 ai] = max([SigVM1([0, 0, K]), SigVM1([0.5, 0, K]), SigVM1([0, 0.5, K]), SigVM1([0.5,
0.5, K]), SigVM1([-0.5, 0, K]), SigVM1([0, -0.5, K]), SigVM1([-0.5, -0.5, K]), SigVM1([0.5, -0.5, K]),
SigVM1([-0.5, 0.5, K])]);
        [TempMaxSigVM2 bi] = max([SigVM2([0, 0, K]), SigVM2([0.5, 0, K]), SigVM2([0, 0.5, K]), SigVM2([0.5,
0.5, K]), SigVM2([-0.5, 0, K]), SigVM2([0, -0.5, K]), SigVM2([-0.5, -0.5, K]), SigVM2([0.5, -0.5, K]),
SigVM2([-0.5, 0.5, K])]);
        if TempMaxSigVM1 >= TempMaxSigVM2
            TempMaxSigVM = TempMaxSigVM1;
            ci = ai;
            n = 1;
        else
            TempMaxSigVM = TempMaxSigVM2;
```

```matlab
                ci = bi;
                n= 2;
            end
        if TempMaxSigVM > MaxSigVm
            MaxSigVm = TempMaxSigVM;
            Side = n;
            switch ci
                case 1
                    yn = 0;
                    zn = 0;
                    nl = K;
                case 2
                    yn = 0.5;
                    zn = 0;
                    nl = K;
                case 3
                    yn = 0;
                    zn = 0.5;
                    nl = K;
                case 4
                    yn = 0.5;
                    zn = 0.5;
                    nl = K;
                case 5
                    yn = -0.5;
                    zn = 0;
                    nl = K;
                case 6
                    yn = 0;
                    zn = -0.5;
                    nl = K;
                case 7
                    yn = -0.5;
                    zn = -0.5;
                    nl = K;
                case 8
                    yn = 0.5;
                    zn = -0.5;
                    nl = K;
                case 9
                    yn = -0.5;
                    zn = 0.5;
                    nl = K;
            end
        end
    end

    % hv = h variable bv = b variable
    if Side == 1
        Sigxx = @(hv, bv) My1(nl)*(zn*hv)/(1/12*(hv^3)*bv) + Mz1(nl)*(yn*bv)/(1/12*(bv^3)*hv) +
Fx(nl)/(bv*hv*0.85);
        TauMaxTorque = @(hv, bv) max(Tx(nl)*(3 + 1.8*bv/hv)/(hv*(bv^2)), Tx(nl)*(3 + 1.8*hv/bv)/(bv*(hv^2)));
        Sigxz = @(hv, bv) 3*Vz1(nl)*(1 - 4*((zn*hv)^2)/(hv^2))/(2*hv*bv) + TauMaxTorque(hv, bv);
        Sigxy = @(hv, bv) 3*Vy1(nl)*(1 - 4*((yn*bv)^2)/(bv^2))/(2*hv*bv) + TauMaxTorque(hv, bv);
    else
        Sigxx = @(hv, bv) My2(nl)*(zn*hv)/(1/12*(hv^3)*bv) + Mz2(nl)*(yn*bv)/(1/12*(bv^3)*hv) +
Fx(nl)/(bv*hv*0.85);
        TauMaxTorque = @(hv, bv) max(Tx(nl)*(3 + 1.8*bv/hv)/(hv*(bv^2)), Tx(nl)*(3 + 1.8*hv/bv)/(bv*(hv^2)));
        Sigxz = @(hv, bv) 3*Vz2(nl)*(1 - 4*((zn*hv)^2)/(hv^2))/(2*hv*bv) + TauMaxTorque(hv, bv);
        Sigxy = @(hv, bv) 3*Vy2(nl)*(1 - 4*((yn*bv)^2)/(bv^2))/(2*hv*bv) + TauMaxTorque(hv, bv);
    end
    SigVM = (2^-0.5)*((2*(Sigxx(h, b)).^2 + 6*((Sigxz(h, b)).^2 + (Sigxy(h, b)).^2))).^0.5;

    SelectOpt;
    if SelectOpt == 1
        KoptSigVM = Kopt;
    else
        KoptSigVM = SigVM;
    end

end

% Define maximum boundary dimensions
    hmax = 0.04;
    bmax = 1;
    lmax = 0.12;

% Maximum allowable reversed stress
    SigMax = 240E6;
% x = h b l
    Kopt = @(x) Stiffness(R, x(3), x(2), x(1), wo, 1);
```

```matlab
    H = @(x) -1*Stiffness(R, x(3), x(2), x(1), wo, 2) + SigMax;

    [hbl] = sqp([h, b, l],Kopt,[],H,[0.001, 0.001, 0.001],[hmax, bmax, lmax],20);

    hnew = hbl(1)
    bnew = hbl(2)
    lnew = hbl(3)

[Redundant kx ky kz kmx kmy kmz] = Stiffness(R, lnew, bnew, hnew, wo, 1);

end
```